

Air Force Institute of Technology

AFIT Scholar

Theses and Dissertations

Student Graduate Works

3-2001

Using GPS as a Reference System to Hit a Moving Target

Daryl J. Burnette

Follow this and additional works at: <https://scholar.afit.edu/etd>



Part of the [Signal Processing Commons](#)

Recommended Citation

Burnette, Daryl J., "Using GPS as a Reference System to Hit a Moving Target" (2001). *Theses and Dissertations*. 4583.

<https://scholar.afit.edu/etd/4583>

This Thesis is brought to you for free and open access by the Student Graduate Works at AFIT Scholar. It has been accepted for inclusion in Theses and Dissertations by an authorized administrator of AFIT Scholar. For more information, please contact AFIT.ENWL.Repository@us.af.mil.

20010706 172



USING GPS AS A REFERENCE SYSTEM TO HIT A MOVING TARGET

THESIS

Daryl J. Burnette, Captain, USAF

AFIT/GE/ENG/01M-04

**DEPARTMENT OF THE AIR FORCE
AIR UNIVERSITY**

AIR FORCE INSTITUTE OF TECHNOLOGY

Wright-Patterson Air Force Base, Ohio

APPROVED FOR PUBLIC RELEASE; DISTRIBUTION UNLIMITED.

The views expressed in this thesis are those of the author and do not reflect the official policy or position of the United States Air Force, Department of Defense, or the U. S. Government.

USING GPS AS A REFERENCE SYSTEM TO HIT A MOVING TARGET

THESIS

Presented to the Faculty

Department of Electrical and Computer Engineering

Graduate School of Engineering and Management

Air Force Institute of Technology

Air University

Air Education and Training Command

In Partial Fulfillment of the Requirements for the
Degree of Master of Science in Electrical Engineering

Daryl J. Burnette, B.S.E.E.

Captain, USAF

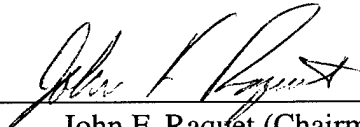
March 2001

APPROVED FOR PUBLIC RELEASE; DISTRIBUTION UNLIMITED.

USING GPS AS A REFERENCE SYSTEM TO HIT A MOVING TARGET

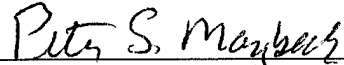
Daryl J. Burnette, B.S.E.E.
Captain, USAF

Approved:



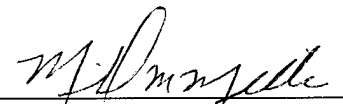
John F. Raquet (Chairman)

6 MAR 01
Date



Peter S. Maybeck (Member)

6 MAR 01
Date



Mikel M. Miller (Member)

6 MAR 01
Date

Acknowledgments

First and foremost I must acknowledge and give thanks to my Lord and personal Savior, Jesus Christ for His everlasting love and blessings. I thank Him for loving me enough to die on the cross that I may be free in Him. "But they that wait upon the Lord shall renew their strength; they shall mount up with wings as eagles; they shall run and not get weary; and they shall walk, and not faint." (*Isaiah 40:31*)

To my family, I love and thank you for all your calls of support and confidence in my ability to make it. I thank God for the blessing of being your child. , you are my heart and I know you will continue to succeed and out do your big brother.

you just don't know how much of an inspiration and support you have been since I laid eyes on you. I appreciate and "live" you.

To my advisor, Major Raquet, I deeply appreciate all of your support, time and sacrifice in the completion of the research. Major Raquet, Dr. Peter Maybeck and Lt Col Mikel Miller you gentlemen have given me an experience at AFIT that I will not forget. Not only for your professionalism, knowledge, and willingness to help, but I won't forget your Godly example. May the Lord continue to bless you and your families.

To Nico "Suave," it has been wild 18 months. I think I have had enough two-person classes to last me a lifetime. To all my fellow AFIT graduates, may God continue to bless you and your families.

To DARPA, I thank you for your help and the opportunity to work with this project.

Daryl J. Burnette

Table of Contents

	Page
Acknowledgments	iv
Table of Contents	v
List of Figures	ix
List of Tables	xii
Abstract	xiii
1. Introduction	1
1.1. Background	2
1.1.1. Global Positioning System Overview	2
1.1.2. AMSTE Program.....	5
1.2. Problem Statement	6
1.3. Scope	6
1.3.1. Assumptions	7
1.4. Methodology	8
2. Background	9
2.1. Overview	9
2.2. Differential GPS (DGPS).....	9
2.3. GPS Errors.....	11
2.4. Satellite Errors	12
2.4.1. Satellite Clock (δt_{sv}).....	12
2.4.2. Ephemeris Errors (δt_{eph}).....	13
2.5. Atmospheric Errors	13

2.5.1.	Ionosphere (δt_{iono})	13
2.5.2.	Troposphere (δt_{trop})	15
2.6.	Receiver Errors.....	18
2.6.1.	Receiver Clock (δt_u)	18
2.6.2.	Multipath (δt_{mp})	18
2.6.3.	Measurement Noise (δt_{noise})	21
2.7.	DGPS Effect on GPS Errors.....	22
2.8.	Synthetic Aperture Radar/Ground Moving Target Indicator	23
2.8.1.	SAR Errors	24
2.9.	System Kalman Filter	25
2.9.1.	State and Measurement Model Equations	26
2.9.2.	Measurement Model Linearization	27
2.9.3.	Extended Kalman Filter Propagate and Update Equations	28
2.10.	Environment Model.....	29
3.	Modeling Methodology.....	31
3.1.	Overview	31
3.2.	True Environment Modeling.....	31
3.2.1.	Sensors Environment Models.....	32
3.2.2.	Munition Environment Model.....	33
3.2.3.	Target Environment Model	34
3.2.4.	GPS Environment Model	35
3.2.4.1.	Environment Model True Ranges and Range Rates	35
3.2.4.2.	GPS Troposphere Environment Model	36

3.2.4.3.	GPS Environment Satellite Clock Model.....	36
3.2.4.4.	GPS Environment Ephemeris Model	37
3.2.4.5.	GPS Environment Receiver Clock Model	37
3.2.4.6.	GPS Environment Receiver Noise Model.....	38
3.2.4.7.	GPS Environment Multipath Model	38
3.2.5.	SAR/GMTI Environment Range and Range Rate Models	39
3.2.5.1.	SAR/GMTI Environment Atmosphere Range Error.....	39
3.2.5.2.	SAR/GMTI Environment Range/Range Rate Noise Error	41
3.2.6.	True Environment Summary	41
3.3.	Kalman Filter.....	42
3.3.1.	Filter Model State Vector	42
3.3.2.	Filter Dynamics Model of Sensor 1, Sensor 2, and the Bomb	45
3.3.3.	Filter Dynamics Model for Target	48
3.3.4.	Filter Model for Sensors 1 & 2 and Bomb Receiver Clocks.....	49
3.3.5.	System Model for SAR scale factor for the target	50
3.3.6.	Filter Model for Common GPS Errors	51
3.3.7.	System Measurement Models	51
3.3.7.1.	Filter Measurement Model - GPS Code Measurements.....	52
3.3.7.2.	System Measurement Model – SAR range measurement	53
3.3.7.3.	System Measurement Model – SAR Range Rate Measurement.....	54
3.4.	Calculations to Find Accuracy in Bomb-to-Target Vector	55
4.	Simulation Results.....	57
4.1.	Overview	57

4.2.	System Kalman Filter Results Setup.....	57
4.3.	Filter Output and Tuning.....	59
4.4.	Filter Parameters and Case Definitions.....	66
4.4.1.	Number of GPS satellites.....	66
4.4.2.	Estimating the SV Errors.....	67
4.4.3.	Tracking the Bomb and Target.....	67
4.4.4.	Case Descriptions.....	68
4.4.5.	Case 1 – All Satellites, Modeling Satellite Error, Bomb Tracking.....	68
4.5.	Results Summary.....	71
4.5.1.	All-in-View Satellite Cases.....	72
4.5.2.	Limited (-2) Satellite Cases.....	73
4.5.3.	Limited 4 Satellite Cases.....	74
4.5.4.	Case Summary.....	75
5.	Conclusions and Recommendations.....	77
5.1.	Conclusions.....	77
5.2.	Recommendations.....	78
Appendix	Graphs of the Bomb-to-Target (Cases 2-12).....	81
Bibliography	114
Vita	119

List of Figures

	Page
Figure 1. Illustrated Description of GPS Navigation Solution [9].....	4
Figure 2. Differential GPS Concept	9
Figure 3. GPS Errors [12]	11
Figure 4. Ionosphere Total Electron Content (TEC) Unit.....	14
Figure 5. Multipath-Induced Error as a Function of Relative Delay and Phase of Multipath [35].....	19
Figure 6. DGPS Concept.....	22
Figure 7. Synthetic Aperture Radar Techniques[46].....	24
Figure 8. True Environment Model.....	31
Figure 9. East-North view of Sensor 1 and Sensor 2 Flight Profiles	33
Figure 10. True Environment Bomb Altitude	34
Figure 11. Environment Receiver Clock model.....	37
Figure 12. Multipath Error Example for Sensor 1	38
Figure 13. SAR Atmosphere error model (value is doubled for transmission & reception)	40
Figure 14. SAR/GMTI Environment Atmosphere Error	41
Figure 15. Performance evaluation of the Kalman filter.....	58
Figure 16. Error in Bomb Position –East	60
Figure 17. Error in Bomb Position – North.....	61
Figure 18. Error in Bomb Position – Up	62
Figure 19. Error in Target Position – East	63

Figure 20. Error in Target Position – North	64
Figure 21. Atmosphere scale factor of Sensor 1 to Target.....	65
Figure 22. Error in Target Acceleration – East	66
Figure 23. Case 1- East Error for Bomb-to-Target Vector	69
Figure 24. Case 1-North Error Bomb-to-Target.....	70
Figure 25. Case 1- Up Error Bomb-to-Target	71
Figure 26. Case 2 - East Error Bomb-to-Target	81
Figure 27. Case 2- North Error Bomb-to-Target.....	82
Figure 28. Case 2- Up Error Bomb-to-Target	83
Figure 29. Case 3- East Error Bomb-to-Target	84
Figure 30. Case 3- North Error Bomb-to-Target.....	85
Figure 31. Case 3- Up Error Bomb-to-Target	86
Figure 32. Case 4- East Error Bomb-to-Target	87
Figure 33. Case 4- North Error Bomb-to-Target.....	88
Figure 34. Case 4- Up Error Bomb-to-Target	89
Figure 35. Case 5 – East Error Bomb-to-Target	90
Figure 36. Case 5 – North Error Bomb-to-Target.....	91
Figure 37. Case 5 – Up Error Bomb-to-Target	92
Figure 38. Case 6 – East Error Bomb-to-Target	93
Figure 39. Case 6 – North Error Bomb-to-Target.....	94
Figure 40. Case 6 – Up Error Bomb-to-Target	95
Figure 41. Case 7 – East Error Bomb-to-Target	96
Figure 42. Case 7 – North Error Bomb-to-Target.....	97

Figure 43. Case 7 – Up Error Bomb-to-Target	98
Figure 44. Case 8 – East Error Bomb-to-Target	99
Figure 45. Case 8 – North Error Bomb-to-Target	100
Figure 46. Case 8 – Up Error Bomb-to-Target	101
Figure 47. Case 9 – East Error Bomb-to-Target	102
Figure 48. Case 9 – North Error Bomb-to-Target	103
Figure 49. Case 9 – Up Error Bomb-to-Target	104
Figure 50. Case 10 – East Error Bomb-to-Target	105
Figure 51. Case 10 – North Error Bomb-to-Target	106
Figure 52. Case 10 – Up Error Bomb-to-Target	107
Figure 53. Case 11 – East Error Bomb-to-Target	108
Figure 54. Case 11 – North Error Bomb-to-Target	109
Figure 55. Case 11 – Up Error Bomb-to-Target	110
Figure 56. Case 12 – East Error Bomb-to-Target	111
Figure 57. Case 12 – North Error Bomb-to-Target	112
Figure 58. Case 12 – Up Error Bomb-to-Target	113

List of Tables

	Page
Table 1. DGPS Effect on GPS Errors	23
Table 2. Racetrack shape of Sensor 1 and 2.....	33
Table 3. Summary of Environment Measurements and Errors	42
Table 4. Filter Model States	43
Table 5. Case Descriptions.....	68
Table 6. All-in-view Satellite Cases (1-4).....	72
Table 7. Limited (-2) Satellite Cases (5-8).....	74
Table 8. Limited (only 4) Satellite Cases (9-12).....	74
Table 9. All Cases Summary.....	75

Abstract

The Affordable Moving Surface Target Engagement (AMSTE) project attempts to develop affordable solutions to the precise moving target surface target engagement problem. Up to this point, most of the error analysis performed for the AMSTE project has been at the error variance level, generating root-sum-square (RSS) total errors from error budgets consisting of constant error variances. In reality, the level of error for both Global Positioning System (GPS) positioning and radar targeting systems is highly dependent upon the given situation (such as the distance between sensor and target, the altitude differences, etc.)

This research generates a more comprehensive model of the GPS errors based upon the underlying physics of the situation. It focuses on differential tropospheric errors and multipath, as these are the primary error source in a differential GPS targeting system.

In addition to the error model development, a code-based differential GPS and differential ranging approach is implemented in simulation using a Kalman filter. This approach uses GPS measurements collected by each of the sensors and the weapon, and it uses ranging measurements from the sensors to the bomb and the target. Multiple cases are run varying 1) the number of GPS satellite measurements tracked by each receiver, 2) whether or not the common GPS errors are estimated, and 3) whether or not the bomb is tracked with the same radar sensors that are tracking the target. The horizontal DRMS position error during the terminal phase of the bomb trajectory drops from about 6 meters to about 3.5 meters.

USING GPS AS A REFERENCE SYSTEM TO HIT A MOVING TARGET

1. Introduction

Over time, the method of damaging an enemy's surface infrastructure or hardware has changed dramatically. In the earliest days of cannons, two or three test shots were required to determine the range to the targets. Environmental and technical factors such as weather and poor targeting repeatability made the firing of cannons a guessing game. In today's warfighter environment, the ability to engage and destroy fixed or stationary surface targets has been honed due to modern technology. As adversaries begin to adopt mobility as a means of survival, an affordable and precise moving surface target engagement capability will be necessary. Currently the use of precise guided munitions (PGMs) using laser-guidance with a "man-in-the-loop" has some benefits for mobile targeting [44]. In the effort to redefine close air support (CAS), there is the desire to have the ability to transmit updated information about moving targets to a weapon in flight [41]. The Affordable Moving Surface Target Engagement (AMSTE) program's goal is to provide such a capability.

In the development of any network or weapon system, there is a need to model expected errors. To this point, most of the error analysis performed for the AMSTE program has been at the error variance level, generating root-sum-square (RSS) total errors from error budgets consisting of constant error variances. In reality, the level of error for GPS positioning and targeting systems is highly dependent upon the current

environment in which it is employed (i.e., distance between sensor and target, altitude, time of day, etc.)

The purpose of this study is to generate more comprehensive models, primarily of the GPS errors, and look at the sensor errors, based upon the underlying physics of the situation. Differential tropospheric and multipath errors will be the focus, since these are the primary error sources for a differential GPS targeting system to be employed by the AMSTE program.

1.1. Background

In this section, the Global Positioning System (GPS) will be briefly covered. Additionally, the purpose and goals of the AMSTE program will be discussed.

1.1.1. Global Positioning System Overview

The Global Positioning System (GPS) is a satellite-based radio-navigation system established by the U.S. Department of Defense for military positioning applications and, as a by-product, it is also serving the civilian community. The system provides accurate, continuous, worldwide, three-dimensional position, velocity, and time information to users with the appropriate receiving equipment.

GPS is broken into three segments: the space segment, the control segment and the user segment. The space segment is the constellation nominally consisting of 24 satellites arranged in 6 orbital planes with 4 satellites per plane. Each satellite orbit has a period of approximately 12 hours and a 55° inclination angle with respect to the equatorial plane. The control segment is a worldwide ground control/monitoring network monitoring the health and status of the satellites. These monitor stations measure signals

from the satellites (SVs) that are incorporated into orbital models for each satellite. The models compute precise orbital data (ephemeris) and SV clock corrections for each satellite. The Master Control Station uploads ephemeris and clock data to the SVs. The Master Control facility is located at Schriever Air Force Base in Colorado. The third segment is the user segment. This consists of all GPS receivers. The receivers convert the satellite signals into position, velocity, and time estimates [19].

Currently, the satellites transmit two carrier signals. The L1 frequency (1575.42 MHz) carries the navigation message, Coarse Acquisition code (C/A code), and Precise code (P-Code) signals. This frequency is available to civil users as the Standard Positioning Service (SPS). The L2 frequency is modulated by the P-Code. Authorized users with cryptographic equipment and keys along with specially equipped receivers use the L2 frequency, part of the Precise Positioning Service (PPS).

The navigation message is a 50 Hz signal consisting of data bits that describe parameters such as the GPS week, range accuracy prediction, satellite health, clock corrections, and broadcast ephemerides. The C/A code is a repeating 1.023 MHz Pseudo Random Noise (PRN) Code. This “noise-like” code spreads the spectrum over approximately a 1MHz bandwidth. It repeats every 1023 bits (one millisecond). Each satellite has its own unique PRN code. The C/A code on the L1 carrier is the basis for the civil SPS. The P-Code is a very long (seven days) 10.23 MHz PRN code. In the Anti-Spoofing (AS) mode of operation, the P-Code is encrypted into the Y-Code. The encrypted Y-Code requires a classified AS Module for each receiver channel. This is for use only by authorized users with cryptographic keys. This P (Y)-Code is the basis for the PPS. Navigating by the pseudo-ranges can be described in Figure1.

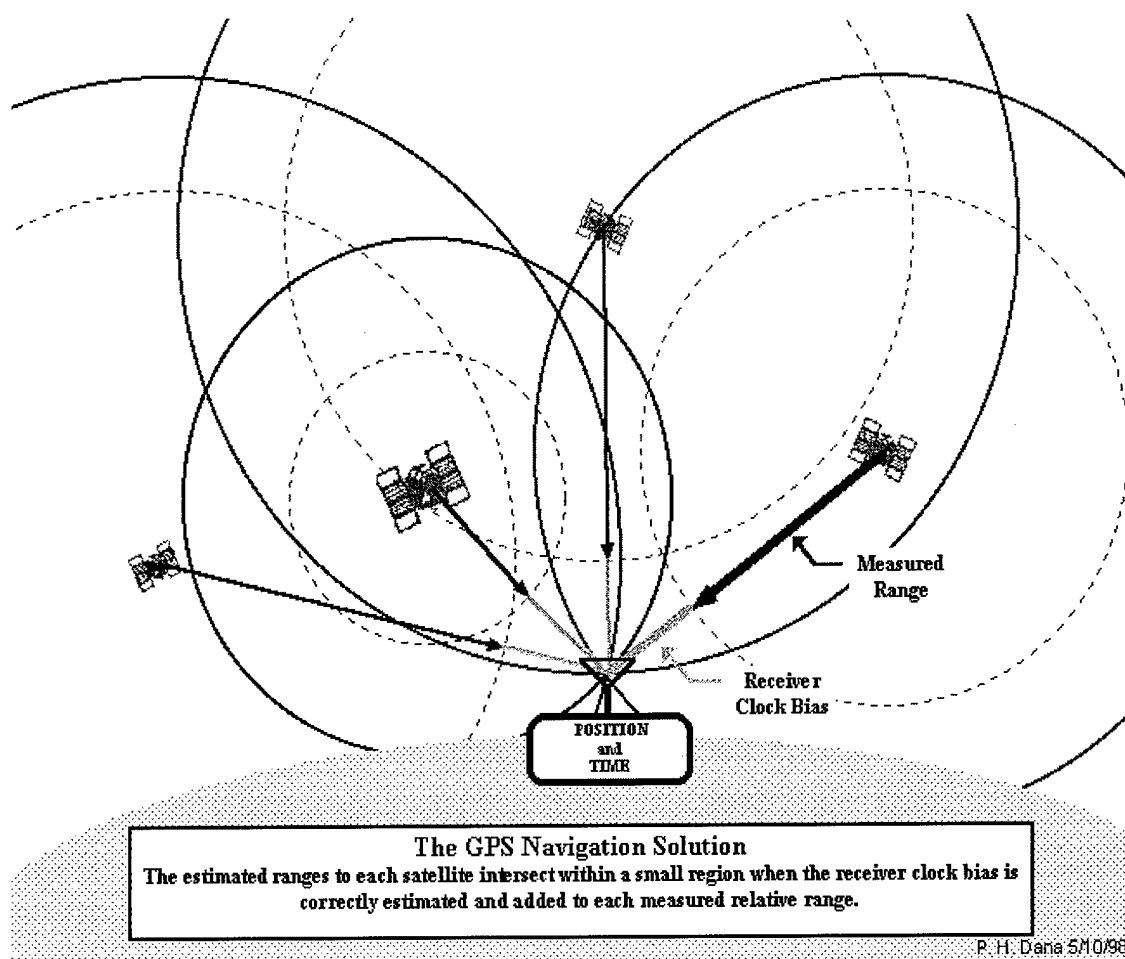


Figure 1. Illustrated Description of GPS Navigation Solution [9]

The position of the receiver is where the pseudo-ranges from a set of satellites intersect. It is determined from multiple pseudo-range measurements at a single measurement epoch. The pseudorange measurements are used together with satellite position estimates based on the ephemeris data sent by the satellites. This orbital data allows the receiver to compute the satellites' positions in three dimensions the instant they sent their respective signals. A minimum of four satellites is required to determine the three position dimensions and time. Time is used to correct the offset in the receiver clock, allowing receiver clocks to be less expensive and less accurate. Using five or

more satellites provides redundancy, greater fix certainty, and can allow detection of out-of-tolerance signals [9].

1.1.2. AMSTE Program

Existing technology (e.g., sensors, communications, and weaponry) supports moving surface target engagement, but generally requires sophisticated seeker systems, humans-in-the-loop, or dispersive area-effect munitions [43]. These approaches can result in expensive weapon systems, high risk to human life, and the potential for collateral damage to unintended vehicles[43]. The goal of the AMSTE program is to develop and demonstrate a new strike capability: the ability to target moving surface threats from long range and to engage rapidly those threats with precision, stand-off weapons. This capability will ultimately enable a robust, dynamically-controlled system to engage multiple dispersed mobile targets accurately in complex traffic and all weather conditions [6]. The key areas are described as:

- Dynamic - contains the inherent flexibility to create a custom solution for each engagement
- Robust - degrades gracefully with dynamic changes
- Accurate - provides precision tracking and weapon guidance to destroy the moving or stationary target of interest
- Multiple - has the ability to plan, maintain track, and conduct parallel engagements
- Dispersed - has flexibility to operate over an entire theater
- Mobile targets - robust to target move-stop-move behavior cycles
- Complex traffic – maintains target track in dense background traffic environment

- All weather - provides a targeting solution in any weather condition

The AMSTE program investigates the concept of leveraging recent advances in sensor technology to provide an affordable solution to precise moving surface target engagement [1]. The fundamental concept investigated is to use a network of ground moving target indicating (GMTI) radar and synthetic aperture radar (SAR) systems to provide a precision fire control tracking solution on moving and intermittent surface targets. These sensors provide all-weather capability, and the use of multiple GMTI sensors provides the required precision targeting and will be provided to update low-cost, precision guided munitions in-flight for precise engagement of a moving surface target [2].

Current studies have shown that obtaining the required level of accuracy is possible with expected advancements [11]. The real challenge is maintaining a precise estimate of the location of the target [1].

1.2. Problem Statement

The problem for this research are to 1) identify GPS errors that are significant for the AMSTE program, and 2) determine, through simulation, the effects of GPS and radar errors on the navigation solution, for a variety of implementation schemes. Additionally, the simulation results will be used to demonstrate the benefit of tracking both the munition and target with the same sensor.

1.3. Scope

Although the AMSTE program has a vested interest in the development and accuracies of the GMTI/SAR sensors, this thesis focuses on GPS and its contributing

errors. The GMTI/SAR sensors will be modeled using a fairly straightforward range/range-rate representation, as described in Chapter 3.

1.3.1. Assumptions

Typical of any simulation, assumptions are made in this thesis to reduce the complexity of the development, design, and analysis of the GPS-based system environment model and Kalman filter simulations.

1. *There is only one target that will be in view of the system sensors throughout the scenario.*
2. *While start and stopping and hiding in the terrain (e.g. forests, mountains) would be an excellent ploy to counteract a moving target system, this thesis limits the target to an environment similar to a desert where the vehicle will *always be moving.**
3. *The location of the Kalman filter processing is not a concern, and the data from all sensors is sent without computation or transmission delays.*
4. *Minimizing the error in the relative distance between munition and target is the focus.* The absolute position of the munition and the target is not critical.
5. *The receivers on the platforms and munition are all identical.* While each receiver will have different multipath and receiver noise, they are the same type, so their clocks will be modeled with the same error parameters.
6. *Only GPS pseudorange measurements will be used.* While using carrier smoothed or phase measurements would lead to more accurate results, these procedures are outside the scope of this thesis.

7. *Dual frequency receivers will be used.* This neglects the ionosphere error which will be discussed in Chapter 2.
8. Except for measurement noise, *the GMTI/SAR sensors are identical.*

1.4. Methodology

The premise of this thesis lies in the modeling and building of a true environment model and a system upon which a Kalman filter is to be based. The environment will be built using the true ranges and rates of all the satellites, platforms, munition and target. Appropriate errors will be added to the true ranges and rates to generate simulated measurements. These simulated measurements will be used by the algorithm, which is essentially a Kalman filter, to estimate the position and velocities of the sensors, bomb, and target.

2. Background

2.1. Overview

This chapter provides background that is needed to understand the true environment model and system Kalman filter. It will describe differential GPS, the errors associated with the GPS system, how differential GPS affects those errors, and errors related to SAR range and range rate. The chapter closes by describing the basis of the extended Kalman Filter.

2.2. Differential GPS (DGPS)

The differential GPS concept is used to enhance standalone GPS accuracy by removing common or correlated errors from two or more receivers viewing the same satellites. Figure 2 gives a graphical representation of DGPS.

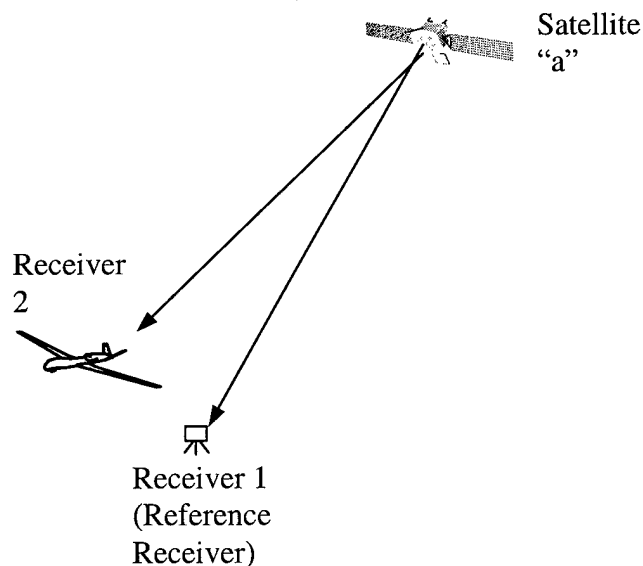


Figure 2. Differential GPS Concept

In the basic form of DGPS, one of these receivers is called the reference receiver. This receiver's precise position is known. Because of this, it can determine the errors in the pseudorange measurement from each satellite in view by subtracting the pseudorange from the satellite-to-reference station geometric range. Some of these errors would be common to other nearby receivers (atmospheric delays, satellite clock). The reference station would then send out those errors, called differential corrections, to the mobile receiver which subtracts these common errors from their pseudoranges. This results in a more accurate position solution, on the order of 1-4m (1σ) with a code-only solution [19, 30, 43].

There are many different ways to implement DGPS, leading to different levels of accuracy. As mentioned above, using code-only measurements (the easiest to implement) has an accuracy of 1-4m (1σ). Carrier-smoothed code, which combines the carrier-phase precision with the code absolute (but noisy) measurement, can have an accuracy of 0.1-0.5 m (1σ) [30, 34]. A third technique is to use the carrier-phase measurement and resolve the carrier-phase integer ambiguities. While carrier-phase ambiguity resolution yields an accuracy on the centimeter level (1σ), carrier-phase is the most difficult to implement because of the need to determine the integer ambiguity in the measurement [19, 21, 30].

For this study, only code (i.e., pseudorange) measurements are used. There are a few benefits to using code measurements: 1) military receivers generally only give pseudorange measurements, and 2) it is the best place to start because it is the simplest form and easy to implement.

2.3. GPS Errors

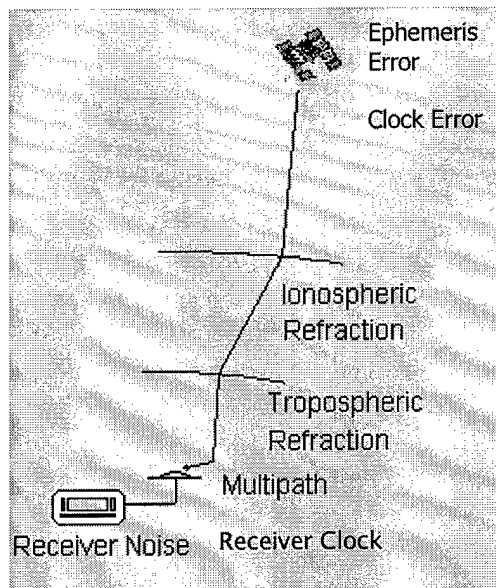


Figure 3. GPS Errors [12]

Figure 3 shows some of the GPS errors that affect the signal from the satellite to the receiver. GPS errors are usually classified into three areas: satellite, atmospheric, and receiver errors. These errors along with the true range between the satellite and receiver make up the pseudorange, as shown in the following equation:

$$\rho = r + c(\delta t_u - \delta t_{sv} + \delta t_{trop} + \delta t_{iono} + \delta t_{noise} + \delta t_{mp}) \quad (2-1)$$

where:

- r = geometric range
- c = speed of light
- δt_u = receiver clock error
- δt_{sv} = satellite clock error
- δt_{eph} = error due to broadcast ephemeris
- δt_{trop} = delay due to the troposphere
- δt_{iono} = delay due to the ionosphere
- δt_{noise} = receiver noise
- δt_{mp} = multipath error

Each of these errors will now be discussed in detail.

2.4. Satellite Errors

There are two errors associated with the satellite. These are satellite clock and satellite ephemeris errors.

2.4.1. Satellite Clock (δt_{sv})

GPS satellites use atomic clocks to control the onboard timing operations, including the generation of the broadcast signal. Atomic clocks, which are typically cesium or rubidium, are inherently stable. Nevertheless, they do drift, and over time the δt can be as big as 1msec [19]. This can translate up to a 300-km pseudorange error. Clock correction parameters are sent in the navigation message and are implemented by the receiver to produce estimates of the actual clock errors. The correction parameters are implemented by the receiver using the following second-order polynomial:

$$\delta t = a_{fo} + a_{f1}(t - t_{oc}) + a_{f2}(t - t_{oc})^2 + \Delta t_r \quad (2-2)$$

where

- a_{fo} = clock bias
- a_{f1} = clock drift
- a_{f2} = frequency drift
- t_{oc} = clock data reference time
- t = current time epoch
- Δt_r = correction due to relativistic effects

Although the clock error estimate removes most of the error, some residual error remains, and this residual error is what contributes to ranging errors in the pseudorange measurements. The resulting ranging errors induced by the satellite clock are typically on the order of 3.0m (1σ)[19].

2.4.2. Ephemeris Errors (δt_{eph})

Ephemeris errors result when the GPS message does not transmit the correct satellite location. Estimates of ephemerides, as in the clock corrections, are uplinked to the satellite and broadcast in the navigation message. Typically, the radial component of this error is the smallest. The tangential and cross-track errors may be larger by an order of magnitude. Fortunately, the larger components do not affect ranging accuracy to the same degree as the radial component [36]. Generally, the ephemeris errors result in a 3m (1σ) in the pseudorange [30]. However if post-processing is an option, precise ephemeris data can be used. Precise orbits of the satellites are calculated using days of data from hundreds of reference stations. Precise orbits are available from various sources (such as National Geodetic Survey), and they are typically accurate to within 6 cm (1σ) [30].

2.5. Atmospheric Errors

If a vacuum existed between the satellites and the receiver, there would not be any error due to the propagation of the signal. The atmosphere, however, affects the transmission and the reception of the signal. The effects of the ionosphere and the troposphere are normally treated as separate errors.

2.5.1. Ionosphere (δt_{iono})

The ionosphere is the part of the atmosphere consisting of free electrons that ranges from approximately 50km to 1000km above the surface of the Earth [19,22, 36]. It is a result of the ultraviolet radiation from the sun splitting the atmospheric molecules into ions and free electrons. The density of these electrons determines the magnitude of effect on the GPS signal. Electron density is normally quantified by counting the number of

electrons in a vertical column with a cross-sectional area of 1m^2 . This is called the Total Electron Content (TEC). Figure 4 gives an illustration of the TEC [34].

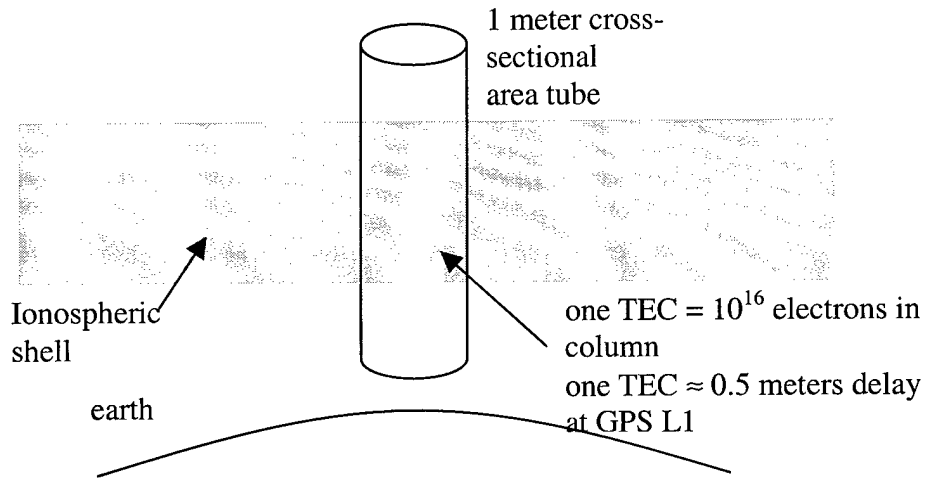


Figure 4. Ionosphere Total Electron Content (TEC) Unit.

TEC (units of electrons/ m^2) varies with time of day, user location, satellite elevation angle, season, ionizing flux, magnetic activity, sunspot cycle, and scintillation [19].

The amount of delay of the group (pseudorange) can be expressed as:

$$\Delta S_{iono,g} = \frac{40.3 \text{ TEC}}{f^2} \quad (2-3)$$

where

$$\begin{aligned} \Delta S_{iono,g} &= \text{group (pseudorange) delay (m)} \\ f &= \text{carrier frequency (L1 or L2 for GPS)} \end{aligned}$$

The delay of the carrier-phase delay is

$$\Delta S_{iono,p} = -\frac{40.3 \text{ TEC}}{f^2} \quad (2-4)$$

The ionosphere advances the carrier-phase by the same magnitude of the group delay.

Due to this, a dual frequency receiver can estimate the ionospheric delay and remove it.

The L1 ionospheric delay is calculated by

$$\Delta S_{iono,corr_{L1}} = \left(\frac{f_2^2}{f_2^2 - f_1^2} \right) (\rho_{L1} - \rho_{L2}) \quad (2-5)$$

where

$$\begin{aligned} \Delta S_{iono,corr_{L1}} &= \text{L1 ionospheric delay (m)} \\ f_1, f_2 &= \text{L1 and L2 carrier frequencies} \\ \rho_{L1}, \rho_{L2} &= \text{L1 and L2 pseudorange measurements} \end{aligned}$$

The L2 delay can be calculated by

$$\Delta S_{iono,corr_{L2}} = \left(\frac{f_1}{f_2} \right)^2 \Delta S_{iono,corr_{L1}} \quad (2-6)$$

While applying these ΔS delay terms completely removes the ionospheric error, multipath and noise are still present, adding some additional error [19,30]. For this thesis, it is assumed that dual frequency receivers have removed the ionospheric delay.

2.5.2. *Troposphere* (δt_{trop})

The troposphere is the atmosphere that extends from the ground to approximately 10 km above [19, 47,48]. Unlike ionosphere, the tropospheric delay is not frequency dependent. Within the range of the GPS frequencies, the troposphere delays both the code and carrier observations. This delay is dependent on the tropospheric refractive index, which is a function of the local temperature, pressure, and relative humidity.

The tropospheric effect can be divided into a hydrostatic (dry) delay and a wet delay. The hydrostatic delay, which is the larger effect (90 to 95% of the total refraction), is caused primarily by N_2 and O_2 molecules [36]. The hydrostatic delay at zenith (i.e., straight up) is normally around 2.3m, and it varies with local temperature and atmospheric pressure in a reasonably predictable manner [36, 47]. Due to its

predictability, it can be modeled and removed with an accuracy of a few millimeters or better using a surface model (including pressure, temperature, and humidity) [47].

The second part, the wet delay, is generally smaller, with delays of 1-80 cm at zenith (depending on humidity levels) [36]. However, since the wet component can vary 10-20% in a few hours [36], it is more difficult to model and remove based on standard tropospheric models using surface measurements [36,47]. The residual tropospheric delay remaining after the applied model is mostly due to the wet component.

The troposphere delay can be expressed as

$$\Delta S_{tropo} = \int (n - 1) ds \quad (2-7)$$

or

$$\Delta S_{tropo} = 10^{-6} \int N ds \quad (2-8)$$

where

- n = index of refraction
- N = refractivity

The refractivity N can be divided into hydrostatic and wet components. Hence the above equation can be written as

$$\Delta S_{tropo} = 10^{-6} \int N_{Hydro} ds + 10^{-6} \int N_{Wet} ds \quad (2-9)$$

or symbolically,

$$d_{tropo} = d_{Hydro} + d_{Wet} \quad (2-10)$$

where

- d_{tropo} = total tropospheric delay
- d_{Hydro} = hydrostatic delay
- d_{Wet} = wet delay

Propagation delays at various elevation angles are determined from the zenith delays and mapping functions. As the zenith delay can be expressed as the sum of the hydrostatic and wet components, mapping functions can be developed in order to map separately the hydrostatic and wet components [48]. In general the tropospheric delay is represented as

$$d_{tropo} = d_{Hydro}^Z \times m_{Hydro}(\varepsilon) + d_{Wet}^Z \times m_{Wet}(\varepsilon) \quad (2-11)$$

where

- d_{Hydro}^Z = hydrostatic zenith delay
- d_{Wet}^Z = wet zenith delay
- $m_{Hydro}(\varepsilon)$ = hydrostatic mapping function
- $m_{Wet}(\varepsilon)$ = wet mapping function
- ε = elevation angle

Much research has gone into the creation and testing of tropospheric models to compute the refractivity N along the path of signal travel [8,10,27,33,35,47,48]. The various tropospheric models differ primarily with respect to the assumptions made regarding the vertical refractivity profiles and the mapping of the vertical delay with elevation angles [56]. Even though a tropospheric model removes most of the error, there is almost always a residual unmodeled error.

While there are many suitable models available, this research, employed the modified Hopfield model because it has proven to be a reliable model for a wide variety of environments. The thorough explanation of this model is available in [56].

2.6. Receiver Errors

While there are various types and models of receivers, all are affected by receiver clock errors, multipath errors, and receiver noise. Each of these receiver-based errors will be described in the sections that follow.

2.6.1. Receiver Clock (δt_u)

Similar to satellite clock errors, receiver clock error is caused by the inaccuracies in the receiver clock. However unlike the satellite clocks, which use atomic oscillators, the receivers typically use quartz crystals, which have much worse long-term frequency stability. Due to this poor stability, receiver clock errors are typically large, but this error is explicitly estimated as part of the navigation solution.

2.6.2. Multipath (δt_{mp})

Multipath, the phenomena whereby a signal travels from a transmitter to a receiver via multiple paths, is due to reflection and diffraction. It is a major source of error remaining when using differential GPS, because it is uncorrelated between receivers, so it does not cancel out [4,15, 28,32,35]. It distorts the signal modulation (code) and degrades accuracy in conventional and differential systems. Multipath also distorts the phase of the carrier and hence degrades the accuracy of the carrier-phase-based systems [3,4]. Additionally, because carrier-phase algorithms often employ pseudorange measurements for initialization (ambiguity resolution) purposes, multipath contamination of the pseudorange can increase the time required for initialization [3,4]. Multipath-induced errors are more difficult to quantify, because they are a function of the environment in which the particular GPS receiver is operating, as well as the receiver design [3,4].

Multipath has been the subject of much research and can be characterized by four basic parameters:

δ : the relative time delay between the direct and reflected signals

α : the amplitude of the multipath signal relative to that of the direct signal

φ : the phase of the multipath signal relative to that of the direct signal

$\dot{\varphi}$: the rate of change of the phase of the multipath signal relative to that of the direct signal

Figure 5 gives an illustration of the relationship between the relative phase and delay of multipath and the resultant range error.

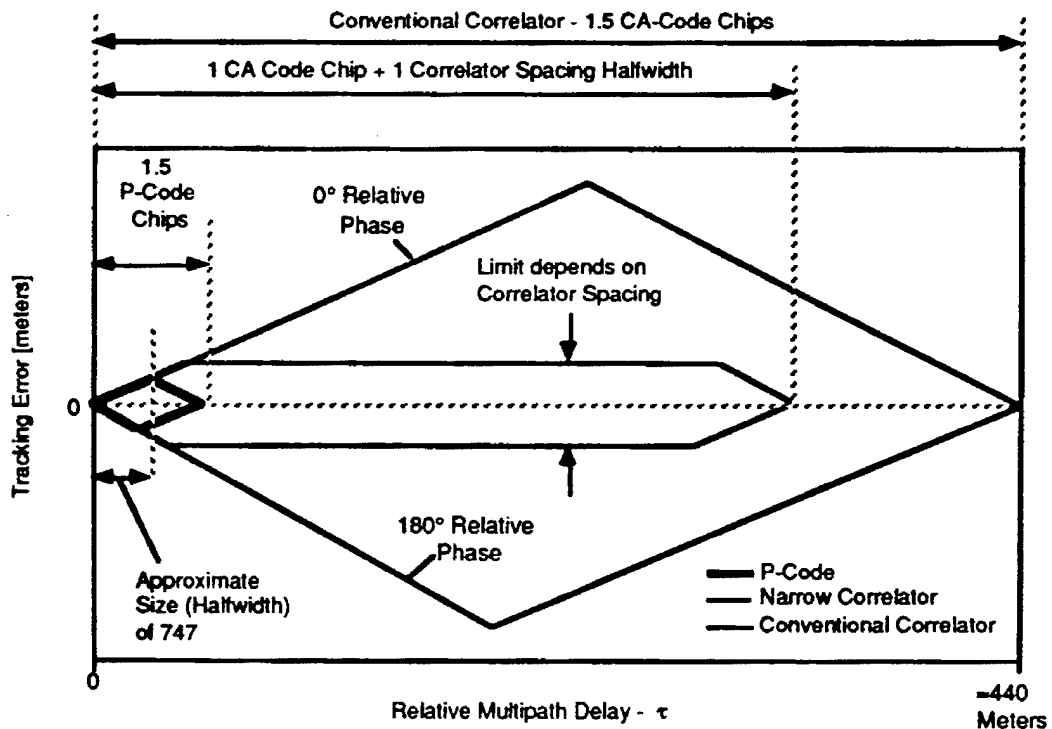


Figure 5. Multipath-Induced Error as a Function of Relative Delay and Phase of Multipath [35].

The theoretical basis for Figure 5 is well developed in [4]. The nature of the spread-spectrum GPS signal causes multipath delayed by more than 1.5 chips to be rejected. However, multipath with shorter delays may cause ranging errors. The value of the error due to multipath can be either positive or negative, depending on the phase of the multipath relative to that of the direct signal. The amplitude and shape of the error envelope depends on the relative amplitude of the multipath signal. As the amplitude of the multipath increases, the error bounds in Figure 5 grow larger, and the error envelope becomes increasingly asymmetrical. Therefore, the magnitude of the ranging error due to multipath is a function of δ , α , and φ . The spectral characteristics of the multipath error are dependent on $\dot{\varphi}$ [28].

For this thesis, the focus of multipath is its effect on the airborne platforms and the munition. On airborne platforms, the relative delay δ is limited by the size of the airplane. By limiting δ , the magnitude of the multipath ranging error is also limited. A study of multipath delay on Boeing 777, 747-400 and 737 aircraft showed a 20 to 60 cm 1- σ ranging error using pseudorange measurements [28].

To determine the effects of multipath on a munition, a study on multipath effects on a satellite is used as a point of comparison. This is due to the similarity in the amount of surface area in which a signal could reflect off and enters the antenna as delay. A study by Godet found that the error range in differential phase measurements to be in the millimeter range [15]. As forementioned, this thesis does not use phase measurements. However, due to the very small limit on the amount of delay possible from a reflected

signal on a munition, code multipath is expected to be on the order of 10 cm or less for falling munitions [5].

Another factor in munition multipath is the ground. As an airplane (or munition) approaches the ground, the geometry between the airplane, the satellite, and any multipath sources on the ground is changing rapidly. Hence the relative phase, φ , and the relative time delay, δ , are likewise changing rapidly. As the phase continually changes, the multipath-induced error changes rapidly from negative to positive, making it appear noise-like in appearance when periodically sampled [28]. Smoothing the code measurements with the carrier-phase measurement can reduce this multipath.

Multipath is generally worse for fixed receivers, such as DGPS ground stations. Depending on the ground environment (location of obstacles from which signals can reflect), antenna location, and receiver type, multipath errors could be anywhere from 0 to 5 meters [5]. Since this research does not use a ground reference station, this level of multipath error is not a concern.

2.6.3. Measurement Noise (δt_{noise})

Measurement or receiver noise errors are due to the measurement processes used within the receiver. These include the design of the antenna, the method used for the analog to digital conversion, the correlation processes, and the tracking loops and bandwidths [36]. Similar to the multipath, the level is dependent on the signal that is tracked. The C/A code measurement noise will be approximately one order of magnitude greater than P-code measurements. One-sigma values are usually on the order of 1.5m for the C/A code and 20 cm on the P-code [19]. The measurement noise due to carrier-phase is usually between 1.2mm and 1.6 mm [30,31]. These errors are uncorrelated, and they are typically modeled as pure white noise.

2.7. DGPS Effect on GPS Errors

Using DGPS is known to produce more accurate solutions than stand-alone GPS. While DGPS may reduce or remove some common errors, it can also cause some errors to be added or even amplified.

Figure 6 shows a typical DGPS setup, where $Meas_1$ is the measurement from the satellite to the reference receiver and $Meas_2$ is the measurement from the satellite to receiver 2.

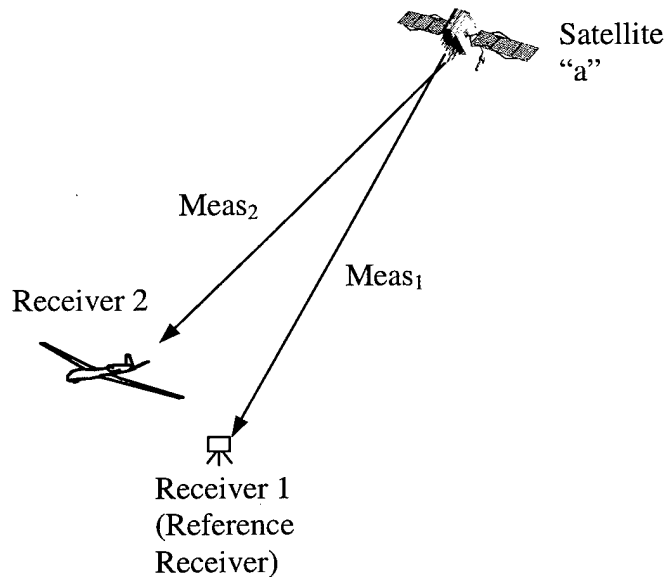


Figure 6. DGPS Concept

The comparison between the measurements and the DGPS effect on the error are found in Table 1[30].

Table 1. DGPS Effect on GPS Errors

Error Type	Comparison between Meas ₁ and Meas ₂	DGPS Effect on Error
Satellite clock error	Same	Removed
Receiver clock error	Different (uncorrelated)	Added
Ephemeris error ¹	Very similar ²	Reduced ²
Ionospheric delay	Very similar ²	Reduced ²
Tropospheric delay	Very similar ²	Reduced ²
Multipath	Different (uncorrelated)	Added (and amplified)
Measurement noise	Different (uncorrelated)	Added (and amplified)

¹Effect of ephemeris error on positioning (actually only affects the calculated range, not the actual measurement)

²Errors grow as the separation distance between receivers 1 and 2 increases. (The errors are the same and are removed for very short baselines distances)

The satellite clock error is cancelled. Differential ephemeris, ionospheric, and tropospheric errors are based upon the distance between the two receivers. At a close range, the differential errors are reduced because of the correlation between the errors, but as the distance grows, the amount of error slowly increases. Multipath and the measurement noise are uncorrelated errors, so they do not cancel. In fact not only are the errors summed, but also they are amplified by the double difference.

2.8. Synthetic Aperture Radar/Ground Moving Target Indicator

Synthetic Aperture Radar (SAR) produces high-resolution images of surface areas and has the ability to operate in all-weather conditions. SAR can be used on many different platforms, including airplanes, the Space Shuttle, and satellites [38]. Because radar imagery resolution is a function of the radar sensor's aperture, a larger aperture produces higher resolution imagery. A SAR uses the motion of the airborne platform to synthesize a large aperture antenna from the true, smaller aperture antenna. Typical SAR sensors provide two modes of operation: search and spotlight. In search mode, a SAR will radiate a swath of land providing a large area (and usually lower resolution) image.

In spotlight mode, the SAR radiates a smaller area multiple times producing a higher resolution image. Figure 7 shows a SAR mission with both search and spotlight mode. A SAR utilizes typical radar techniques by measuring the time between the transmission and reception of a SAR signal [23].

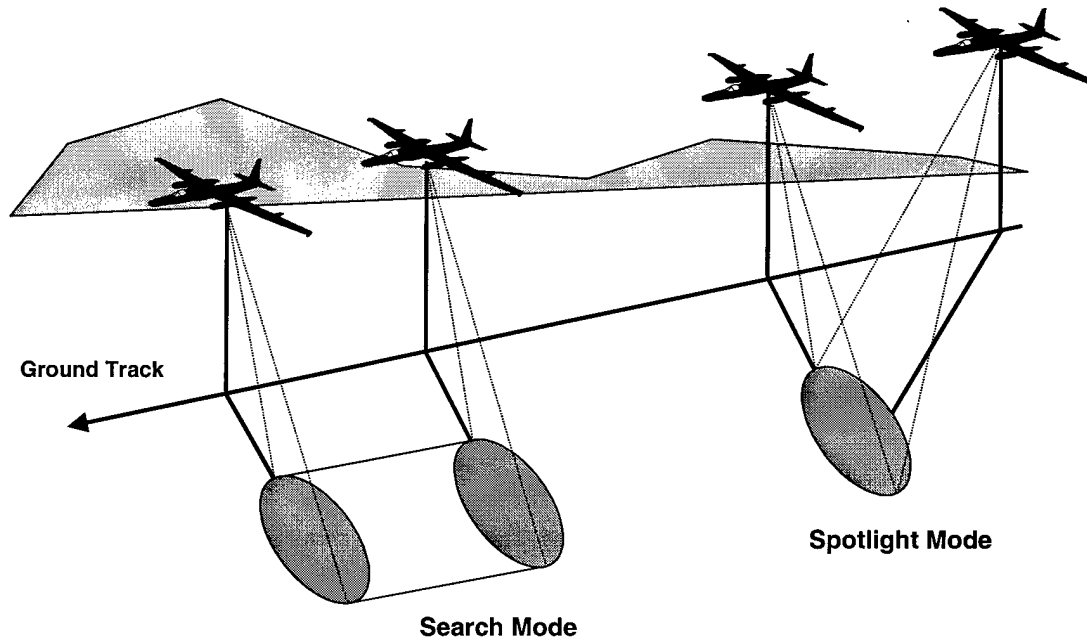


Figure 7. Synthetic Aperture Radar Techniques[46]

SAR targets are typically stationary. However, the Ground Moving Target Indicator (GMTI) is a radar mode that can pickup moving targets. The radar returns echoes from moving vehicles on the ground are separated from the ground clutter on the basis of their Doppler frequencies [6].

2.8.1. SAR Errors

For this research, the measurements received from the SAR are assumed to be a range and range rate. In early AMSTE studies, SAR measurements were range and range rates

[6]. The errors for the range can occur as a bias and/or a noise, where biases have a long correlation time and noises have a short correlation time.

Some bias-like range errors include range clock, and atmospheric refraction [23].

Range measurements are made by measuring the time difference between the transmitted pulse and its return. Consequently, any error found in the clock rate will result in a range measurement error [23]. In general, a clock runs either slightly fast or slightly slow with very slowly changing variations in the rate [23]. Given the assumption of no time latency in this thesis, this effect goes away. The atmospheric refraction error is similar to the troposphere error in GPS. It is a function of how the particles in the air affect the path of the signal.

Noises on the range can include quantization errors and range timing errors. The quantization errors result from resolution errors. The range timing error results from the time delay needed to perform SAR processing. Both of these errors are modeled as white noise.

The range rate errors are primarily noise-like in character. The radar's receiver noise and internal motion resolution errors can add various levels of error. Calibration, if it is not precise, can add a bias-like error to the range rate. More quantitative details of SAR errors are given in Chapter 3.

2.9. *System Kalman Filter*

The Kalman filter is an optimal recursive data processing algorithm [25,26]. The filter is optimal referring that the entire history of measurements available to the filter is processed and incorporated as information in the form of dynamics model, measurement model, and statistical descriptions of noises and uncertainties. The filter is recursive in

that the filter does not require all of the previous data to be kept in storage and reprocessed every time a new measurement becomes available. The Kalman filter processes all available measurements of interest, regardless of their accuracy, based on knowledge of the system and measurement dynamics, the statistical description of the system noises, measurement errors, and model uncertainties [25,26]. The models may be linear, in certain cases, but most system models are nonlinear in nature. For nonlinear system models, the extended Kalman filter (EKF) is implemented. The extended Kalman Filter is not “optimal,” but only a first-order approximation to the (infeasible, infinite-dimensional) optimal non-linear filter [25,26]. The EKF linearizes the nonlinear system model about a nominal point in the trajectory, utilizing the linear assumptions and equations described in the following sections. During operation, an EKF is relinearized based on the most current optimal estimate of the variable of interest.

2.9.1. State and Measurement Model Equations

In developing the Extended Kalman filter for this research, let the system model be defined as a state equation in the following form in Equation (2-12),

$$\mathbf{x}(t_i) = \Phi(t_i, t_{i-1})\mathbf{x}(t_{i-1}) + \mathbf{G}_d(t_{i-1})\mathbf{w}_d(t) \quad (2-12)$$

where

- $\mathbf{x}(t_i)$ = state vector at time t_i
- $\mathbf{x}(t_{i-1})$ = state vector at time t_{i-1}
- $\Phi(t_i, t_{i-1})$ = linear discrete state dynamics matrix
- $\mathbf{G}_d(t_{i-1})$ = noise distribution matrix (the identity matrix for this system)
- $\mathbf{w}_d(t)$ = white Gaussian noise with a mean value of zero and strength

$$E[\mathbf{w}_d(t)] = \mathbf{0} \quad (2-13)$$

$$E[\mathbf{w}_d(t_i)\mathbf{w}_d^T(t_j)] = \begin{cases} \mathbf{Q}_d(t_i) & \text{for } t_i = t_j \\ \mathbf{0} & \text{for } t_i \neq t_j \end{cases} \quad (2-14)$$

where

$$\mathbf{Q}_d(t_i) = \text{covariance of } \mathbf{w}_d(t_i)$$

The discrete time measurements, $\mathbf{z}(t_i)$, are modeled in Equation (2-15)

$$\mathbf{z}(t_i) = \mathbf{h}[\mathbf{x}(t_i), t_i] + \mathbf{v}(t_i) \quad (2-15)$$

where

$\mathbf{h}[\mathbf{x}(t_i), t_i]$ = nonlinear function of the state vector and time

$\mathbf{v}(t_i)$ = discrete time measurement noise vector with a zero-mean white noise process, which is independent of $\mathbf{w}(t_i)$, and having covariance $\mathbf{R}(t_i)$ defined by:

$$E[\mathbf{v}(t)] = \mathbf{0} \quad (2-16)$$

$$E[\mathbf{v}(t_i)\mathbf{v}^T(t_j)] = \begin{cases} \mathbf{R}(t_i) & \text{for } t_i = t_j \\ \mathbf{0} & \text{for } t_i \neq t_j \end{cases} \quad (2-17)$$

2.9.2. Measurement Model Linearization

Since the measurements are nonlinear, the EKF filter equations must be linearized to produce the prediction of the measurement vector $\mathbf{z}(t_i)$ before it arrives, to process a measurement update cycle of the filter. The linearization is performed by taking the partial derivative of $\mathbf{h}[\mathbf{x}(t_i), t_i]$ to produce $\mathbf{H}[\mathbf{x}_n(t_i), t_i]$

$$\mathbf{H}[t_i; \hat{\mathbf{x}}(t_i^-)] = \left. \frac{\delta \mathbf{h}[\mathbf{x}(t), t]}{\delta \mathbf{x}} \right|_{\mathbf{x}=\hat{\mathbf{x}}(t_i^-)} \quad (2-18)$$

Normally, if the true state trajectory differs from the desired state trajectory, large errors could occur. The EKF reduces this effect by allowing a relinearization about the most recent state estimate as shown in Equation (2-18), as opposed to the linearized Kalman filter which only uses the nominal state value. Using the EKF method allows for the declaration of a new nominal pre-computed trajectory (emanating from the most

recent state estimate) at every estimate. This ensures deviations from the nominal trajectory remains small as long as the error model stays accurate.

2.9.3. *Extended Kalman Filter Propagate and Update Equations*

This section addresses the EKF propagate and update equations implemented in this research effort. Equation (2-12) is the discrete-time dynamics model and Equation (2-15) is the discrete-time measurement model. As previously mentioned, a Kalman filter is a recursive algorithm. There are two steps involved in this recursion: propagation and update. The state estimate, $\hat{\mathbf{x}}(t)$, and the covariance of that estimate, $\mathbf{P}(t)$, are both propagated from the last time sample, t_{i-1} , and updated at every time, t_i . Sampled data EKF equations utilize the following notations:

t_i^- - value of a variable after propagation from t_{i-1} but just prior to a measurement update at time t_i .

t_i^+ - value of a variable after propagation from t_{i-1} and the measurement update at time t_i .

The subscript i is used to describe the discrete time points when measurements are available. Using these time notations, the state estimates $\hat{\mathbf{x}}(t_i^-)$ and covariance values $\mathbf{P}(t_i)$ are propagated from t_{i-1} to t_i using the following discrete equations:

$$\hat{\mathbf{x}}(t_i^-) = \Phi(t_i - t_{i-1})\hat{\mathbf{x}}(t_{i-1}^+) \quad (2-19)$$

$$\mathbf{P}(t_i^-) = \Phi(t_i - t_{i-1})\mathbf{P}(t_{i-1}^+)\Phi^T(t_i - t_{i-1}) + \mathbf{Q}_d \quad (2-20)$$

These equations are for time-invariant system model and stationary noise model. When discrete time measurements, \mathbf{z}_i , become available, the EKF update cycle is performed using the following equations:

$$\mathbf{K}(t_i) = \mathbf{P}(t_i^-) \mathbf{H}^T [t_i; \hat{\mathbf{x}}(t_i^-)] \{ \mathbf{H} [t_i; \hat{\mathbf{x}}(t_i^-)] \mathbf{P}(t_i^-) \mathbf{H}^T [t_i; \hat{\mathbf{x}}(t_i^-)] + \mathbf{R}(t_i) \}^{-1} \quad (2-21)$$

where

$\mathbf{K}(t_i)$ = Kalman Filter Gain

$$\hat{\mathbf{x}}(t_i^+) = \hat{\mathbf{x}}(t_i^-) + \mathbf{K}(t_i) \{ \mathbf{z}_i - \mathbf{h}[\hat{\mathbf{x}}(t_i^-), t_i] \} \quad (2-22)$$

$$\mathbf{P}(t_i^+) = (\mathbf{I} - \mathbf{K}(t_i) \mathbf{H} [t_i; \hat{\mathbf{x}}(t_i^-)]) \mathbf{P}(t_i^-) (\mathbf{I} - \mathbf{K}(t_i) \mathbf{H} [t_i; \hat{\mathbf{x}}(t_i^-)])^T + \mathbf{K}(t_i) \mathbf{R}(t_i) \mathbf{K}(t_i)^T \quad (2-23)$$

For more details and a complete derivation of the above equations, the reader is referred to [25,26].

2.10. *Environment Model*

The Environment Model will be the truth model for the system model. A truth model results from a detailed analysis of the system, and it includes errors and other characteristics that may be assumed negligible by the system model. It should also be the best possible representation of the “real world.” Typically, a truth model contains many more state variables than the system filter design model and a higher level of accuracy. However due to the nonlinear deterministic nature of some errors (troposphere in particular), meaning that they can be found with known parameters and are not truly random in nature, the “truth” environment model is not only driven by white noise. In addition, the environment model will begin with profiles of exact position, velocity and acceleration (if necessary) for each platform, the munition, satellites and target. Random values representing the errors in the measurements will be added. For example, the true range between satellite #1 and sensor platform #1 at a given time is known from the

profiles. GPS errors such as satellite clock and ephemeris along with atmospheric (troposphere, ionosphere) and receiver errors will be added, producing a known pseudorange. Other neglected errors (neglected in the filter design model) such as multipath and the unmodeled troposphere errors will also be added. This will show what effect not modeling them in the filter design model has on the resulting total error. The actual elements of the environment model will be discussed in detail in the next chapter.

3. Modeling Methodology

3.1. Overview

This chapter focuses on the development of the true environment model and the system models, integration methods, and simulation techniques used in this research effort. Section 3.2 describes the true environment and all the models that produce the GPS measurements and the SAR range and range rate measurements used by the Kalman filter. Section 3.3 examines the elements of the Kalman filter. Section 3.4 provides the equations and calculations necessary to examine to error in the range from the bomb to the target.

3.2. True Environment Modeling

The true environment model is illustrated in Figure 8:

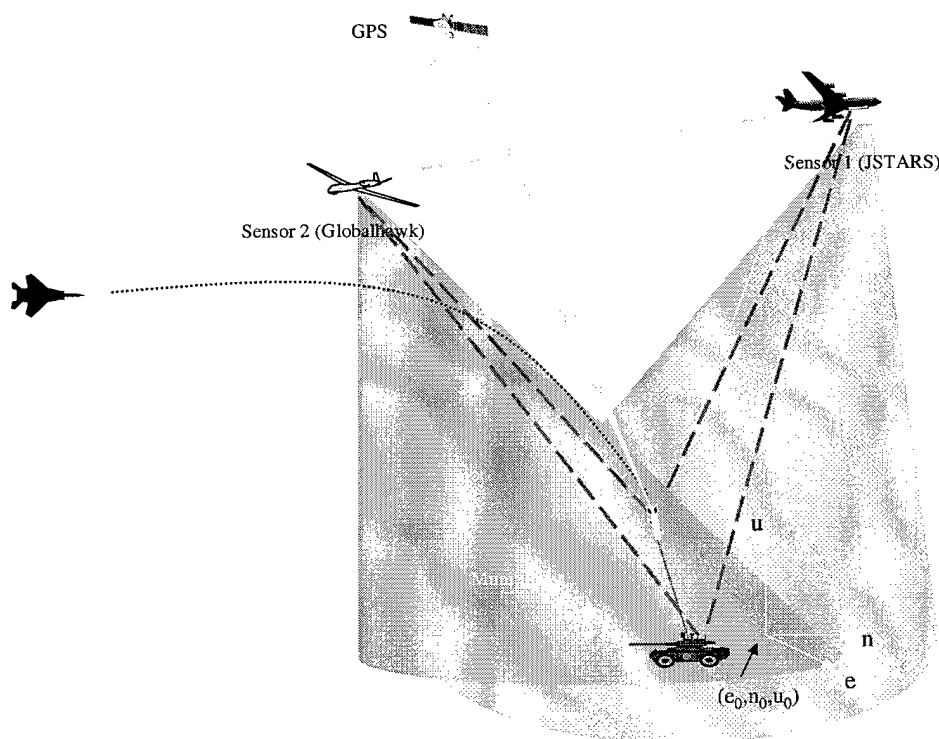


Figure 8. True Environment Model

The true environment consists of two sensor platforms (a Global Hawk and a JSTARS), the munition delivered by a fighter, a target, and the GPS constellation of satellites in view to the receivers on the sensor platforms and munition. The lightning-like lines represent the pseudorange measurements from the GPS satellites to the GPS receivers. The gray dashed lines from the sensors to the bomb and target represent the SAR range and range rates. The dotted line from the fighter to the bomb represents the flight path of the bomb to impact the target. The three-way axis represents the local-level, East-North-Up (ENU) coordinate frame. The line from the bomb to the target represents the range between the two and is the primary focus of the simulations: to minimize the error in the range from the bomb to the target. The scenario is 750 seconds in length and was based on preliminary work for the AMSTE program [17,43].

3.2.1. Sensors Environment Models

The models of the two sensors, also referred to as Sensor 1 and 2, were built in MATLAB using PROGEN, a flight profile generator [2]. PROGEN is a local-level flight trajectory generator suitable for short-distance, short-duration flights. Sensor 1 is at an altitude of 10 kilometers, and sensor 2 at 16.7 kilometers, and both fly the same rectangular racetrack shape trajectory. Table 2 defines this shape. They are separated by a nearly constant look angle to the target of 40 degrees. Figure 9 shows a top view of the two sensor flight profiles along with the top view of the bomb and target. The target is offset from the profile to allow it to be seen.

Table 2. Racetrack shape of Sensor 1 and 2

Fly straight 180 sec
Roll right 45 deg
Turn 90 deg
Roll back to level
Travel for 90 sec
Roll right 45 deg
Turn 90 deg
Roll back to level
Travel for 180 sec
Roll right 45 deg
Turn 90 deg
Roll back to level
Travel for 90 sec

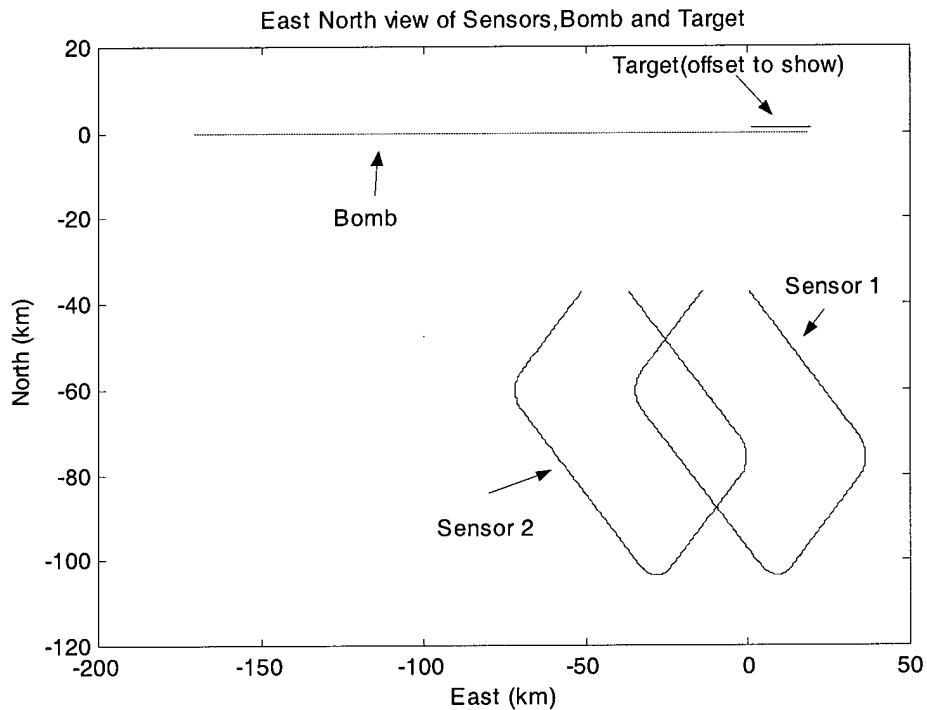


Figure 9. East-North view of Sensor 1 and Sensor 2 Flight Profiles

3.2.2. Munition Environment Model

The profile for the munition, or bomb, is described as a bomb being carried by a fighter that flies at a constant altitude of 7620 meters for 630 seconds. The bomb is then dropped such that it impacts the target from a nearly vertical direction. By coming in

vertically, the error in the Up direction of the target, which will be discussed later, becomes less of a factor in accurately destroying the target. Figure 10 gives the profile of the bomb altitude for the scenario.

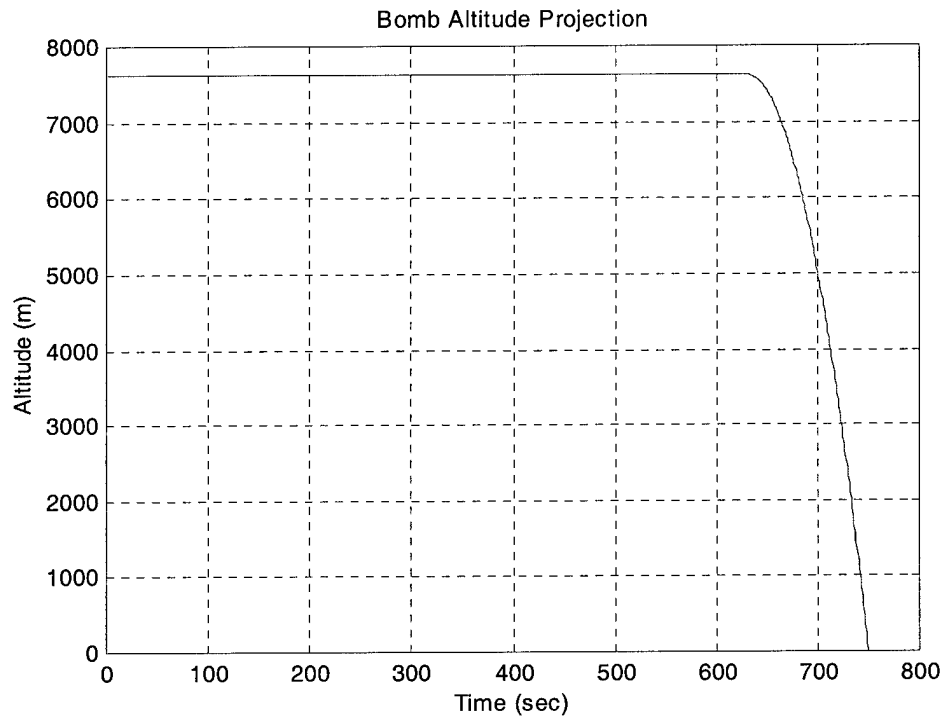


Figure 10. True Environment Bomb Altitude

3.2.3. Target Environment Model

The target model is very simple. To maintain the assumptions of only one visible and constantly moving vehicle, the target begins at the origin of the ENU coordinates and moves eastward at a constant velocity of 24.2 m/s. The trajectories are designed so that the bomb impacts the target at $t=750$ seconds. This is important because this research is only looking at the navigation, not the guidance of the bomb.

3.2.4. GPS Environment Model

The GPS environment model is built by a randomly picked ephemeris data file. The ephemeris data file is randomly chosen to provide variety in the satellite constellations for Monte-Carlo simulations. The ephemeris file is used to calculate the positions of the satellites that are visible to the three receivers. The next few sections explain the GPS and SAR environment true ranges and range rates and the errors that are added to the true ranges/range rates to produce the measurements.

3.2.4.1. Environment Model True Ranges and Range Rates

This section shows the equations used to build the true GPS ranges and the SAR range and range rates. The GPS ranges are found by calculating the distance between the GPS satellites and the receiver positions [30]. This is repeated for each receiver and the satellites visible to the receiver.

$$\begin{aligned} GPS_{pseudorange} = & \sqrt{(x_{sv} - x_r)^2 + (y_{sv} - y_r)^2 + (z_{sv} - z_r)^2} + c\delta t_u - c\delta t_{sv} \\ & + c\delta t_{trop} + c\delta t_{noise} + c\delta t_{mp} + \delta r_{eph} \end{aligned} \quad (3-1)$$

where

- x_{sv}, y_{sv}, z_{sv} = ENU positions of the satellite
- x_r, y_r, z_r = ENU positions of the receiver
- $c\delta t_u$ = receiver clock error
- $c\delta t_{sv}$ = satellite clock error
- $c\delta t_{eph}$ = error due to broadcast ephemeris
- $c\delta t_{trop}$ = delay due to the troposphere
- $c\delta t_{iono}$ = delay due to the ionosphere
- $c\delta t_{noise}$ = receiver noise
- $c\delta t_{mp}$ = multipath error
- δr_{eph} = ephemeris error

The model for each error will be discussed in the next sections.

3.2.4.2. GPS Troposphere Environment Model

As mentioned in chapter 2, the modified Hopfield model was used to determine the tropospheric error. The modified Hopfield model uses the receiver's height, elevation, and relative humidity to estimate the error that needs to be subtracted from the pseudorange. There is usually a residual error after the model has been applied. This residual is the error that gets applied to the true range in the research. To build the residual error, a true relative humidity between 0% and 100% is randomly selected and the true tropospheric error is determined. The model is run again, but this time the relative humidity is set at 50%. This value is chosen because normally a value of 50% is used when the true humidity is not known. The two model estimates are then subtracted from each other to represent the residual error. This error can be 10^{-4} to 4×10^{-3} meters of error for the sensors and 0.1 to 0.6 meters of error for the bomb. The amount of error is dependent on the height of the receiver.

3.2.4.3. GPS Environment Satellite Clock Model

The correction coefficients for the satellite clock error are transmitted as part of the navigation message (a_{f0}, a_{f1}, a_{f2}). Once the corrections have been applied in the real world, the resulting 1- σ residual error is typically 10ns or 3m [19]. In the environment model, the satellite clock error is modeled as a constant bias for the duration of the scenario. For the length of time of the scenario (750 seconds), this error does not change significantly. The bias, chosen independently for each satellite, is a normally distributed random variable with a standard deviation of 10ns. This error is multiplied by the speed of light to convert to meters.

3.2.4.4. GPS Environment Ephemeris Model

The satellite ephemeris error model uses the satellite positions sent in the navigation message and precise satellite positions from post-processed data. The difference between the transmitted navigation message position and precise positions is the ephemeris error. These errors are transformed from the downtrack, crosstrack and radial directions to the ENU coordinate frame. Calculating the projection of the error onto the unit line of sight of the receiver gives the appropriate level of error, about 3m (1σ) [38].

3.2.4.5. GPS Environment Receiver Clock Model

The environment receiver clock model is described in Figure 11. The strength of the white noises, u_7 and u_8 , are functions of Allan variance parameters [31]. Their values are calculated in the following equations:

$$S_f = 2 \times h_0 \quad (3-2)$$

$$S_g = 8\pi^2 \times h_{-2} \quad (3-3)$$

where

S_f = Strength of white noise u_7

S_g = Strength of white noise u_8

h_0, h_{-2} = Allan variance parameters typical quartz crystal, $h_0 = 2E-19, h_{-2} = 2E-20$

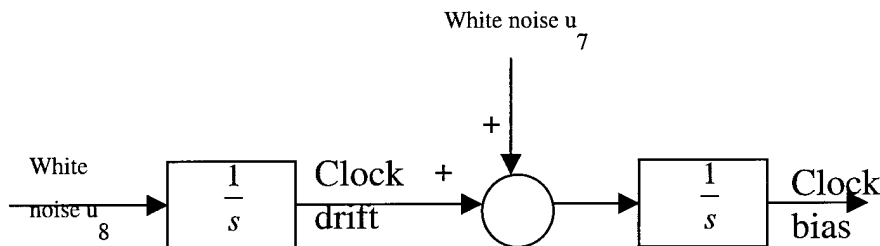


Figure 11. Environment Receiver Clock model

3.2.4.6. GPS Environment Receiver Noise Model

The noise of a receiver is uncorrelated with the noise of any other receiver [31]. Each receiver's noise is modeled as a white Gaussian noise with a standard deviation of 0.1m, which is a noise value typical for P-code measurements [19].

3.2.4.7. GPS Environment Multipath Model

The multipath environment model for both the sensor platforms and the bomb is modeled as a first order Gauss-Markov process. This model is consistent with [5]. The first-order Markov model parameters are a standard deviation 1 meter with a time constant of 30 seconds. The bomb has multipath of 10cm (1σ) and a time constant of 30 seconds. Figure 12 gives an example of multipath for an airplane.

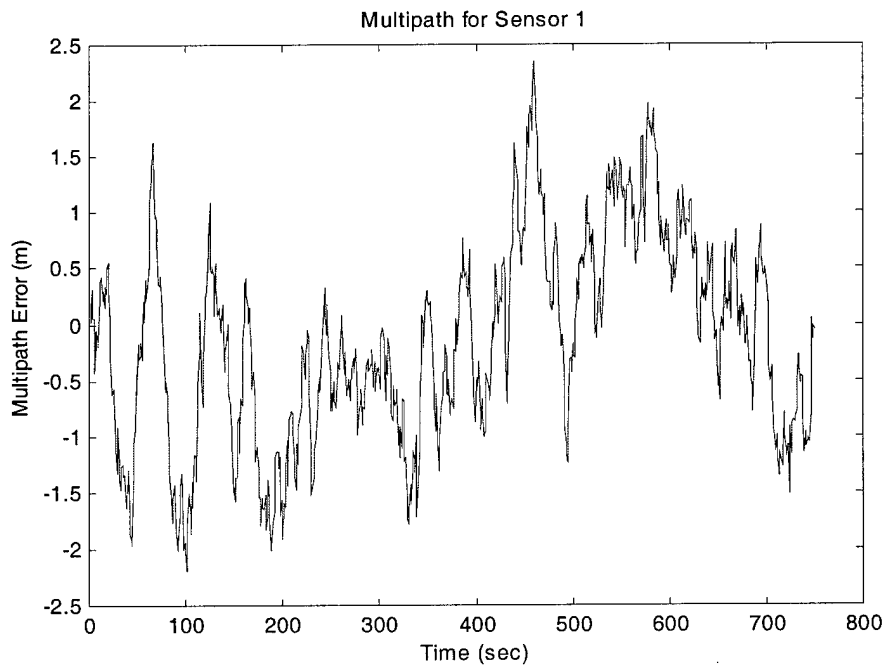


Figure 12. Multipath Error Example for Sensor 1

3.2.5. SAR/GMTI Environment Range and Range Rate Models

The SAR/GMTI true ranges to the bomb and target are calculated from the positions of the profiles. The SAR true range is calculated in the same manner as the GPS range, except it is the difference between the sensor and the bomb or the target [23,46]. The errors added to the range and range rate to produce the SAR measurements are discussed in the following sections.

$$SAR_{range} = \sqrt{(x_P - x_t)^2 + (y_P - y_t)^2 + (z_P - z_t)^2} + \delta \text{ trop} + v_{noise} \quad (3-4)$$

where

- x_P, y_P, z_P = ENU positions of the sensor
- x_t, y_t, z_t = ENU positions of the target/bomb
- $\delta \text{ trop}$ = SAR atmospheric error
- v_{noise} = SAR range noise

The SAR range rate is a function of the difference of velocities projected along the line of sight

$$SAR_{rangerate} = \frac{\mathbf{P}_P - \mathbf{P}_t}{\sqrt{(x_P - x_t)^2 + (y_P - y_t)^2 + (z_P - z_t)^2}} \bullet (\mathbf{v}_P - \mathbf{v}_t) + v_{noise} \quad (3-5)$$

where

- \mathbf{P}_P = position vector of the sensor
- \mathbf{P}_t = position vector of the target/bomb
- \mathbf{v}_P = velocity vector of the sensor
- \mathbf{v}_t = velocity vector of the target/bomb
- v_{noise} = SAR range rate noise
- \bullet = dot product

3.2.5.1. SAR/GMTI Environment Atmosphere Range Error

The environment range atmosphere error is similar to the tropospheric error for the GPS signal. In the case of the SAR range, the troposphere not only delays the

transmission of the signal, but also the return. The error is modeled in the same manner as the troposphere error is modeled, however an additional 0.1° error (1σ) is added to the elevation angle to model the mapping function errors. The mapping function errors are due to the interpolation of the model for elevation angle. The difference of the two calculated atmosphere errors, which is multiplied by 2 to account for the transmission and return, becomes the error due to the atmosphere. This is illustrated in Figure 13.

The process is repeated for the bomb. The bomb starts at a higher altitude, where there are lower atmospheric errors. As the bomb drops altitude and approaches the target, the value of the bomb and target atmospheric errors converges. Figure 14 gives a graphical depiction of a sample case. The changes in the magnitude of error are due to the changes in elevation angle.

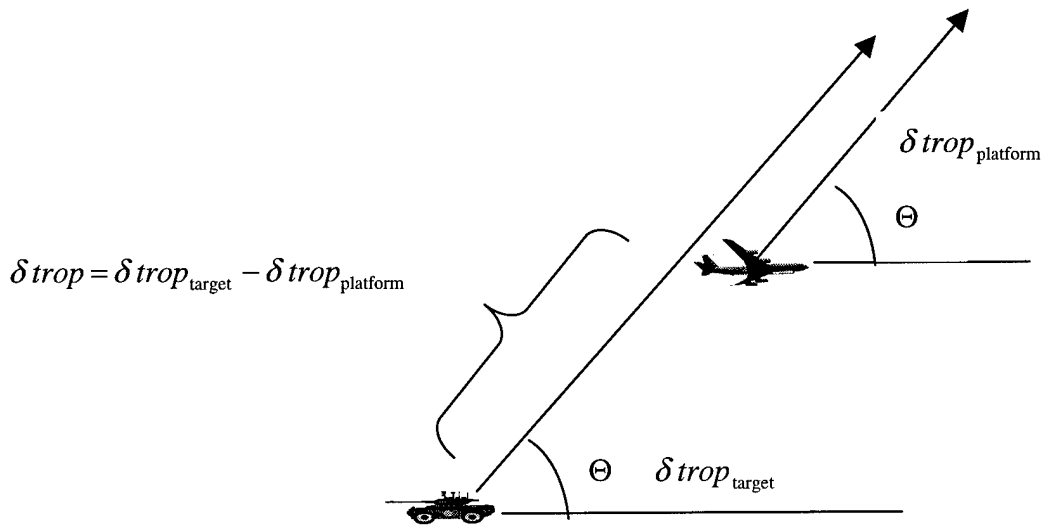


Figure 13. SAR Atmosphere error model (value is doubled for transmission & reception)

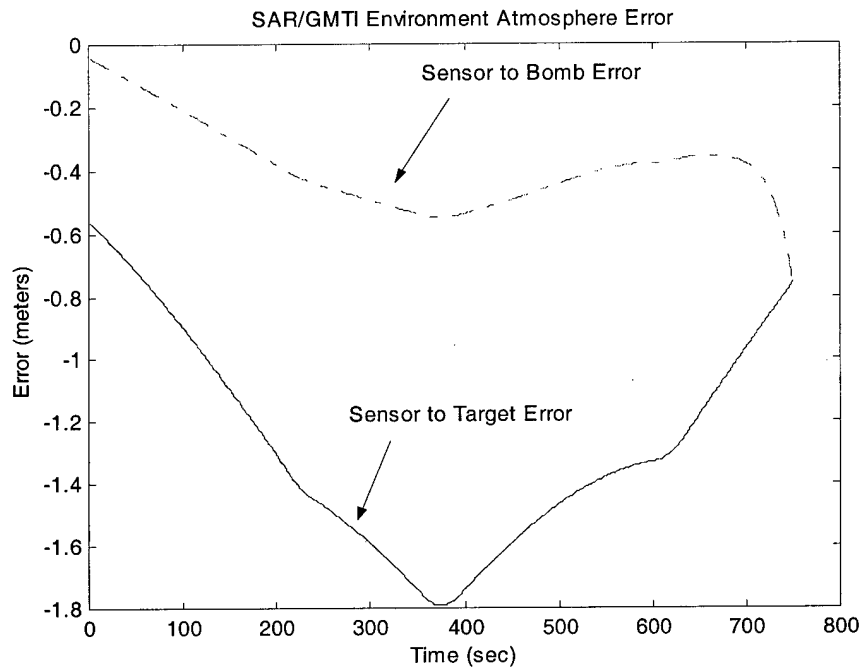


Figure 14. SAR/GMTI Environment Atmosphere Error

3.2.5.2. SAR/GMTI Environment Range/Range Rate Noise Error

There are a number of factors that add noise-like errors to a range or range rate, including timing and quantization errors [23]. The modeling of the range and range rate noises come from the work done in [23, 46]. Taking the root mean square of all the noise terms, the range noise error is 3.17 meters (1σ) and the range rate noise error is 0.04 meters/sec (1σ).

3.2.6. True Environment Summary

All of the components and error models have been described. Table 3 summarizes the true ranges and the associated errors added to the ranges to produce the measurements used by the System Model.

Table 4. Filter Model States

State #	Symbol	Description	State #	Symbol	Description
1	x_{P1}	East position of Sensor 1 (m)	22	\dot{x}_B	East velocity of Bomb (m/s)
2	y_{P1}	North position of Sensor 1 (m)	23	\dot{y}_B	North velocity of Bomb (m/s)
3	z_{P1}	Up position of Sensor 1 (m)	24	\dot{z}_B	Up velocity of Bomb (m/s)
4	\dot{x}_{P1}	East velocity of Sensor 1 (m/s)	25	\ddot{x}_B	East acceleration of Bomb (m/s ²)
5	\dot{y}_{P1}	North velocity of Sensor 1 (m/s)	26	\ddot{y}_B	North acceleration of Bomb (m/s ²)
6	\dot{z}_{P1}	Up velocity of Sensor 1 (m/s)	27	\ddot{z}_B	Up acceleration of Bomb (m/s ²)
7	\ddot{x}_{P1}	East acceleration of Sensor 1 (m/s ²)	28	x_T	East position of Target (m)
8	\ddot{y}_{P1}	North acceleration of Sensor 1 (m/s ²)	29	y_T	North position of Target (m)
9	\ddot{z}_{P1}	Up acceleration of Sensor 1 (m/s ²)	30	\dot{x}_T	East velocity of Target (m/s)
10	x_{P2}	East position of Sensor 2 (m)	31	\dot{y}_T	North velocity of Target (m/s)
11	y_{P2}	North position of Sensor 2 (m)	32	\ddot{x}_T	East acceleration of Target (m/s ²)
12	z_{P2}	Up position of Sensor 2 (m)	33	\ddot{y}_T	North acceleration of Target (m/s ²)
13	\dot{x}_{P2}	East velocity of Sensor 2 (m/s)	34	$c\delta t_{P1}$	Clock bias Sensor 1 (m)
14	\dot{y}_{P2}	North velocity of Sensor 2 (m/s)	35	$c\delta \dot{t}_{P1}$	Clock drift Sensor 1 (m/s)
15	\dot{z}_{P2}	Up velocity of Sensor 2 (m/s)	36	$c\delta t_{P2}$	Clock bias Sensor 2 (m)
16	\ddot{x}_{P2}	East acceleration of Sensor 2 (m/s ²)	37	$c\delta \dot{t}_{P2}$	Clock drift Sensor 2 (m/s)
17	\ddot{y}_{P2}	North acceleration of Sensor 2 (m/s ²)	38	$c\delta t_{P1}$	Clock bias Bomb (m)
18	\ddot{z}_{P2}	Up acceleration of Sensor 2 (m/s ²)	39	$c\delta \dot{t}_{P2}$	Clock drift Bomb (m/s)
19	x_B	East position of Bomb (m)	40	sf_{P1}	SAR scale factor of target - platform1 (m/m)
20	y_B	North position of Bomb (m)	41	sf_{P2}	SAR scale factor of target - platform 2 (m/m)
21	z_B	Up position of Bomb (m)	42+	$sv\#_{err}$	Satellite #_ errors (m)

The next sections describe the dynamics models for these states and give the initial value and covariances. The dynamics models for these states can be in either continuous

form or an equivalent discrete-time form. Both forms are shown in the following equations.

$$\begin{aligned}\dot{\mathbf{x}} &= \mathbf{F}\mathbf{x} + \mathbf{B}\mathbf{u} + \mathbf{G}\mathbf{w} \\ \mathbf{x}(t_i) &= \Phi\mathbf{x}(t_{i-1}) + \mathbf{B}_d\mathbf{u}(t_{i-1}) + \mathbf{w}_d(t_{i-1})\end{aligned}\quad (3-6,3-7)$$

where

- \mathbf{F}, Φ = continuous, discrete-time forms of the dynamics matrix
- \mathbf{B}, \mathbf{B}_d = continuous, discrete-time forms of the input matrix (zero matrix for study)
- $\mathbf{u}, \mathbf{u}(t_{i-1})$ = continuous, discrete-time forms of the vector of input states (zero for this study)
- $\mathbf{w}, \mathbf{w}_d(t_{i-1})$ = continuous, discrete-time forms of the vector of driving white noise

For these descriptions, the state vector will be split into segments. For example, the position, velocity, and acceleration states of sensor 1 are one segment. The Φ and the \mathbf{Q}_d matrices are shown below in block form.

$$\Phi = \begin{bmatrix} FOGMA_{P_1} & 0 & 0 & 0 & 0 & 0 & 0 \\ 0 & FOGMA_{P_2} & 0 & 0 & 0 & 0 & 0 \\ 0 & 0 & FOGMA_B & 0 & 0 & 0 & 0 \\ 0 & 0 & 0 & FOGMA_T & 0 & 0 & 0 \\ 0 & 0 & 0 & 0 & Clock & 0 & 0 \\ 0 & 0 & 0 & 0 & 0 & SAR_{Sf} & 0 \\ 0 & 0 & 0 & 0 & 0 & 0 & SAT_{Err} \end{bmatrix} \quad (3-8)$$

where

- $FOGMA_{P_1}, FOGMA_{P_2}, FOGMA_B$ = 9-by-9 3-D First-Order Gauss-Markov Acceleration models for the sensors, bomb
- $FOGMA_T$ = 6-by-6 2-D First-Order Gauss-Markov Acceleration model for the target
- $Clock$ = three 2-by-2 Clock bias/Clock drift models for the receiver clocks
- SAR_{Sf} = two SAR scale factors for atmosphere error from sensor 1/2 to target
- SAT_{Err} = N-by-N matrix of satellite error models (N= # of satellites)

$$\mathbf{Q}_d = \begin{bmatrix} \mathbf{Q}_{dP1} & 0 & 0 & 0 & 0 & 0 & 0 \\ 0 & \mathbf{Q}_{dP2} & 0 & 0 & 0 & 0 & 0 \\ 0 & 0 & \mathbf{Q}_{dB} & 0 & 0 & 0 & 0 \\ 0 & 0 & 0 & \mathbf{Q}_{dT} & 0 & 0 & 0 \\ 0 & 0 & 0 & 0 & \mathbf{Q}_{d\text{clock}} & 0 & 0 \\ 0 & 0 & 0 & 0 & 0 & \mathbf{Q}_{d\text{SAR}} & 0 \\ 0 & 0 & 0 & 0 & 0 & 0 & \mathbf{Q}_{d\text{Sat}} \end{bmatrix} \quad (3-9)$$

where

$\mathbf{Q}_{dP1}, \mathbf{Q}_{dP2}, \mathbf{Q}_{dB} = 9\text{-by-}9$ Matrices for the white noise on the acceleration states

$\mathbf{Q}_{dT} = 6\text{-by-}6$ Matrix for the white noise on the acceleration states

$\mathbf{Q}_{d\text{clock}} = 6\text{-by-}6$ Matrix for the white noise of the receiver clock bias/clock drift states

$\mathbf{Q}_{d\text{SAR}} = 2\text{-by-}2$ Matrix for the white noise of the SAR modeled random walk

$\mathbf{Q}_{d\text{Sat}} = N\text{-by-}N$ matrix for the white noise of the Gauss-Markov satellite models

3.3.2. Filter Dynamics Model of Sensor 1, Sensor 2, and the Bomb

The dynamics model for each of the two sensors and the bomb is a 9-by-9 3-D FOGMA. The position states are an integral of the velocity states, the velocity states are an integral of the acceleration states and the acceleration states are each modeled as a first-order Gauss-Markov process. The continuous-time form of the FOGMA for a sensor or bomb is represented by \mathbf{F}_1 .

$$\mathbf{F}_1 = \begin{bmatrix} 0 & 0 & 0 & 1 & 0 & 0 & 0 & 0 & 0 \\ 0 & 0 & 0 & 0 & 1 & 0 & 0 & 0 & 0 \\ 0 & 0 & 0 & 0 & 0 & 1 & 0 & 0 & 0 \\ 0 & 0 & 0 & 0 & 0 & 0 & 1 & 0 & 0 \\ 0 & 0 & 0 & 0 & 0 & 0 & 0 & 1 & 0 \\ 0 & 0 & 0 & 0 & 0 & 0 & 0 & 0 & 1 \\ 0 & 0 & 0 & 0 & 0 & 0 & -\frac{1}{T} & 0 & 0 \\ 0 & 0 & 0 & 0 & 0 & 0 & 0 & -\frac{1}{T} & 0 \\ 0 & 0 & 0 & 0 & 0 & 0 & 0 & 0 & -\frac{1}{T} \end{bmatrix} \quad (3-10)$$

where

T = time constant for Gauss-Markov process

For sensor 1 and sensor 2 the time constant is 3 seconds. For the bomb it is 5 seconds. These values are based upon the anticipated correlation between the acceleration at the current time applied to the next time [25,26,31].

In this research, the model is implemented in discrete time. There are many ways to calculate the Φ matrix from the \mathbf{F}_1 matrix. Because \mathbf{F}_1 is non-time varying, the matrix exponential method is used.

$$\Delta t \equiv t_i - t_{i-1} \quad (3-11)$$

$$\Phi(t_i, t_{i-1}) = \Phi(\Delta t) = e^{\mathbf{F}_1 \Delta t} \quad (3-12)$$

The characteristics of the white Gaussian noise values for the FOGMA are represented first in continuous-time form with the following equations:

$$E[\mathbf{w}] = \mathbf{0} \quad (3-13)$$

$$E\{w(t)w^T(t+\tau)\} = \mathbf{Q}\delta(\tau) = \begin{bmatrix} 0 & 0 & 0 & 0 & 0 & 0 & 0 & 0 & 0 \\ 0 & 0 & 0 & 0 & 0 & 0 & 0 & 0 & 0 \\ 0 & 0 & 0 & 0 & 0 & 0 & 0 & 0 & 0 \\ 0 & 0 & 0 & 0 & 0 & 0 & 0 & 0 & 0 \\ 0 & 0 & 0 & 0 & 0 & 0 & 0 & 0 & 0 \\ 0 & 0 & 0 & 0 & 0 & 0 & 0 & 0 & 0 \\ 0 & 0 & 0 & 0 & 0 & 0 & q & 0 & 0 \\ 0 & 0 & 0 & 0 & 0 & 0 & 0 & q & 0 \\ 0 & 0 & 0 & 0 & 0 & 0 & 0 & 0 & q \end{bmatrix} \delta(\tau) \quad (3-14)$$

$$q = \frac{2\sigma^2}{T} \quad (3-15)$$

where

- q = strength of the white noise on the acceleration state
- σ = standard deviation of acceleration in meters/sec²
- T = time constant

The σ value for sensors 1 and 2 is 8 meters and the value is 15 meters for the bomb.

As with the dynamics matrix, the covariance matrix needs to be transformed to discrete time. This is done with the following equation:

$$\mathbf{Q}_d = \int_0^{\Delta} \Phi(\tau)\mathbf{Q}\Phi^T(\tau)d\tau \quad (3-16)$$

$$\mathbf{Q}_d = \begin{bmatrix} D_e & 0 & 0 & E_e & 0 & 0 & G_e & 0 & 0 \\ 0 & D_e & 0 & 0 & E_e & 0 & 0 & G_e & 0 \\ 0 & 0 & D_e & 0 & 0 & E_e & 0 & 0 & 0 \\ E_e & 0 & 0 & K_e & 0 & 0 & L_e & 0 & G_e \\ 0 & E_e & 0 & 0 & K_e & 0 & 0 & L_e & 0 \\ 0 & 0 & E_e & 0 & 0 & K_e & 0 & 0 & L_e \\ G_e & 0 & 0 & L_e & 0 & 0 & M_e & 0 & 0 \\ 0 & G_e & 0 & 0 & L_e & 0 & 0 & M_e & 0 \\ 0 & 0 & G_e & 0 & 0 & L_e & 0 & 0 & M_e \end{bmatrix} \quad (3-17)$$

where

$$\begin{aligned}
D_e &= \frac{1}{2}T_a^5 q_a (1 - e^{-2\Delta t/T_a}) + T_a^4 q_a \Delta t (1 - 2e^{-\Delta t/T_a}) - T_a^3 q_a (\Delta t)^2 + \frac{1}{3}T_a^2 q_a (\Delta t)^3 \\
E_e &= T_a^4 q_a \left(\frac{1}{2}e^{-2\Delta t/T_a} - e^{-\Delta t/T_a} + \frac{1}{2} \right) + T_a^3 q_a \Delta t (e^{-\Delta t/T_a} - 1) + \frac{1}{2}T_a^2 q_a (\Delta t)^2 \\
G_e &= \frac{1}{2}T_a^3 q_a (1 - e^{-2\Delta t/T_a}) - T_a^2 q_a \Delta t e^{-\Delta t/T_a} \\
K_e &= \frac{1}{2}T_a^3 q_a \left(-e^{-2\Delta t/T_a} + 4e^{-\Delta t/T_a} + 2\frac{\Delta t}{T_a} - 3 \right) \\
L_e &= -\frac{1}{2}T_a^2 q_a (-e^{-2\Delta t/T_a} + 2e^{-\Delta t/T_a} - 1) \\
M_e &= -\frac{1}{2}T_a q_a (e^{-2\Delta t/T_a} - 1)
\end{aligned}$$

The initial values of the position states for both sensors and the bomb are the true positions with 9m (1 σ) of error added. The initial values of the velocity and acceleration are zero. \mathbf{P}_{p0} describes the initial covariance

$$\mathbf{P}_{p0} = \begin{bmatrix} 100^2 & 0 & 0 & 0 & 0 & 0 & 0 & 0 & 0 \\ 0 & 100^2 & 0 & 0 & 0 & 0 & 0 & 0 & 0 \\ 0 & 0 & 100^2 & 0 & 0 & 0 & 0 & 0 & 0 \\ 0 & 0 & 0 & 400^2 & 0 & 0 & 0 & 0 & 0 \\ 0 & 0 & 0 & 0 & 400^2 & 0 & 0 & 0 & 0 \\ 0 & 0 & 0 & 0 & 0 & 400^2 & 0 & 0 & 0 \\ 0 & 0 & 0 & 0 & 0 & 0 & 20^2 & 0 & 0 \\ 0 & 0 & 0 & 0 & 0 & 0 & 0 & 20^2 & 0 \\ 0 & 0 & 0 & 0 & 0 & 0 & 0 & 0 & 20^2 \end{bmatrix} \quad (3-18)$$

The large initial values insure that the Kalman filter will place more weight on the initial measurements rather than the unknown initial state [31].

3.3.3. Filter Dynamics Model for Target

The dynamics model for the target is also a FOGMA model except that it is only a 6-by-6 matrix for a 2-D case (East and North). A two-state model is being implemented

because there are only two position measurements available (sensor 1 and sensor 2 ranges). The same matrices and equations apply as above minus the z states for position, velocity and acceleration. The time constant, or T , for the target is 6 seconds and the σ value is 5 meters/sec². The initial state values and covariances are the same as that for the sensors and bomb.

The Up direction of the target is modeled as a Digital Terrain Elevation Data (DTED) measurement. DTED is an estimate of the height of a position given the longitude and latitude coordinates. With the length of the scenario short, the error in height is represented by constant random bias with a 1- σ error of 10m. For the target, the velocity and acceleration in the Up direction is assumed to be zero.

3.3.4. Filter Model for Sensors 1 & 2 and Bomb Receiver Clocks

The filter model for the GPS receiver clock is the same model as that used in the true environment model (as shown in Figure 11). The system model is a two-state model of the clock bias and clock drift. The clock bias accounts for a large, non-white error in the code measurements [31]. While the clock drift is not needed for measurement incorporation, is it useful for propagating the clock bias forward in time and preventing a consistent bias in all the code measurements [31]. Equations (3-19) and (3-20) represent the continuous-time form of the dynamics model that is transformed to the discrete model in the same manner as above. This model is repeated for each receiver.

$$\mathbf{F}_{clock} = \begin{bmatrix} 0 & 1 \\ 0 & 0 \end{bmatrix} \quad (3-19)$$

$$\mathbf{Q}_{clock} = \begin{bmatrix} q_{c1} & 0 \\ 0 & q_{c1} \end{bmatrix} \quad (3-20)$$

where

$$q_{c1} = 0.036 \frac{m^2}{s}$$

$$q_{c2} = 0.141 \frac{m^2}{s^3}$$

The initial value for all clock bias and clock drifts are zero and the initial covariance is

$$\mathbf{P}_{clock0} = \begin{bmatrix} 200^2 & 0 \\ 0 & 1000^2 \end{bmatrix} \quad (3-21)$$

3.3.5. System Model for SAR scale factor for the target

The System model for the SAR range atmosphere error to the target incorporates a scale factor error. This model was implemented in [23,46]. Initially the scale factor was applied to both the target and bomb. However, after some initial runs, the estimation of the atmosphere error was significantly off, because there was very little atmospheric error between the sensor and the bomb. By redefining the state to be just the sensor-to-target atmospheric error, the results gave more reasonable errors. As a result, the measurement model for the sensor-to-bomb SAR range measurements did not include the atmospheric error term until the bomb was in the vicinity of the target (defined as below 4000m altitude.) This is not the best model, and associated concerns will be covered in Chapter 5-Conclusion and Recommendations.

The scale factor is modeled as random walk, as shown in equations (3-22) and (3-23).

$$\mathbf{F}_{SAR} = \begin{bmatrix} 0 & 0 \\ 0 & 0 \end{bmatrix} \quad (3-22)$$

$$\mathbf{Q}_{SAR} = \begin{bmatrix} 1 \times 10^{-6} & 0 \\ 0 & 1 \times 10^{-6} \end{bmatrix} \quad (3-23)$$

The initial value is zero and the initial covariance is $(30 \times 10^{-6})^2$ [23,46].

3.3.6. *Filter Model for Common GPS Errors*

Here, the filter models errors in the GPS measurements that are common to all of the receivers: satellite clock and satellite ephemeris. By estimating the common errors for the satellites and the receiver clock, the differential calculation is performed implicitly within the filter. Not estimating the errors provides a stand-alone GPS solution. In the stand-alone GPS solution case, the satellite clock and ephemeris errors are not cancelled or reduced, but left as part of the pseudorange measurement. This fact will be shown in the next chapter. The number of states is dependent on the number of total satellites visible to the receivers. The common error is modeled as a Gauss-Markov process with a σ of 3m and a time constant of 120 seconds. These values are based on the fact that the combination of the satellite clock and ephemeris errors tend to exhibit 1- σ values of 3m and the long time constant reflects the bias-like character of the state [31]. Modeling the errors as random walk produced unreasonable results, because the errors never converged to a solution. The initial value is zero and the initial variance is 9 meters².

3.3.7. *System Measurement Models*

This section describes the nonlinear measurement model, the linearized partial derivative matrix \mathbf{H} evaluated at the current state estimate, and the covariance of the zero-mean white Gaussian measurement noise \mathbf{v} vector (the \mathbf{R} matrix.) As a reminder, the general form of the measurement equation is

$$\mathbf{z}(t_i) = \mathbf{h}[\mathbf{x}(t_i), t_i] + \mathbf{v}(t_i) \quad (3-24)$$

where

$\mathbf{z}(t_i)$ = discrete-time measurement vector at time t_i
 $\mathbf{h}[\mathbf{x}(t_i), t_i]$ = nonlinear function of the state vector and time

$\mathbf{v}(t_i)$ = discrete time measurement noise vector with a zero-mean white noise process, which is independent of $\mathbf{w}(t)$, and having covariance $\mathbf{R}(t_i)$ defined by:

$$E[\mathbf{v}(t)] = \mathbf{0} \quad (3-25)$$

$$E[\mathbf{v}(t_i)\mathbf{v}^T(t_j)] = \begin{cases} \mathbf{R}(t_i) & \text{for } t_i = t_j \\ \mathbf{0} & \text{for } t_i \neq t_j \end{cases} \quad (3-26)$$

3.3.7.1. Filter Measurement Model - GPS Code Measurements

The number of GPS code measurements is dependent upon the number of satellites visible to the receivers. If there are 8 satellites, all visible to the three receivers (sensor 1, sensor 2 and the bomb), there will be 24 GPS code measurements.

The \mathbf{h} vector models the incoming measurements \mathbf{z} in terms of the estimated states.

For GPS code measurements to sensor 1, the measurement equation is:

$$\rho_{GPS\ P1} = \sqrt{(x_{sv} - x_{P1})^2 + (y_{sv} - y_{P1})^2 + (z_{sv} - z_{P1})^2} + c\delta t_{P1} + v_{P1} \quad (3-27)$$

where

x_{sv}, y_{sv}, z_{sv} = satellite position elements
 x_{P1}, y_{P1}, z_{P1} = sensor 1 position elements
 $c\delta t_{P1}$ = receiver clock error

$$E[v_{P1}] = 0 \quad \text{and} \quad E[v_{P1}(t_i)v_{P1}(t_j)] = 2.6m^2 \text{ sec } \delta_{ij} \quad (3-28)$$

The value of $2.6m^2\text{sec}$ is based on typical multipath and noise values [31].

Recall that the \mathbf{H} matrix represents the partial derivatives of the nonlinear measurement model, evaluated at the current state estimate

$$\mathbf{H}[t_i; \hat{\mathbf{x}}(t_i^-)] = \left. \frac{\partial \mathbf{h}[\mathbf{x}(t), t]}{\partial \mathbf{x}} \right|_{\mathbf{x}=\hat{\mathbf{x}}(t_i^-)} \quad (3-29)$$

Let \mathbf{e} represent the unit line of sight vector. The vector is described as

$$\mathbf{e}^T = [e_1 \ e_2 \ e_3] \quad (3-30)$$

$$e_1 = \frac{(x_{sv} - x_{p1})}{\sqrt{(x_{sv} - x_{p1})^2 + (y_{sv} - y_{p1})^2 + (z_{sv} - z_{p1})^2}} \quad (3-31)$$

$$e_2 = \frac{(y_{sv} - y_{p1})}{\sqrt{(x_{sv} - x_{p1})^2 + (y_{sv} - y_{p1})^2 + (z_{sv} - z_{p1})^2}} \quad (3-32)$$

$$e_3 = \frac{(z_{sv} - z_{p1})}{\sqrt{(x_{sv} - x_{p1})^2 + (y_{sv} - y_{p1})^2 + (z_{sv} - z_{p1})^2}} \quad (3-33)$$

The row of the \mathbf{H} matrix corresponding to the GPS code measurement at sensor 1 is

$$[e_1 \ e_2 \ e_3 \ 0 \ \dots \ 0 \ 1 \ 0 \ \dots \ 0]$$

where the “1” is in the 34th column (corresponding to the sensor 1 clock error.)

The measurements for sensor 2 and the bomb are calculated in the same manner as sensor 1. The difference is the unit vector \mathbf{e} corresponds to the appropriate position states and the “1” to clock error state of sensor 2 or bomb.

3.3.7.2. System Measurement Model – SAR range measurement

For both the bomb and the target, there are two SAR range measurements– one from each sensor. The measurement equation for the SAR range measurement is

$$SAR_{range} = (1 + sf_{p1}) \times \sqrt{(x_{p1} - x_t)^2 + (y_{p1} - y_t)^2 + (z_{p1} - z_t)^2} + v_{p1} \quad (3-34)$$

where

- x_{p1}, y_{p1}, z_{p1} = sensor 1 position coordinates
- x_t, y_t, z_t = target position coordinates
- sf_{p1} = sensor 1 scale factor
- v_{p1} = SAR range noise

$$E[v_{p1}] = 0 \quad \text{and} \quad E[v_{p1}(t)v_{p1}(t+\tau)] = \delta(\tau) \times 3.17^2 m^2 \text{ sec}$$

This number is based from the work done in [29,54].

The row of the \mathbf{H} matrix corresponding to the SAR range measurement is

$$[e_{r1} \ e_{r2} \ e_{r3} \ 0 \ \dots \ 0 \ -e_{r1} \ -e_{r2} \ -e_{r3} \ 0 \ \dots \ 0 \ d \ 0 \ \dots \ 0]$$

where

$$e_{r1} = e_1 \times (1 + sf_{p_-}) \quad (3-35)$$

$$e_{r2} = e_2 \times (1 + sf_{p_-}) \quad (3-36)$$

$$e_{r3} = e_3 \times (1 + sf_{p_-}) \quad (3-37)$$

$$e_1 = \frac{x_{p1} - x_t}{d} \quad (3-38)$$

$$e_2 = \frac{y_{p1} - y_t}{d} \quad (3-39)$$

$$e_3 = \frac{z_{p1} - z_t}{d} \quad (3-40)$$

$$d = \sqrt{(x_{p1} - x_t)^2 + (y_{p1} - y_t)^2 + (z_{p1} - z_t)^2} \quad (3-41)$$

The appropriate unit vectors correspond to the position states of the sensor and target/bomb, and d corresponds to the scale factor state.

3.3.7.3. System Measurement Model – SAR Range Rate Measurement

Just as there are two SAR range measurements per sensor, there are two SAR range rate measurements. The measurement equation for the SAR range rate is

$$SAR_{range\ rate} = \frac{\mathbf{P}_{p1} - \mathbf{P}_t}{\sqrt{(x_{p1} - x_t)^2 + (y_{p1} - y_t)^2 + (z_{p1} - z_t)^2}} \bullet (\mathbf{v}_{p1} - \mathbf{v}_t) + v_{rrp1} \quad (3-42)$$

where

$$\mathbf{P}_{p1} = [x_{p1} \ y_{p1} \ z_{p1}] = \text{sensor 1 position vector}$$

$$\mathbf{P}_t = [x_t \ y_t \ z_t] = \text{target position vector}$$

$$\mathbf{v}_{p1} = [\dot{x}_{p1} \ \dot{y}_{p1} \ \dot{z}_{p1}] = \text{sensor 1 velocity vector}$$

$$\mathbf{v}_t = [\dot{x}_t \ \dot{y}_t \ \dot{z}_t] = \text{vector of target velocities}$$

v_{rrP1} = SAR range rate noise

$$E[v_{rrP1}] = 0 \quad \text{and} \quad E[v_{rrP1}(t_i)v_{rrP1}(t_j)] = 0.04^2(m^2 \text{ sec})$$

These values are based on work done in [23, 46].

The partial derivative \mathbf{H} matrix row for the SAR range rate technically should include terms for the sensor and target/bomb velocities and the sensor and target/bomb positions. While the row (shown below) takes the velocities into account, the terms corresponding to the position are so small that they are ignored. The row corresponding to the SAR range rate between sensor 1 and the target is as follows:

$$[0 \quad \dots \quad 0 \quad e_1 \quad e_2 \quad e_3 \quad 0 \quad \dots \quad 0 \quad -e_1 \quad -e_2 \quad -e_3 \quad 0 \quad \dots \quad 0]$$

3.4. Calculations to Find Accuracy in Bomb-to-Target Vector

The 3-D vector from the bomb to the target is not explicitly estimated in the Kalman filter. Nonetheless, calculating this vector is the primary goal of the filter. The estimate (bomb-to-target) can be calculated from elements in the state vector. Subtracting the true range from the estimate will give the error in the range estimate. The range estimates and covariances are found with the following equations:

$$\begin{aligned} \Delta \hat{x} &= \hat{x}_B - \hat{x}_T = [1 \quad -1] \begin{bmatrix} \hat{x}_B \\ \hat{x}_T \end{bmatrix} \\ \sigma_{\Delta \hat{x}}^2 &= [1 \quad -1] \begin{bmatrix} \sigma_{\hat{x}_B}^2 & \sigma_{\hat{x}_B \hat{x}_T} \\ \sigma_{\hat{x}_B \hat{x}_T} & \sigma_{\hat{x}_T}^2 \end{bmatrix} \begin{bmatrix} 1 \\ -1 \end{bmatrix} \\ \sigma_{\Delta \hat{x}}^2 &= \sigma_{\hat{x}_B}^2 + \sigma_{\hat{x}_T}^2 - 2\sigma_{\hat{x}_B \hat{x}_T} \end{aligned} \quad (3-43)$$

where $\Delta \hat{y}, \Delta \hat{z}, \sigma_{\Delta \hat{y}}^2, \sigma_{\Delta \hat{z}}^2$ are found in the same manner.

The error in the estimate is found with the following equations:

$$\begin{aligned}
\delta \Delta x &= \Delta x_{est} - \Delta x_{true} = \Delta x_{est} - (x_{B_{true}} - x_{T_{true}}) \\
\delta \Delta y &= \Delta y_{est} - \Delta y_{true} = \Delta y_{est} - (y_{B_{true}} - y_{T_{true}}) \\
\delta \Delta z &= \Delta z_{est} - \Delta z_{true} = \Delta z_{est} - (z_{B_{true}} - tar_z)
\end{aligned}
\tag{3-44}$$

tar_z - DTED estimate of the target height

Since the target's height is not estimated, the DTED value is used. Also because the DTED value is deterministic, the covariance is only a function of the bomb's covariance.

4. Simulation Results

4.1. Overview

This chapter presents the results and analysis of the system Kalman filter implemented in MATLAB. The first section explains how the Kalman filter was implemented. The second section shows typical results from the Kalman filter and addresses filter tuning. The next section describes the different simulation parameters and how the combinations of these parameters produce the 12 different simulation cases. Lastly, the results from each case are presented and analyzed.

4.2. System Kalman Filter Results Setup

As mentioned in chapter 3, the measurements built from the true environment were used in the Kalman filter. The true environment produces both true state values and measurements that are used by the Kalman filter. It generates the true states and measurements using a combination of pre-determined parameters (such as the number of satellites to use), randomly chosen parameters (such as the tropospheric humidity term – see Section 3.2.4.2), and white noise (such as pseudorange measurement noise). The Kalman filter then processes the measurements, producing estimates of the true states. Subtracting the true from the estimate gives the error in the estimate. This concept is illustrated in Figure 15.

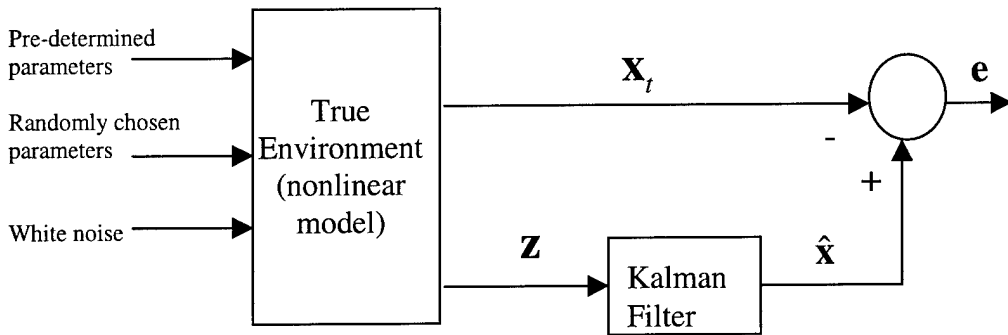


Figure 15. Performance evaluation of the Kalman filter

The objective of the performance analysis is to characterize the error process statistically [31]. To generate the statistical information, a Monte Carlo analysis is performed. Multiple samples of the error processes are generated by the simulations, and the sample statistics are computed directly [31]. For this research, twenty-five samples of the error process are run for each case. From these runs, the mean and 1- σ values of the state values are computed. In addition to viewing the east, north and up errors individually, analyzing the 2-D (horizontal) and 3-D errors can be useful. At each time epoch, the Distance Root Mean Square (DRMS) is calculated by

$$DRMS = \sqrt{\frac{\sum_{i=1}^n [(\delta \Delta x_i)^2 + (\delta \Delta y_i)^2]}{n}} \quad (4-1)$$

where

- n = number of Monte Carlo runs
- $\delta \Delta x_i, \delta \Delta y_i$ = x and y error values for Monte Carlo run i

The DRMS value gives the root-mean-square of the horizontal errors. If the error statistics in the x and y directions are similar, then approximately 63% of the horizontal errors will be less than the DRMS value.

The 3-D version of the DRMS is the Mean Radial Spherical Error (MRSE). This error is calculated by

$$MRSE = \sqrt{\frac{\sum_{i=1}^n [(\delta \Delta x_i)^2 + (\delta \Delta y_i)^2 + (\delta \Delta z_i)^2]}{n}} \quad (4-2)$$

where

n = number of Monte Carlo runs
 $\delta \Delta x_i, \delta \Delta y_i, \delta \Delta z_i$ = x, y, and z error values for Monte Carlo run i

The MRSE value gives the root-mean-square of the spherical errors. If the error statistics in the x, y and z directions are similar, then approximately 61% of the total 3-D errors will be less than the MRSE value.

4.3. *Filter Output and Tuning*

To give an example of the type of results the system filter produces, the next group of figures give the East-North-Up position error statistics for the bomb and the target for an example where all in view satellites are used, the satellite common errors are estimated and the bomb is tracked with the same sensor as the target.

Figure 16 shows the error in the bomb position for the east direction. For the top graph, the multiple dashed lines are the errors from 25 Monte Carlo runs. The solid lines represent the filter-computed standard deviations of the Monte Carlo runs. In the lower plot, the dashed line represents the mean error of the Monte Carlo runs, the solid lines represents the error standard deviation of the Monte Carlo runs, and the dotted lines are the filter-computed 1- σ error value from the runs. The multiple covariance lines are due to the varying satellite geometry (number of satellites and locations).

From the top graph in Figure 16, the runs show little noise in each run up to about 620 seconds. At this point, the two radar sensors are tracking the bomb. These additional range measurements are the cause of the slight increase of noise in the error. The filter standard deviation matches very well with the Monte Carlo simulations. The second graph shows that there is an approximate -0.7 m bias error in the estimate. This bias may be due to a lack of observability. With no true reference point, there is no basis on which to compare relative positions.

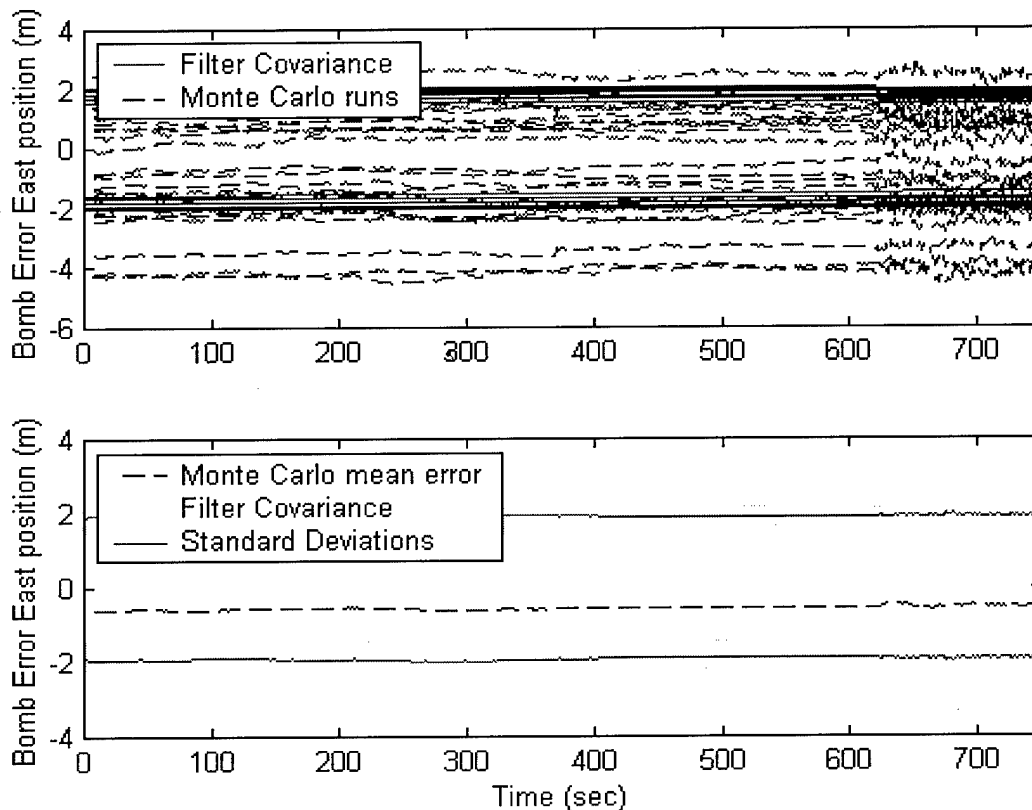


Figure 16. Error in Bomb Position -East

Figure 17 shows the errors in the bomb position in the north direction. The top graph in Figure 17 shows a distinct drop in error around 375 seconds for a few of the runs. This is caused by the loss of a satellite from view. In the second graph, the standard deviation

of the errors also reflects the drop. Again, at time 620 seconds, the growth in noise is due to the added sensor measurements. A positive 0.4 bias appeared in the mean error of graph two.

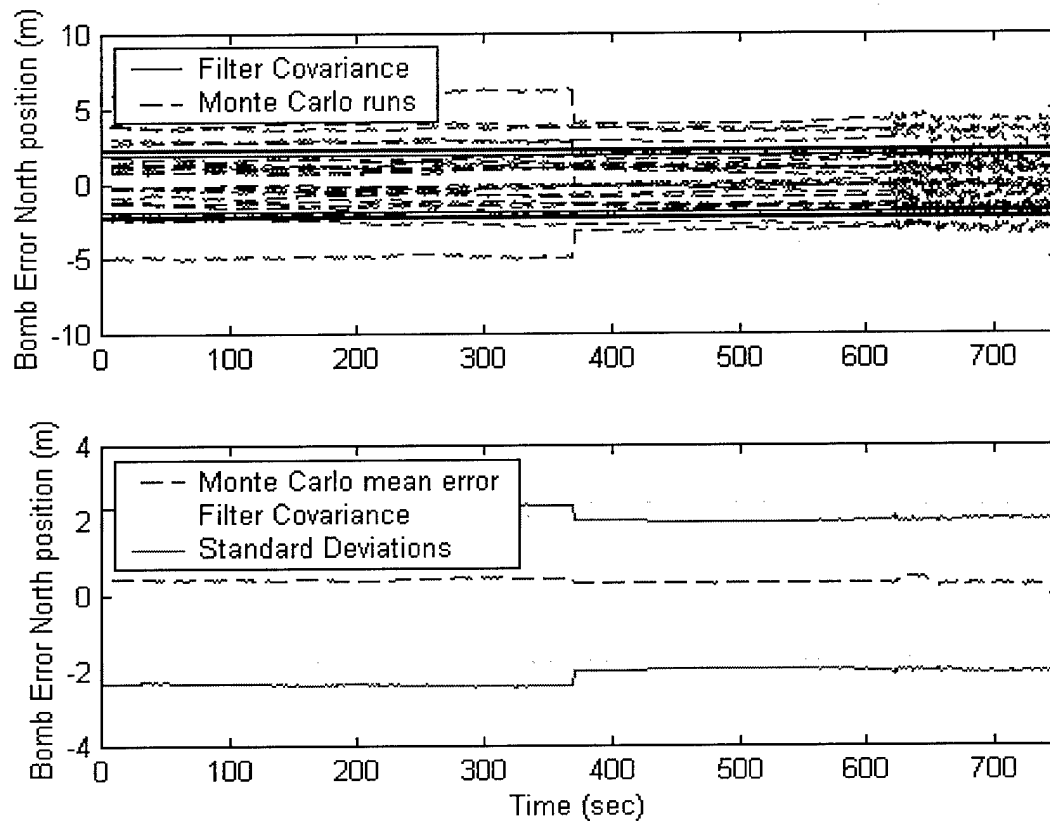


Figure 17. Error in Bomb Position – North

Figure 18 shows the plots for the error in the bomb position in the up direction. The data for the up direction in Figure 18 shows the same satellite drop around 375 seconds. Compared to the east and north direction graphs, there is more noise in the error, and it is consistent the entire time. Also, the constant bias that was evident in the other two directions is not a factor here. Again, the filter covariance matched well with the Monte Carlo results.

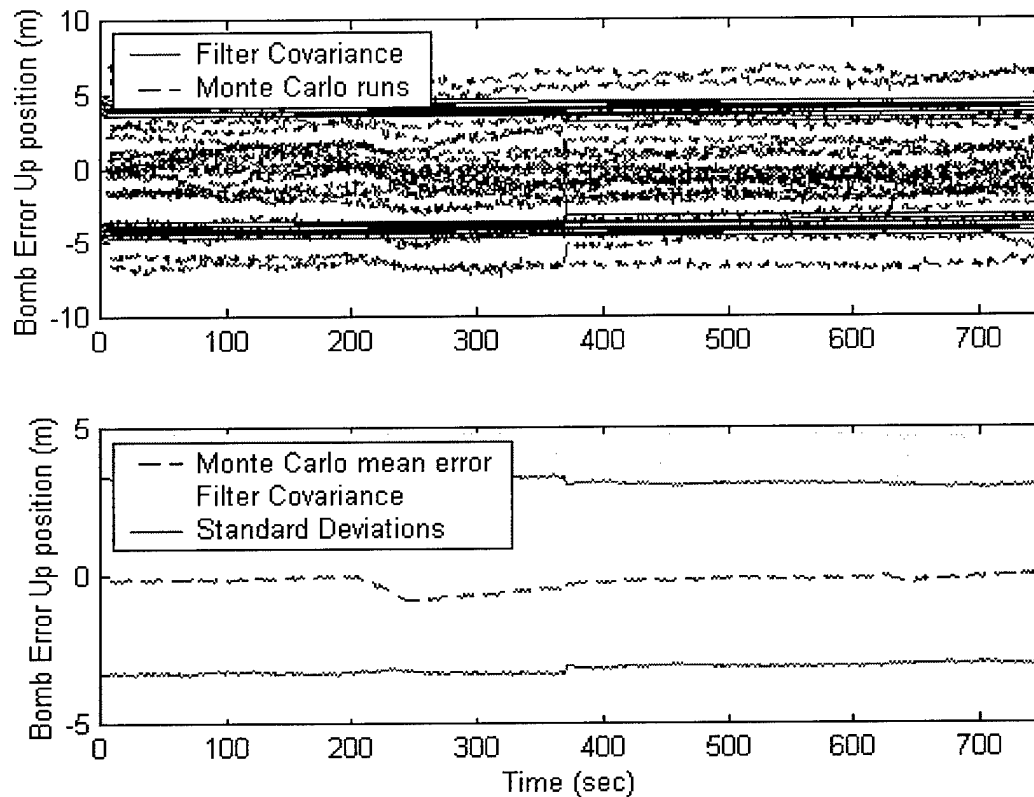


Figure 18. Error in Bomb Position – Up

Figure 19 shows the target position error for the east direction. Comparing these graphs to the position graphs of the bomb, there are several key differences. First, the position of the target comes only from the range measurements of the sensors, while the bomb positions are based on GPS (and sometimes range) measurements. The shape of the filter-computed covariance is a result of the changing geometry between the target and the sensors. The covariance drop at 620 seconds is due to the pickup of the bomb by the radar sensors, and the drop at 720 seconds is from including the atmospheric error (scale factor) in the bomb measurement model, which improves the sensor-to-target measurement accuracy. The two large changes in the mean are due to the turns of the sensors platforms.

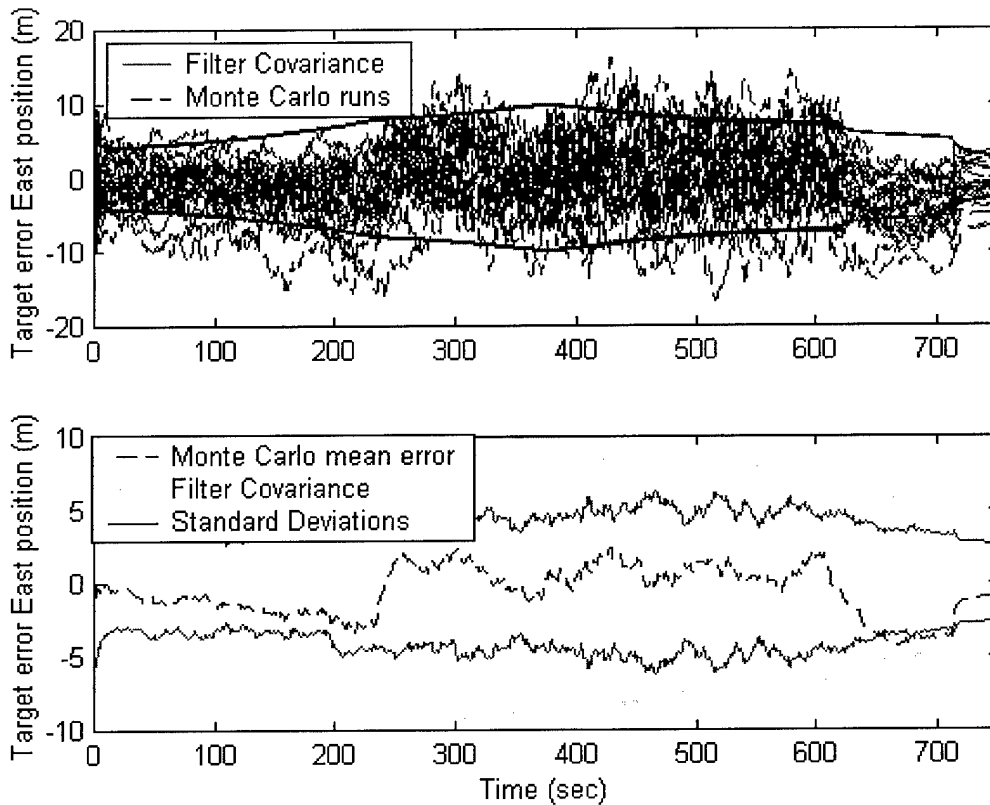


Figure 19. Error in Target Position – East

Figure 20 shows the error in the target position for the north direction, and some characteristics are similar to the north target position error. The two drops in the covariance are again due to the bomb picking up range measurements from the sensors (620 seconds) and the bomb atmosphere error estimated as the target atmosphere error (720 seconds). The steady growth of the error between 230 seconds and 600 seconds could be due to a combination of the modeling of the atmosphere error as a scale bias and geometry of the sensors. As seen in Figure 21, the true atmosphere scale factor is neither constant nor linear. Recommendations to change the model are addressed in the concluding chapter.

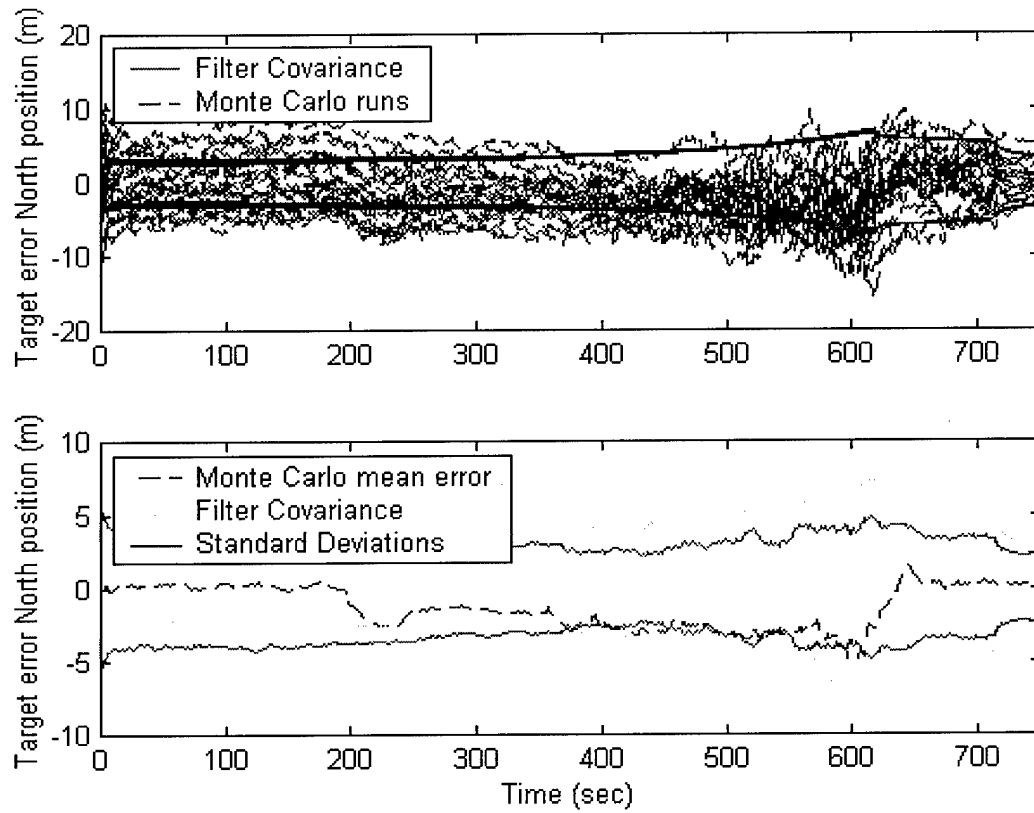
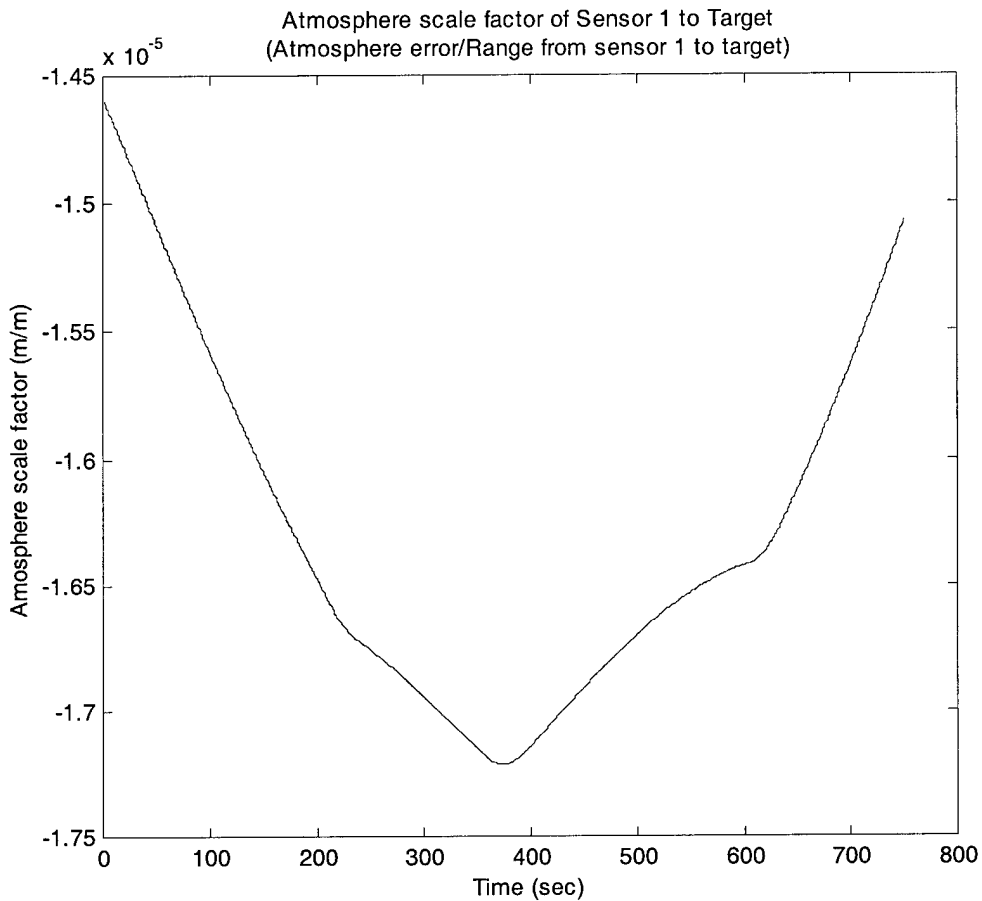


Figure 20. Error in Target Position – North



**Figure 21. Atmosphere scale factor of Sensor 1 to Target
(Atmosphere error/Range from sensor 1 to target)**

Note that the states for all the positions are fairly well tuned (i.e., filter and Monte Carlo $1-\sigma$ values are similar). However this is not the case for all the states. Figure 22 gives an example of the east acceleration state of the bomb. The covariance is much greater than the $1-\sigma$ values. This is not necessarily bad tuning. In an operational filter, the acceleration state process noise is often set conservatively high to ensure that any unexpected acceleration can be tracked by the filter [31]. However, to get more optimal performance of the filter, all states should be correctly tuned.

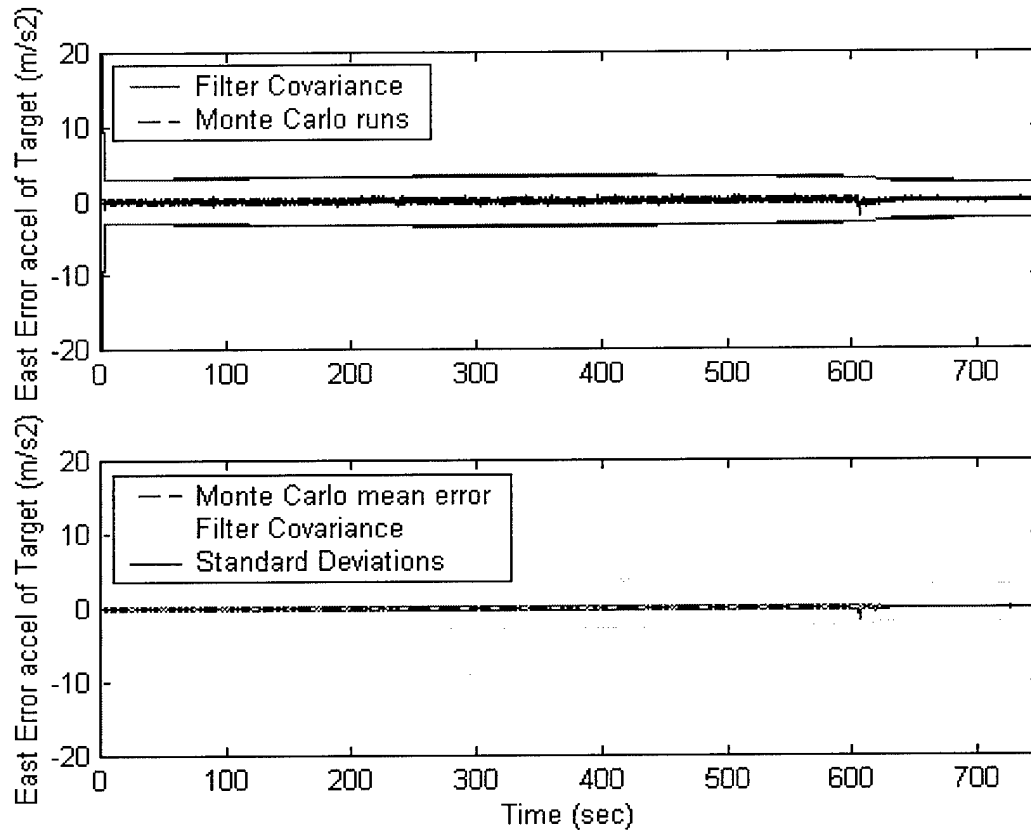


Figure 22. Error in Target Acceleration – East

4.4. Filter Parameters and Case Definitions

For these simulations, there are three parameters of concern: 1) the number of GPS satellites used to produce the navigation solutions, 2) whether or not to estimate the common satellite errors, and 3) whether or not to track the munition with the same radar sensors that are tracking the target. Each of these parameters will now be addressed.

4.4.1. Number of GPS satellites

Regarding the number of satellites, there are three different modes. The first mode is an all-in-view satellite navigation solution. In this mode each receiver uses all visible satellites (any satellite above 5° is considered visible). In the second mode, measurements from two satellites are removed for each receiver. With the dynamics of

the sensor platforms it is quite possible that all visible will not be utilized by the receiver. In the last mode, only four satellites are used to find the solution. This mode simulates most current military receivers, which only track 4 satellites. Like military receivers, only combinations of 4 satellites that result in a good satellite geometry (i.e., that have low Dilute of Precision, or DOP, values) are used.

4.4.2. *Estimating the SV Errors*

As described in Section 2.4, each satellite has errors (ephemeris and clock). These errors are common to receivers that are in close proximity. Estimating these errors should improve the position estimates. When included, the common satellite errors are modeled in states 42 through the end of the state vector (see Table 4).

4.4.3. *Tracking the Bomb and Target*

The benefit of tracking both the bomb and the target with the same sensor is that the errors of the SAR range measurements are correlated, so they can be observed and removed by tracking the bomb (which has a GPS-based position). The SAR range atmospheric error is determined by the amount of atmosphere the signal must travel through. As the bomb approaches the target, the amount of atmosphere between the sensor and the bomb begins to match the atmosphere from the sensor to the target. Therefore the error in the sensor-to-bomb signal and the error in the sensor-to-target signal become more correlated. Since both the sensor and the bomb have relatively precise, GPS-based positions, the distance between them is accurately known as well. The filter can use this information to determine the atmospheric error between the sensor and the bomb, and because of the correlation, information about the sensor-to-target atmospheric error is obtained.

4.4.4. Case Descriptions

By varying the number of satellites, whether or not the satellite common errors are modeled, and whether or not the bomb is tracked by the radar signal, 12 cases were created. Table 5 shows each of the 12 cases.

Table 5. Case Descriptions

Bomb Tracking	SV Error Model	Case 1	Case 5	Case 9
	No SV Error Model	Case 2	Case 6	Case 10
No Bomb Tracking	SV Error Model	Case 3	Case 7	Case 11
	No SV Error Model	Case 4	Case 8	Case 12
		All SVs	Limited SVs 2 fewer SVs per receiver	Limited SVs Total of 4 SVs per receiver

Before the all results are summarized, data from case 1 will be presented to give an example of how the statistics are calculated.

4.4.5. Case 1 – All Satellites, Modeling Satellite Error, Bomb Tracking

The following figures present the results for case 1 in graphical form. Each figure has two graphs: 1) the Monte Carlo runs with the filter-computed $1-\sigma$ bounds, and 2) the mean error and standard deviation from the Monte Carlo runs, along with the filter-computed standard deviation.

Figure 23 shows the East error for the bomb-to-target vector. Looking at the second plot, a large change in the mean occurs approximately at 230 seconds, 620 seconds, and 700 seconds. The first time reflects the first dynamic turn that the sensors perform. The second time, 620 seconds, marks the release of the bomb. The third time marks the time

that the SAR atmosphere range error is applied to the bomb. This is significant because the SAR atmosphere error is now correlated between the target and bomb, resulting in a better estimation. In previous filter implementations, the SAR atmosphere estimate was applied to both the target and bomb. However, the errors in the SAR atmosphere error were significantly wrong. When the SAR atmosphere errors were applied to the bomb only after it was lower than an altitude of 4000 meters, the errors were more reasonable.

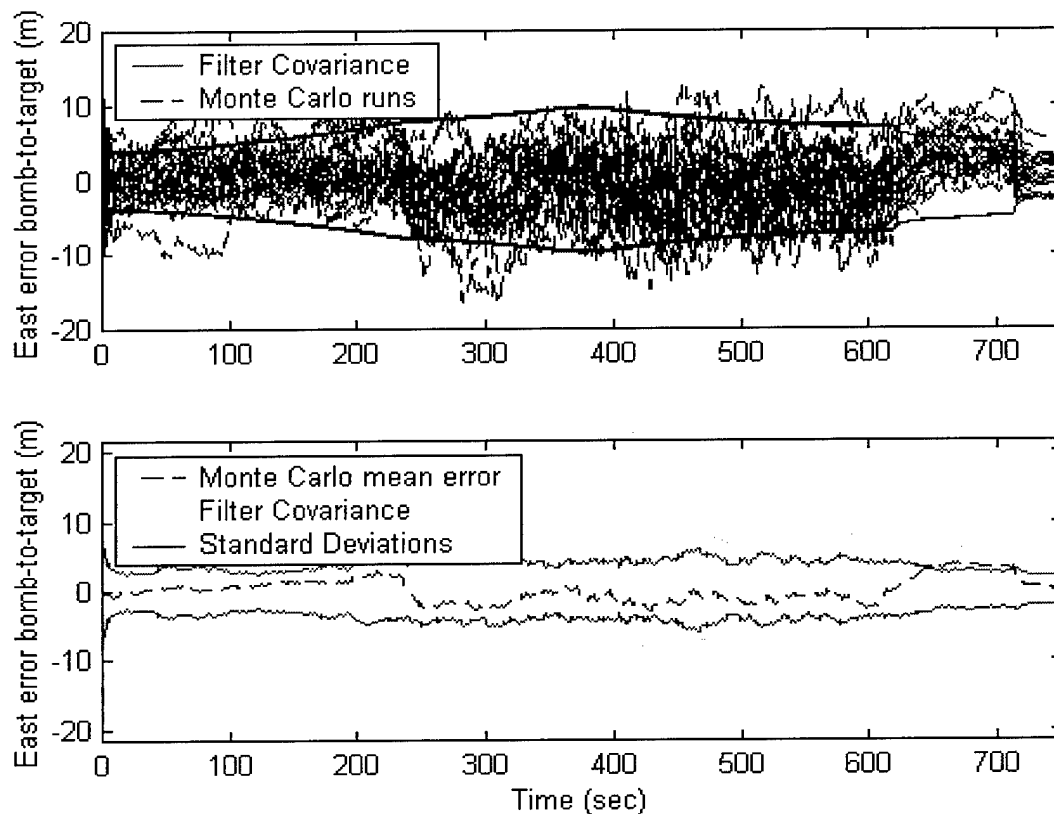


Figure 23. Case 1- East Error for Bomb-to-Target Vector

Figure 24 shows the north errors in the bomb-to-target vector. For the north error, the mean also changes at the first two specified times. In comparing the amount east error with the north, the north error is less. This is due to the geometry of the sensors relative

to the bomb and target. Recall that both sensors are always to the south of the bomb and target (see Figure 9). Therefore, the range measurements provide more information about the north than the east axis.

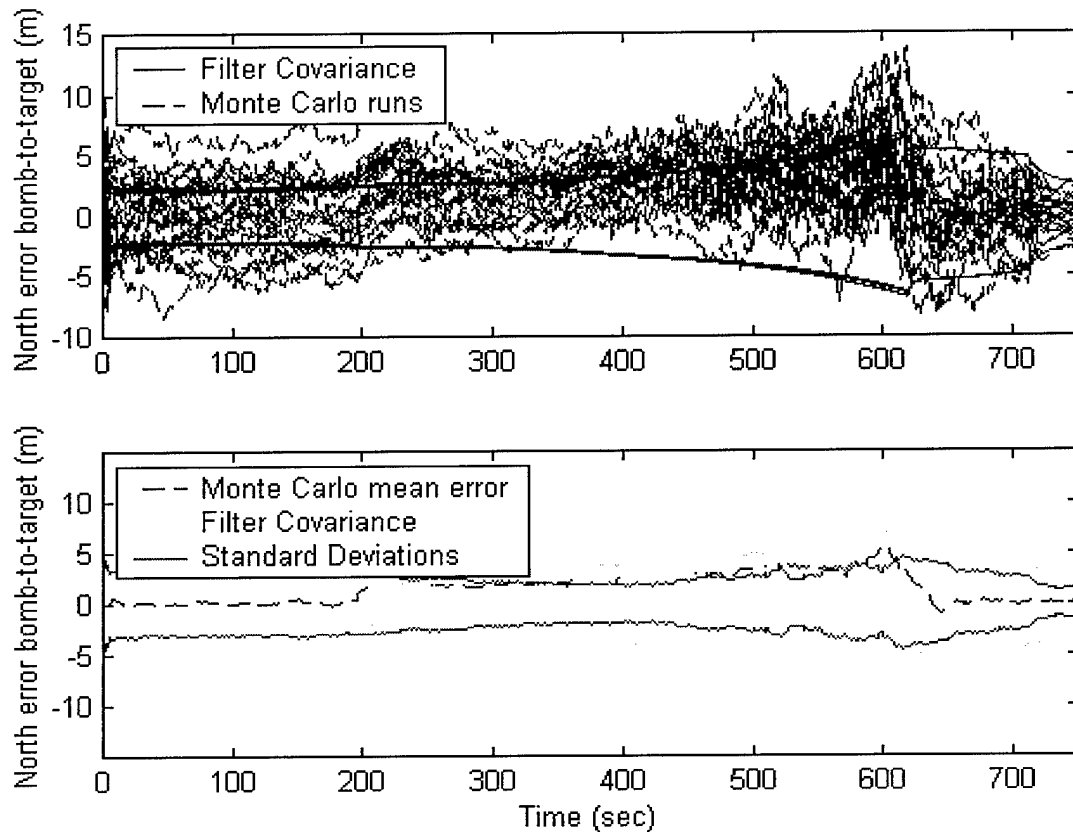


Figure 24. Case 1-North Error Bomb-to-Target

The up direction Monte Carlo runs, shown in Figure 24, have less biased errors and much higher standard deviations than the horizontal axes. This is due to the DTED error, which is a randomly chosen constant for each run. Had the DTED error been ignored, then the results would show less bias (the $1-\sigma$ DTED error value is 10m.)

The graphs from the other 11 cases are available in the Appendix.

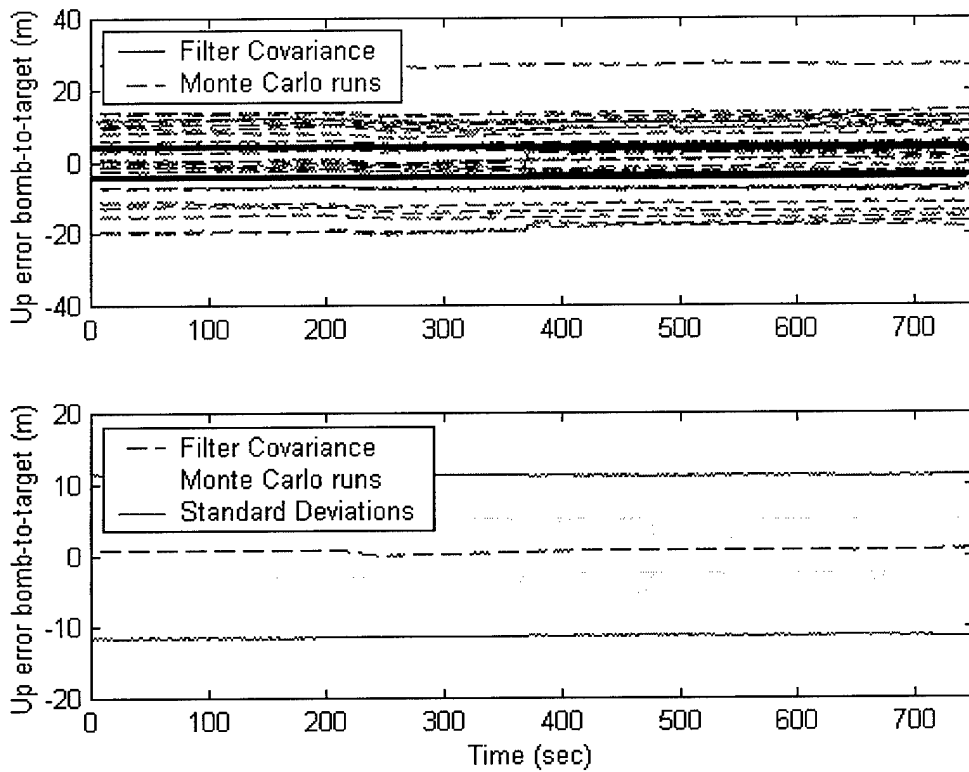


Figure 25. Case 1- Up Error Bomb-to-Target

4.5. Results Summary

To summarize the results of the simulations, the statistics of the various cases have been put into tabular form in order to facilitate comparison. These statistics include the bomb-to-target error means and standard deviations in the ENU frame, the error DRMS in the East and North axis (horizontal), and the Mean Radial Spherical Error (MSRE) in all three axes. Because this is a bomb application, a “terminal period” is specified (defined as the last 50 seconds of the bomb flight). This period is chosen because the final approach is crucial to the navigation solution of a bomb. In order to produce a single number for the whole terminal period, the mean errors are averaged over the time period, and RMS values of the standard deviations, DRMS, and MRSE errors are

calculated over the terminal period. (These RMS values are essentially “average” values for those statistical measures).

The first section (below) compares the four cases with all-in-view satellites solutions. The next section compares the limited satellite cases where two satellites have been pulled from the solution. Thirdly, the four satellite cases are compared. Finally, cross comparisons between the different satellite cases, the bomb tracking, and satellite model estimation are addressed.

4.5.1. All-in-View Satellite Cases

The all-in-view satellite cases are cases 1 through 4. The results are found in Table 7.

Table 6. All-in-view Satellite Cases (1-4)

Case	SV used	Bomb Track?	SV error modeled?	East (m)		North (m)		Up (m)		DRMS (m)	MRSE (m)
				mean	std	mean	std	mean	std		
1	All	Yes	Yes	1.30	2.38	0.05	1.90	0.95	11.32	3.45	11.65
2	All	Yes	No	1.17	2.26	-0.31	2.04	-1.21	11.38	3.46	11.74
3	All	No	Yes	3.75	3.56	-0.39	3.18	2.33	12.47	6.01	13.82
4	All	No	No	3.47	3.55	-0.97	3.17	-1.20	9.72	5.90	11.27

In examining the table, the results provide some insight into whether to estimate the common satellite errors and whether to track the bomb.

Tracking the bomb gives a definite increase in accuracy. When tracking the bomb, the mean error decreases from 3.75 m to 1.30 m in the east direction (see case 3 to case1). Similar results are for the comparison of case 4 to case 2. Tracking also improves the standard deviation values. In tracking the bomb, the standard deviation went from 3.18 meters to 1.90 meters for the north direction. The total DRMS (horizontal) decrease from about 6m to approximately 3.5m is about a 2.5 meter jump in accuracy.

Estimating the satellite errors yields no overall improvement in accuracy in this case. However, it is interesting that the mean errors in the north direction were significantly lower when estimating the satellite errors. For example, the mean error went from -0.3051m to -0.0478m from case 2 to case 1 and -0.97m to -0.39m from case 4 to case 3. There is no obvious reason for this fact, but it could be due to the geometry of sensors and allowing them to take full advantage of what little improvement estimating the satellite errors provide. Also the mean in the east are all positive and biased. This again is the result of the geometry of the sensors.

The up direction does not give much information on the benefits of estimating the satellite errors or tracking the bomb because the DETD error dominates the results. The true height for each case is zero. If the DTED error is close to zero, then the amount of error caused by the DTED estimation is low. To prove this point, the actual DTED errors of the four cases were examined. From this observation, the reason that case 4 has the best results is because case 4 had lower DTED errors than the other cases. Had the DTED errors been forced to be the same for each of test cases, the results would probably be less random and could give some insight on the impact of the parameters in the up direction. However, because the bomb is expected to come in vertically, the impact of the error in the up direction is reduced. For this reason, the results of the up direction and the MRSE will not be included in future tables.

4.5.2. *Limited (-2) Satellite Cases*

Table 7 presents the results of the first limited satellite case, where 2 satellites are removed from each receiver. The results in case 2 are similar to the results in the full satellite cases. The bias in the east direction is again a product of the geometry of the sensor platforms.

Table 7. Limited (-2) Satellite Cases (5-8)

Case	SVs used	Bomb Track?	SV error modeled?	East (m)		North (m)		DRMS (m)
				mean	std	mean	std	
5	-2	Yes	Yes	1.24	2.26	0.11	1.94	3.37
6	-2	Yes	No	1.51	2.62	0.20	1.94	3.71
7	-2	No	Yes	3.37	3.50	-0.68	3.54	5.98
8	-2	No	No	4.22	3.10	-0.35	3.75	6.39

4.5.3. Limited 4 Satellite Cases

Table 8 presents the results of the cases where only 4 satellites measurements are used by each receiver.

Table 8. Limited (only 4) Satellite Cases (9-12)

Case	SVs used	Bomb Track?	SV error modeled?	East (m)		North (m)		DRMS (m)
				mean	std	Mean	std	
9	4	Yes	Yes	1.87	3.10	-0.57	3.23	5.08
10	4	Yes	No	1.59	3.50	-0.71	3.45	5.32
11	4	No	Yes	1.76	3.74	-0.86	3.64	5.63
12	4	No	No	6.12	10.01	-2.90	9.36	15.07

While the first two satellite sets were pretty much the same, the four satellite set results have a few significant differences. The improvement in accuracy for tracking the bomb is not as good, going 5.63m to 5.08m DRMS. The overall accuracy is along the same lines as the all-in-view and minus 2 satellite cases. The results of case 12 are not in line with the other results. All cases on this table used the same data sets, so the only difference is how the filter is implemented. This would imply that there is a significant benefit in modeling the satellite errors in the 4-satellite case, especially when the bomb is not tracked. However, looking at the graphs of results of case 12 in the Appendix, there

seems to be only two or three runs that are out-of-family. Further analysis, to include more runs would be necessary before a definite conclusion could be given.

4.5.4. Case Summary

Table 10 shows the results for all cases. The cases are organized according to whether the bomb is tracked and the satellite common error is estimated.

Table 9. All Cases Summary

Case	SVs used	Bomb Track ?	SV error modeled?	East (m)		North (m)		DRMS (m)
				mean	Std	mean	std	
1	All	Yes	Yes	1.30	2.38	0.05	1.90	3.45
5	-2	Yes	Yes	1.24	2.26	0.11	1.94	3.37
9	4	Yes	Yes	1.87	3.10	-0.57	3.23	5.08
2	All	Yes	No	1.17	2.26	-0.31	2.04	3.46
6	-2	Yes	No	1.51	2.62	0.20	1.94	3.71
10	4	Yes	No	1.59	3.50	-0.71	3.45	5.32
3	All	No	Yes	3.75	3.56	-0.39	3.18	6.01
7	-2	No	Yes	3.37	3.50	-0.68	3.54	5.98
11	4	No	Yes	1.76	3.74	-0.86	3.64	5.63
4	All	No	No	3.47	3.55	-0.97	3.17	5.90
8	-2	No	No	4.22	3.10	-0.35	3.75	6.39
12	4	No	No	6.12	10.01	-2.90	9.36	15.07

Overall, the tracking of the bomb is the parameter that most improves the accuracy of the system. As the bomb is tracked, using the all or all but two satellites generally produces the same level of accuracy. Both modes are an improvement to the four satellite case; approximately 1.2 meters DRMS.

The satellite error estimation typically generally does not improve the accuracy. A vast improvement of approximately 9 meters occurred with four satellites and no bomb tracking. To confirm this, more Monte Carlo runs should be made to see if there would be a change in the value.

There is a positive bias in the east direction mean error values. This may be caused by a lack in observability issue of the states. In this system filter, there is no “absolute position” which is different than the typical differential GPS setup with a “known” reference system. One way to combat this problem would be to declare one of the receivers to be the “reference,” and all other positions are based from its position. Also a residual analysis could be conducted to determine if estimating the errors decreases the other residuals. As it stands, estimating the errors does not yield much benefit (except in the 4 satellite case), and in a real-time system, would add processing time to the calculations.

The amount of error in the up direction is sporadic. This is due to the poor implementation of the DTED errors. A better model could be used. Actual DTED data could be used and it would eliminate the entire issue.

Since the north axis is more precise than the east axis (due to the geometry of the sensors) changing the location of one or both of the sensors could increase the accuracy for both directions.

In summary, it has been shown that tracking the bomb with the same sensors that are tracking the target has a significant benefit to reducing the overall DRMS error. When comparing the all-in-view and the all but two satellites cases, there is no improvement. However, the four satellite cases had a drop in accuracy compared to the first two. Estimating the satellite errors showed no real value except in the case of four satellites and not tracking the bomb, but these results need further analysis.

5. Conclusions and Recommendations

5.1. Conclusions

Up to this point in time, most of the error analysis performed for the AMSTE program has been at the error variance level, generating root-sum-square (RSS) total errors from error budgets consisting of constant error variances. In reality, the level of error for GPS positioning and targeting systems is highly dependent upon the current environment in which it is employed (i.e., the distance between sensor and target, altitude, time of day, etc.). This thesis presented a comprehensive study of GPS errors and their effect on a differential GPS bombing system. Satellite clock, ephemeris, receiver clock, troposphere, ionosphere, receiver noise and multipath errors were all addressed. Ionospheric effects were not a concern, with the assumption that is the receiver uses ionospheric-free measurements. Of all of these errors, the most critical for the AMSTE scenario are on differential tropospheric errors and multipath. Differential tropospheric error causes problems because, even after a model is applied, the unmodeled tropospheric error is unpredictable and can increase as the baseline and height difference between the receivers increase. Regarding multipath, between 20 to 60 cm (1σ) of pseudorange multipath error is common for aircraft in flight. Also, multipath on a munition should be 10 cm or less due to the limited surface from whence the signal may bounce.

An environment model was developed which consisted of two SAR radar sensors with GPS receivers, a falling munition with a GPS receiver, the visible GPS satellite constellation, and a moving target. The environment used the true ranges and rates of all the satellites, sensor platforms, munition and target. Appropriate errors were added to the

true ranges and rates to generate simulated measurements. These simulated measurements will be used by the Kalman filter, to estimate the position and velocities of the sensors, bomb, and target.

Twelve cases were run (25 Monte Carlo runs each) in the Kalman filter. These cases involved variations in the number of satellites used in the position solution, the estimation of common satellite errors, and the tracking of the bomb to the target with the same radar sensor. The all-in-view or the minus 2 satellite mode did not change the accuracy. However, the four satellite case produced results that were not as precise or accurate.

Overall, estimating the common satellite errors did not provide significant increase in accuracy. However, in the case of 4 satellites and no bomb tracking, the estimation of the satellite errors decreased the DRMS accuracy by 10 meters.

The most beneficial mode is the tracking of the bomb with the same sensor as the target. In most cases, the horizontal DRMS accuracy improved from about 6 meters to approximately 3.5 meters, just by tracking the bomb. This improvement was due to modeling the bomb radar atmosphere error with the target atmosphere error.

5.2. Recommendations

While most of the GPS models in this thesis have been used extensively [22,36,50], the SAR model used in this research has only been used on three occasions [29,54].

The following recommendation are provided to extend this research:

1. Use a more realistic SAR model. The results of the simulations in this thesis should not be used in absolute number terms because the SAR model is not analytically correct.

2. Enhance Kalman filter to use more advanced differential setups. Carrier smoothed code and carrier-phase measurements are more accurate forms of DGPS and could increase the accuracy.
3. Include different targeting sensors. Using laser-guided sensors or other combinations of sensors could prove beneficial.
4. Change the flight profiles and number of sensors to see it affects the accuracy. By simply moving the location of the sensors, a determination on the effect of sensor geometry could be explored. Additionally, changing the number of sensors and the rate at which the sensors provide data are ways to improve the efficiency of the resources. A GPS jamming scenario where the bomb loses GPS and only sensor measurements are used could also prove beneficial.
5. Track the bomb with only one sensor and vary the tracking rates.
6. Include INS data with the GPS measurements. This would allow for a large jamming scenario. Also, different integration techniques (loose, tight, ultra-tight) could be explored.
7. Increase the complexity of the target. For this research, a basic model was used. A more advanced model of the target could include stops or continuity jumps in the sensor data. The length and times of these jumps could effect the accuracy.
8. Tune the Kalman filter to obtain optimal performance. A single scenario could be run under different \mathbf{Q} and \mathbf{R} values to find the best accuracy.
9. Add more Monte Carlo runs. You can never have too many Monte Carlo runs.
10. Use real DTED data. Real DTED data would ensure that the effects of DTED errors are accurately reflected in the results.

11. Designate one of the receivers as the “master receiver”. The master receiver would have all other elements referenced to it. This may reduce the observability concerns that effected the usefulness in estimating the satellite errors.

Appendix Graphs of the Bomb-to-Target (Cases 2-12)

This appendix contains the graphs of the other 11 cases for the bomb-to-target vector.

Case 1 is shown in Section 4.4.5.

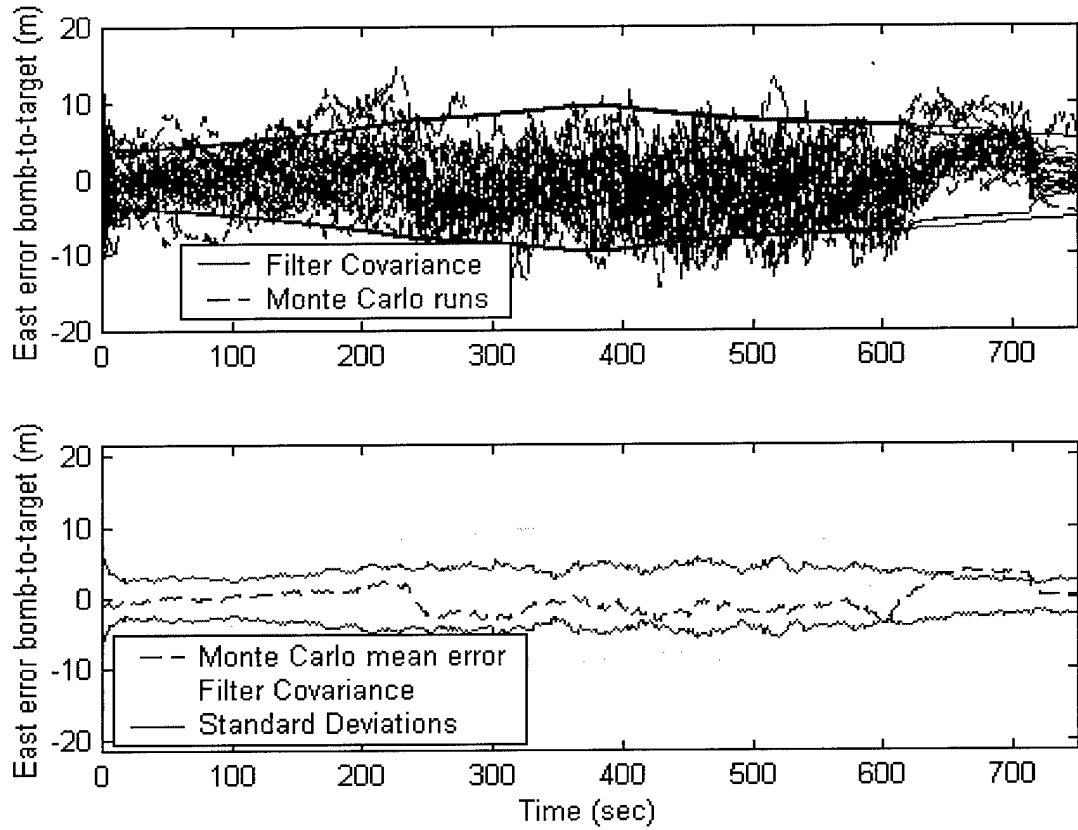


Figure 26. Case 2 - East Error Bomb-to-Target

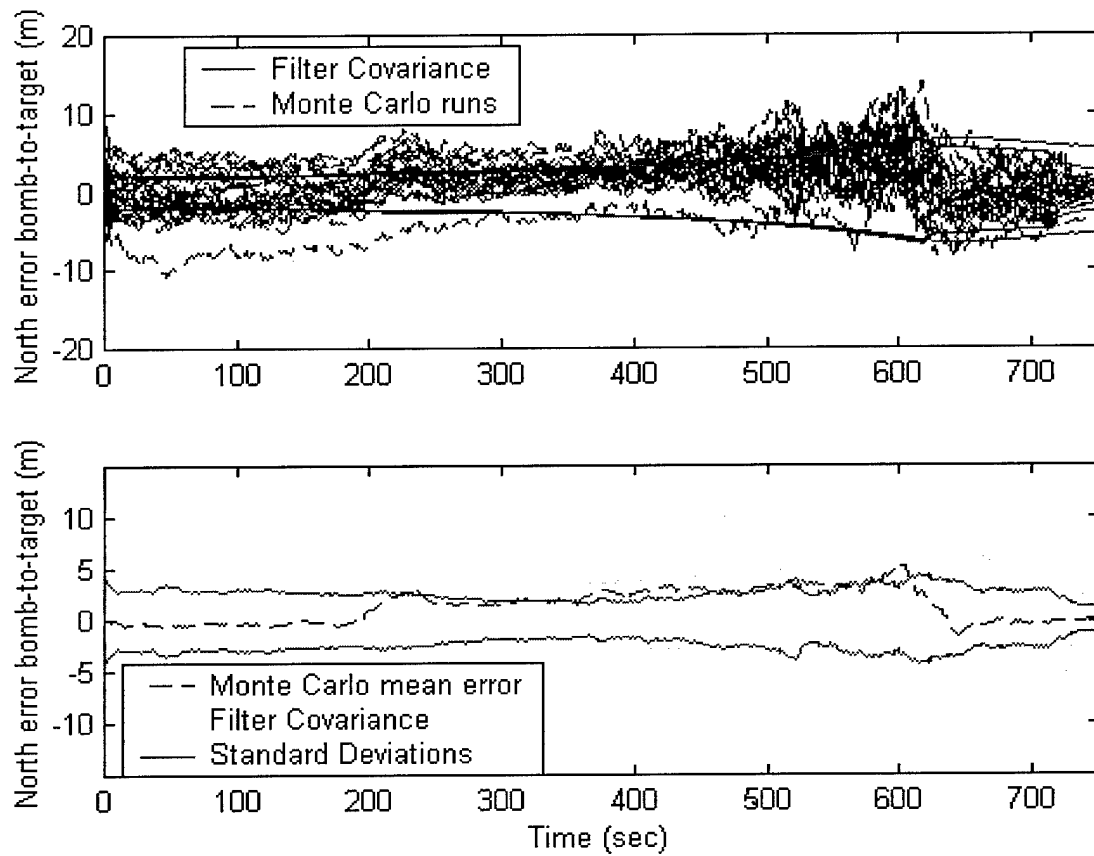


Figure 27. Case 2- North Error Bomb-to-Target

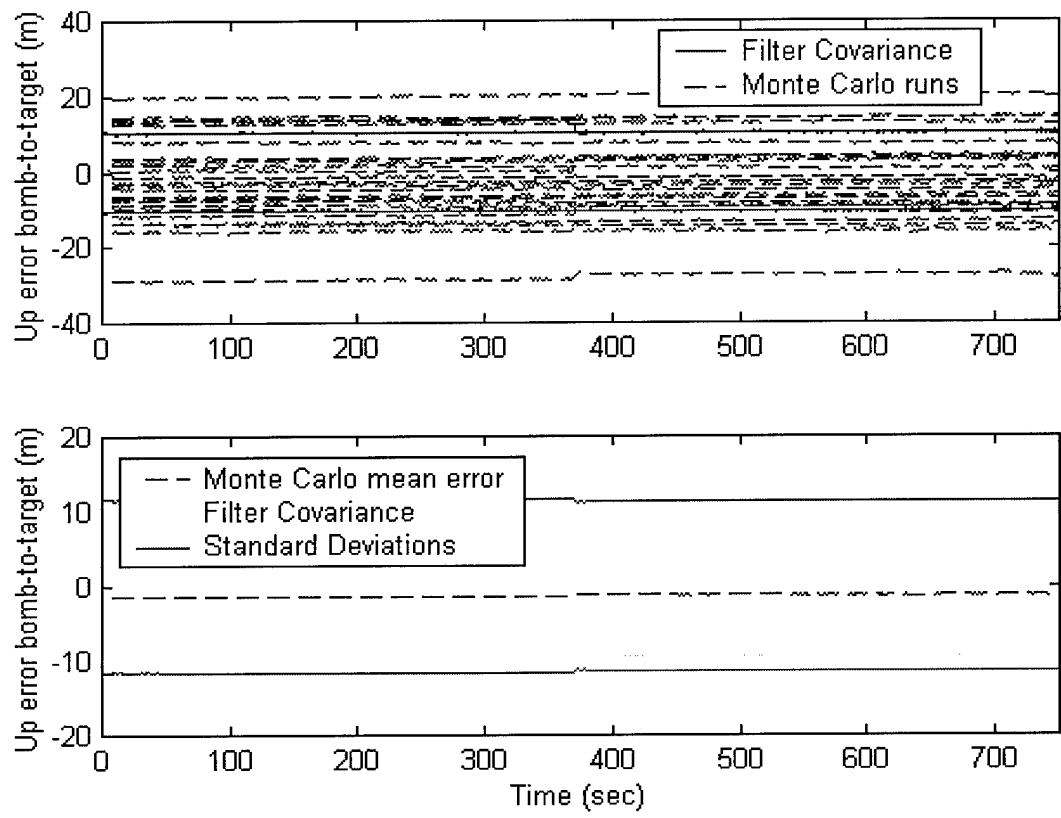


Figure 28. Case 2- Up Error Bomb-to-Target

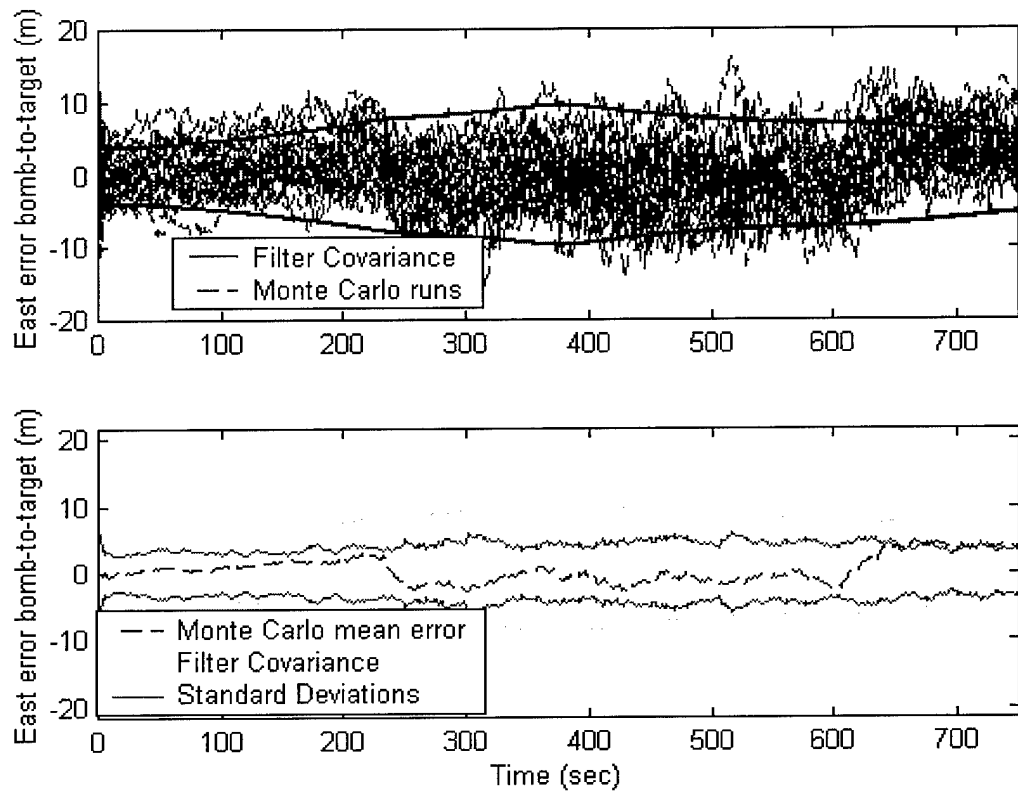


Figure 29. Case 3- East Error Bomb-to-Target

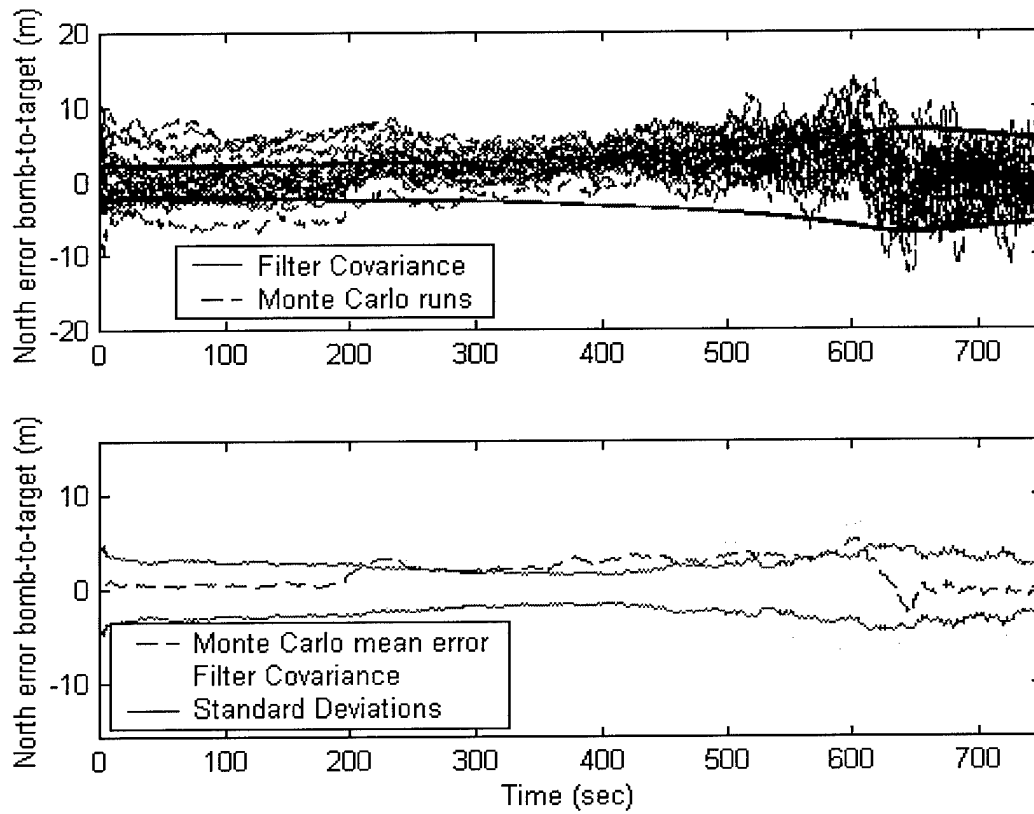


Figure 30. Case 3- North Error Bomb-to-Target

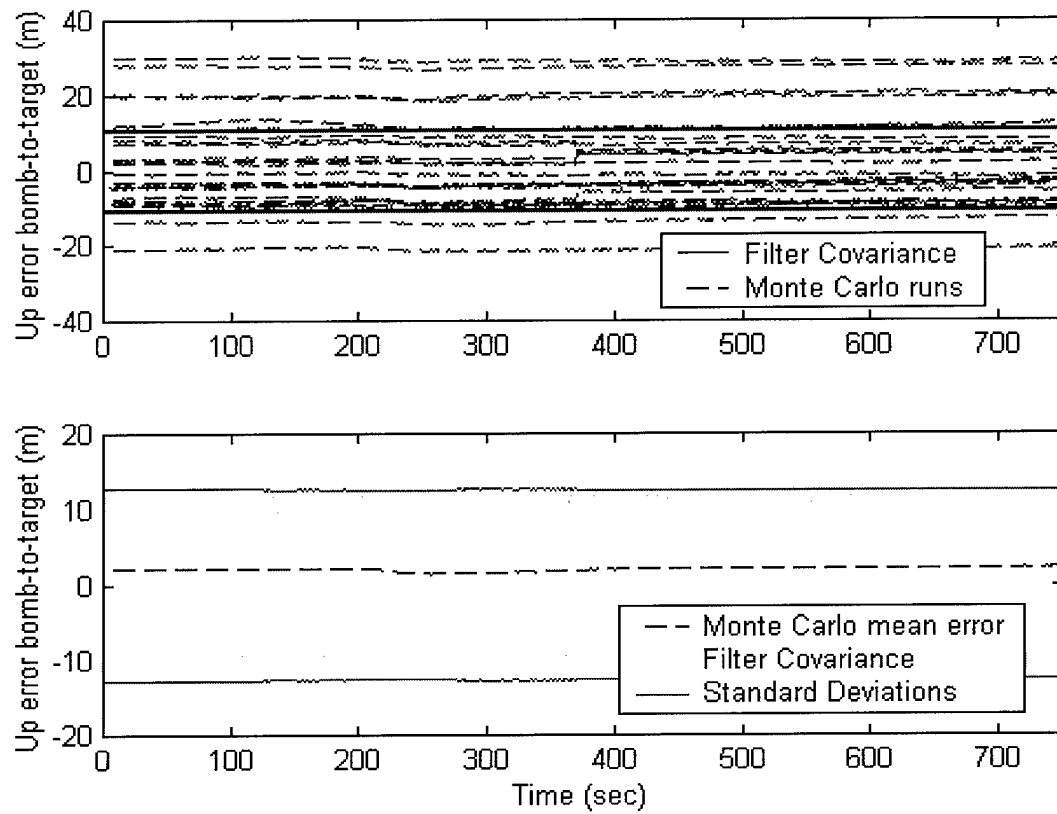


Figure 31. Case 3- Up Error Bomb-to-Target

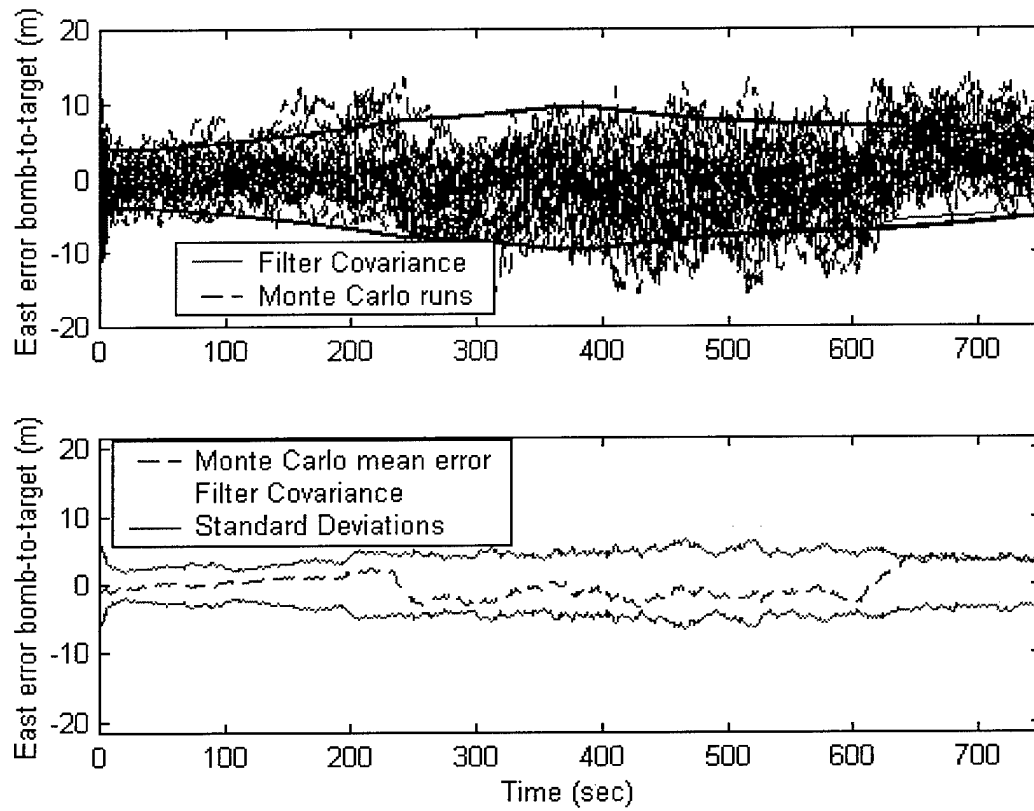


Figure 32. Case 4- East Error Bomb-to-Target

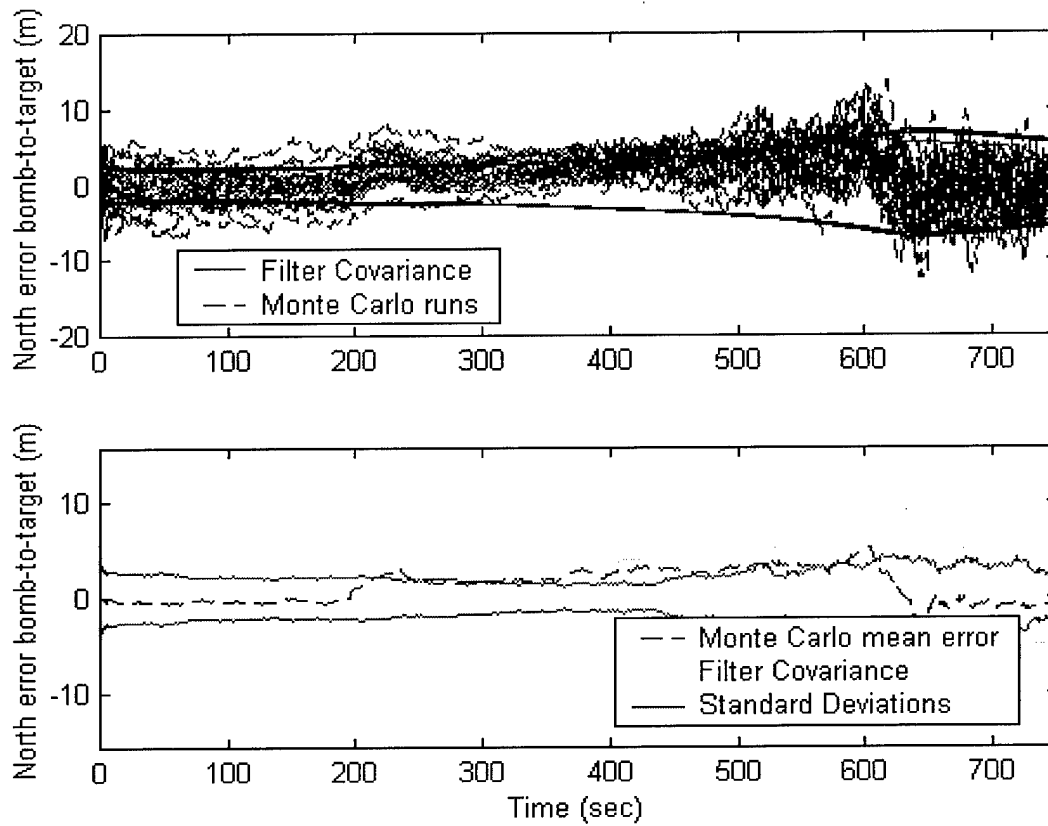


Figure 33. Case 4- North Error Bomb-to-Target

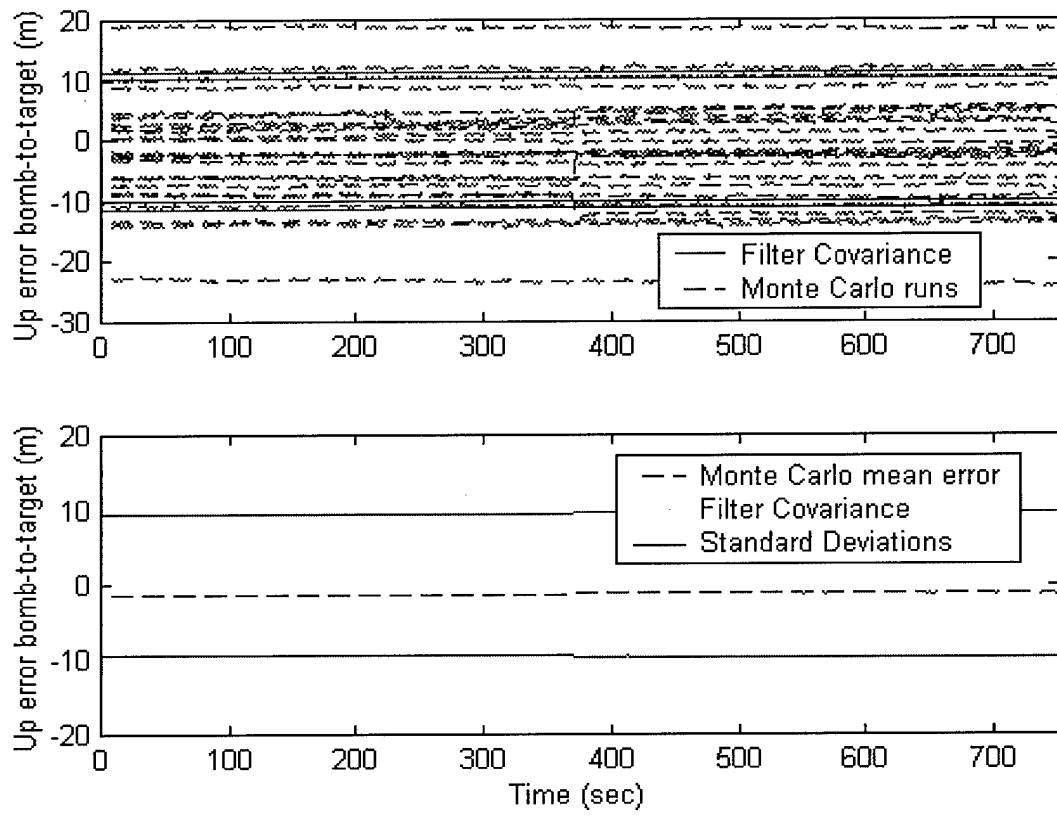


Figure 34. Case 4- Up Error Bomb-to-Target

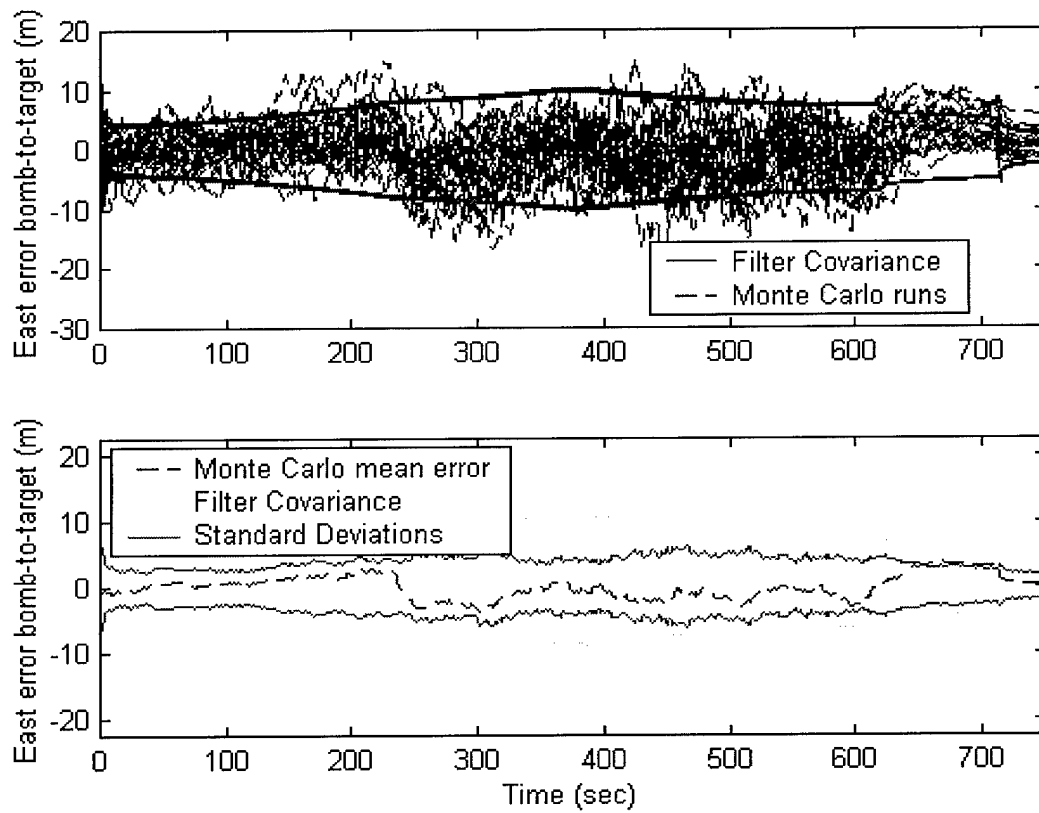


Figure 35. Case 5 – East Error Bomb-to-Target

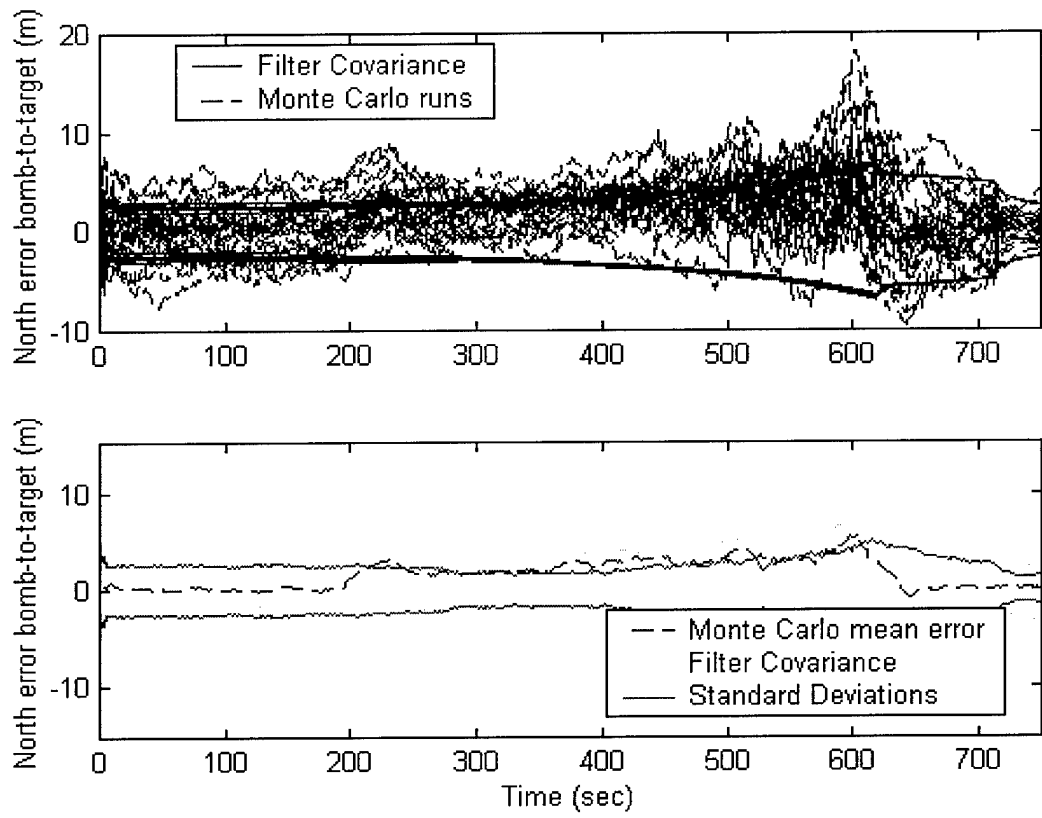


Figure 36. Case 5 – North Error Bomb-to-Target

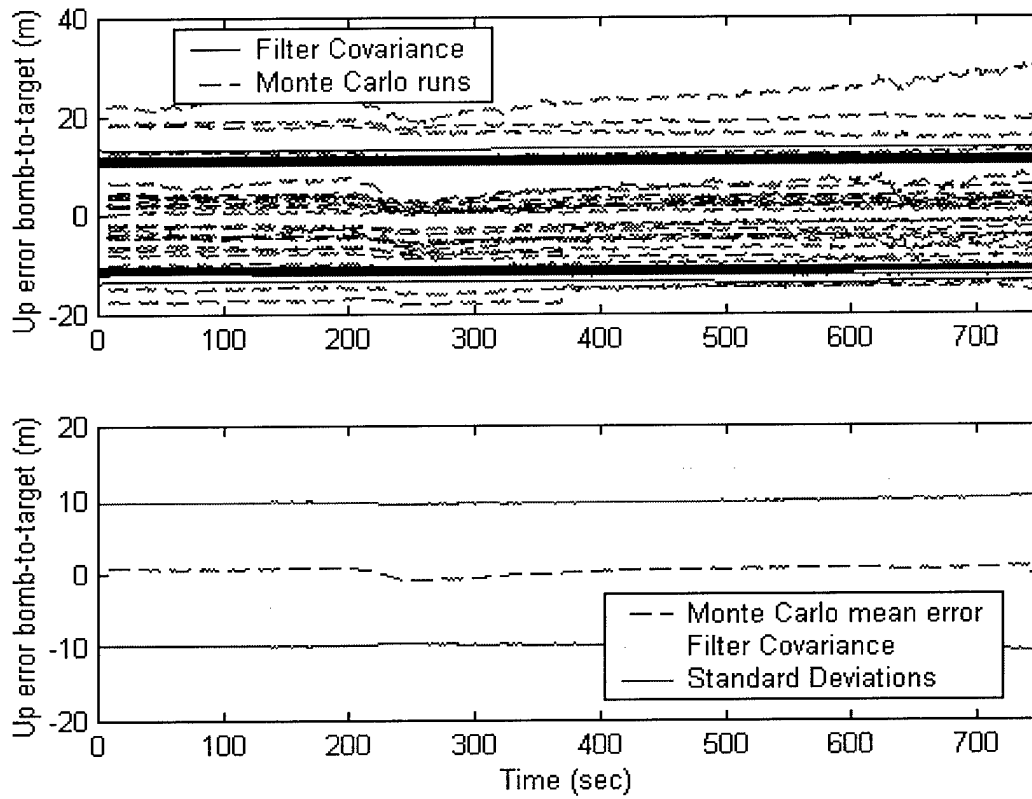


Figure 37. Case 5 – Up Error Bomb-to-Target

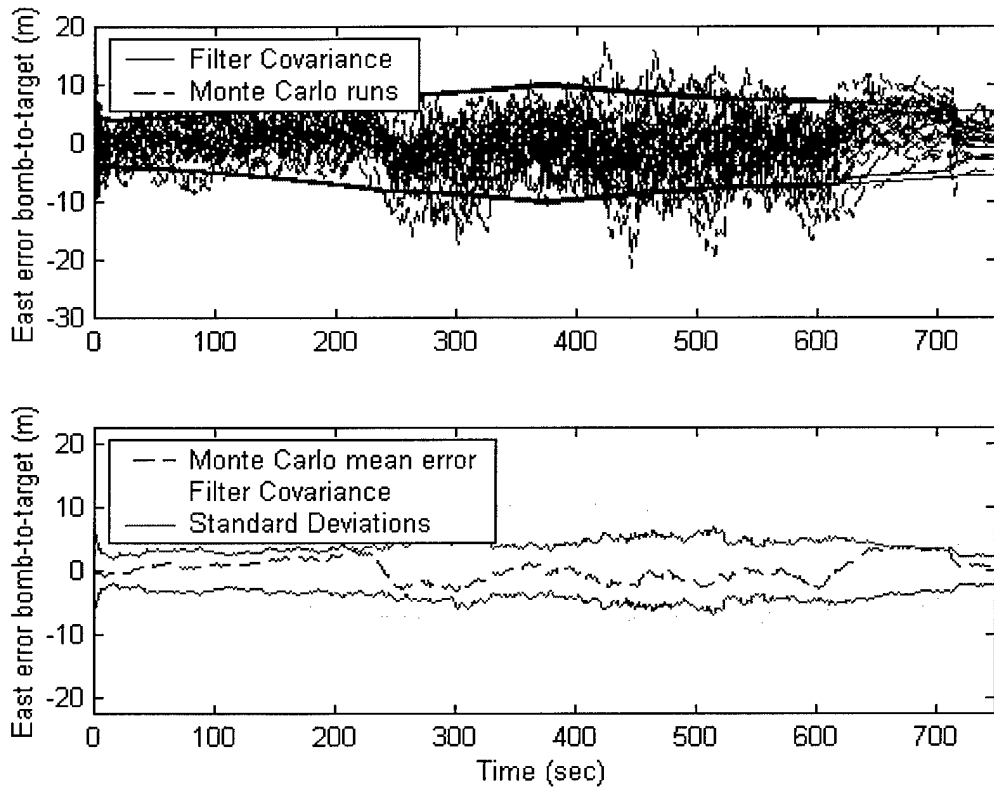


Figure 38. Case 6 – East Error Bomb-to-Target

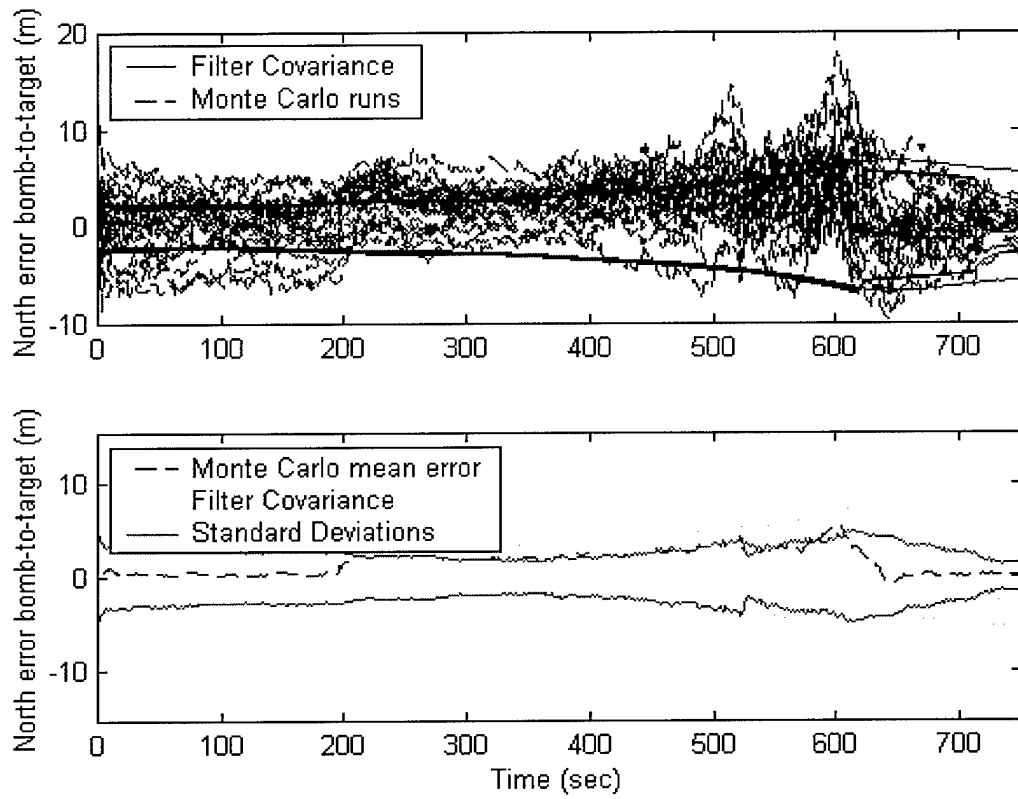


Figure 39. Case 6 – North Error Bomb-to-Target

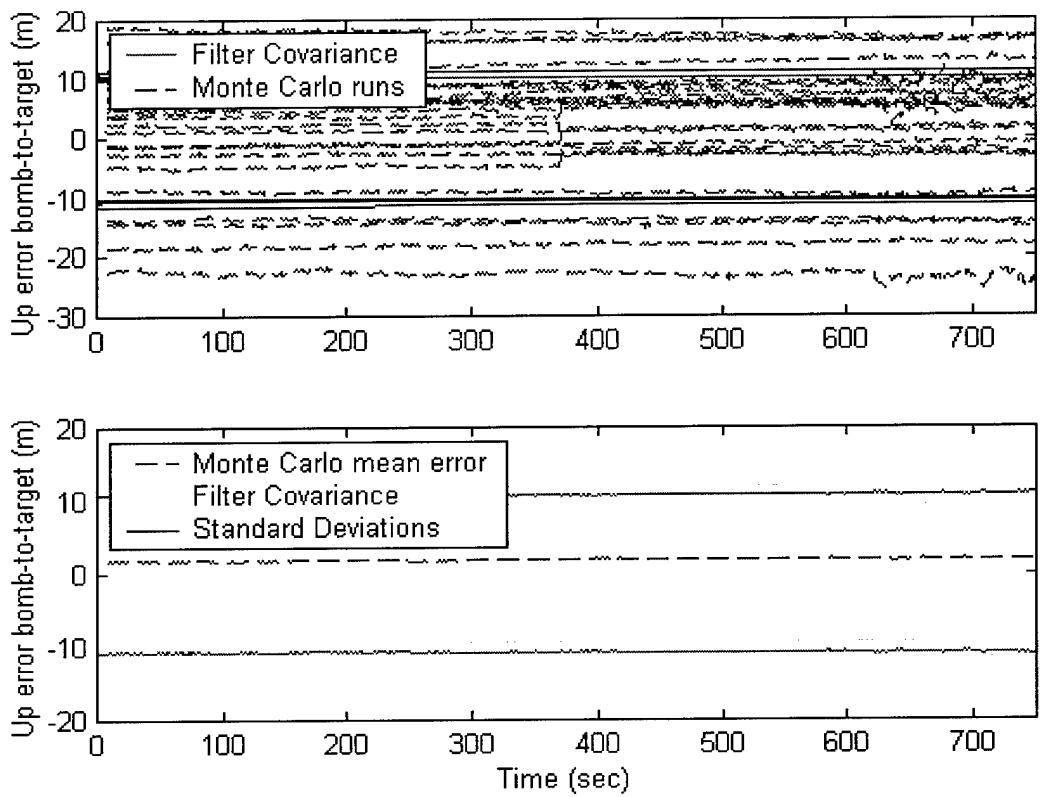


Figure 40. Case 6 – Up Error Bomb-to-Target

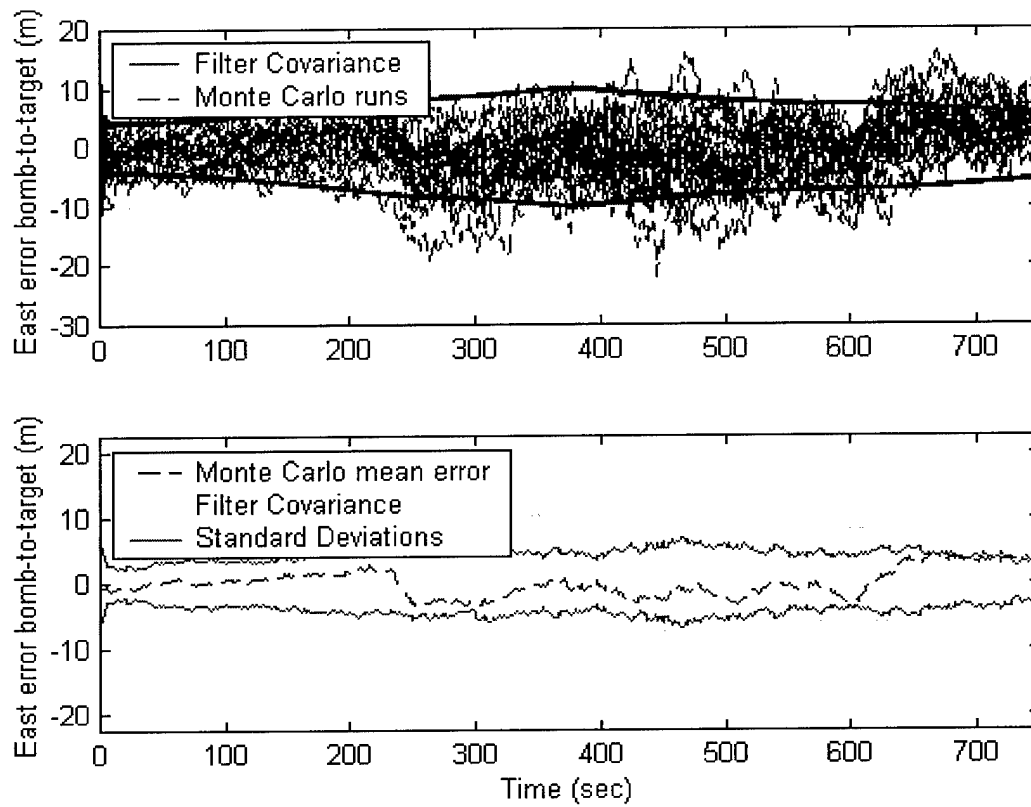


Figure 41. Case 7 – East Error Bomb-to-Target

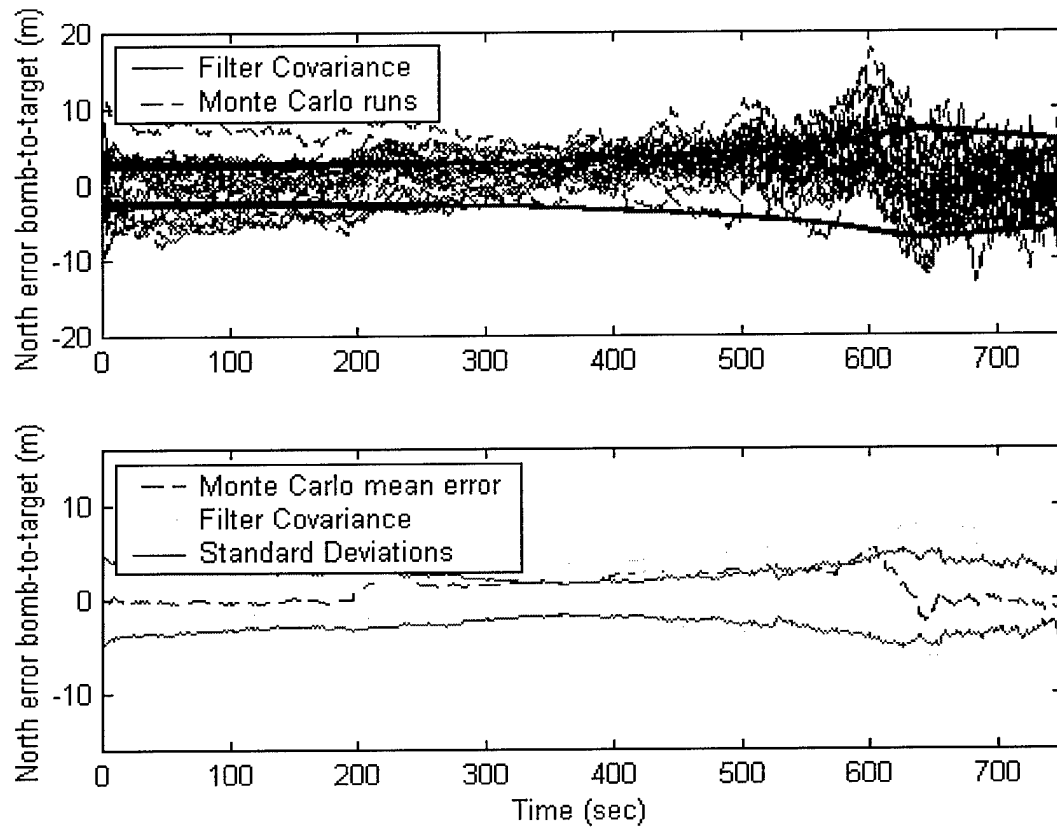


Figure 42. Case 7 – North Error Bomb-to-Target

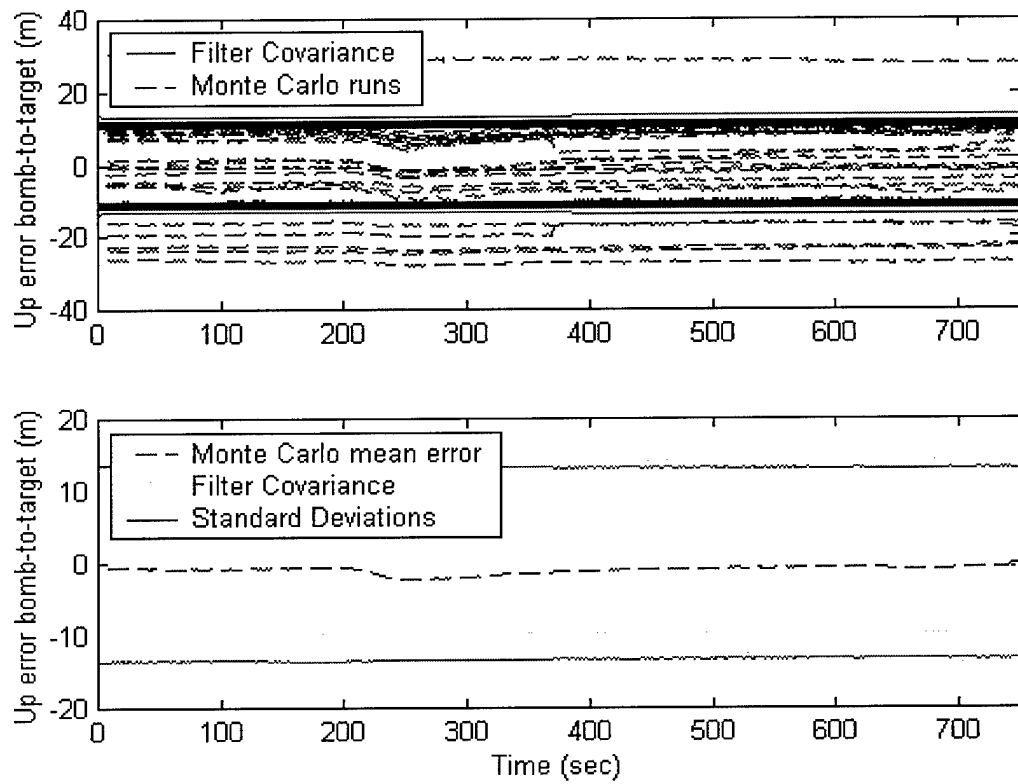


Figure 43. Case 7 – Up Error Bomb-to-Target

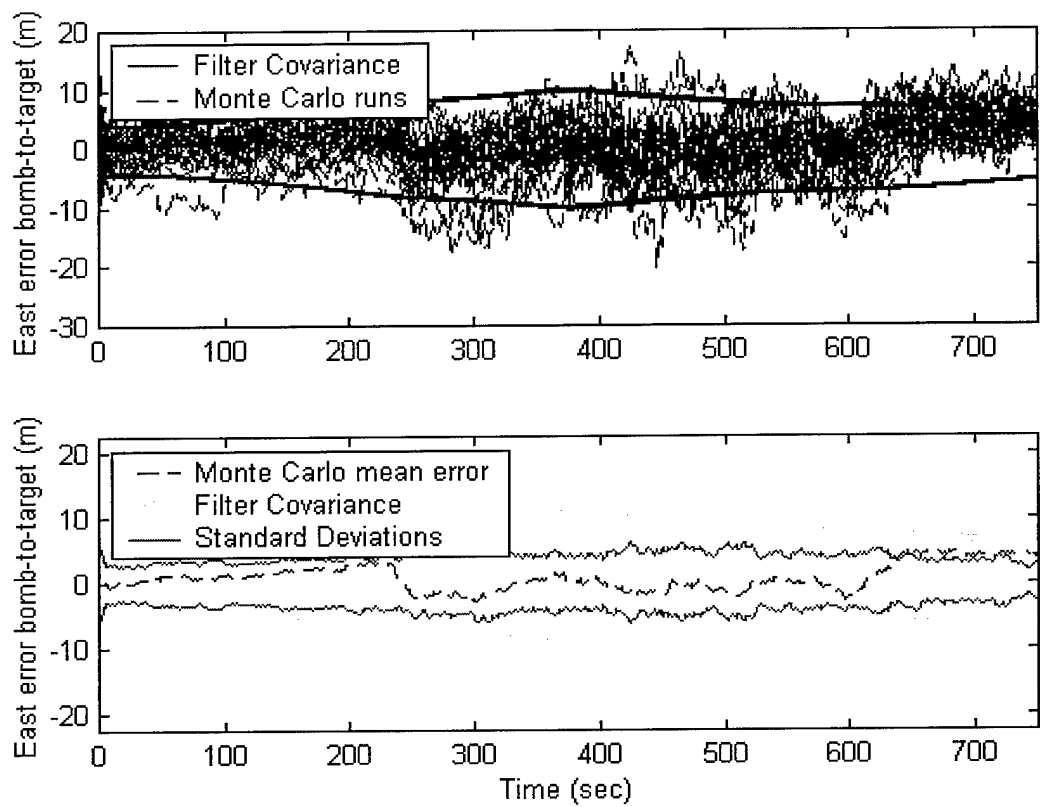


Figure 44. Case 8 – East Error Bomb-to-Target

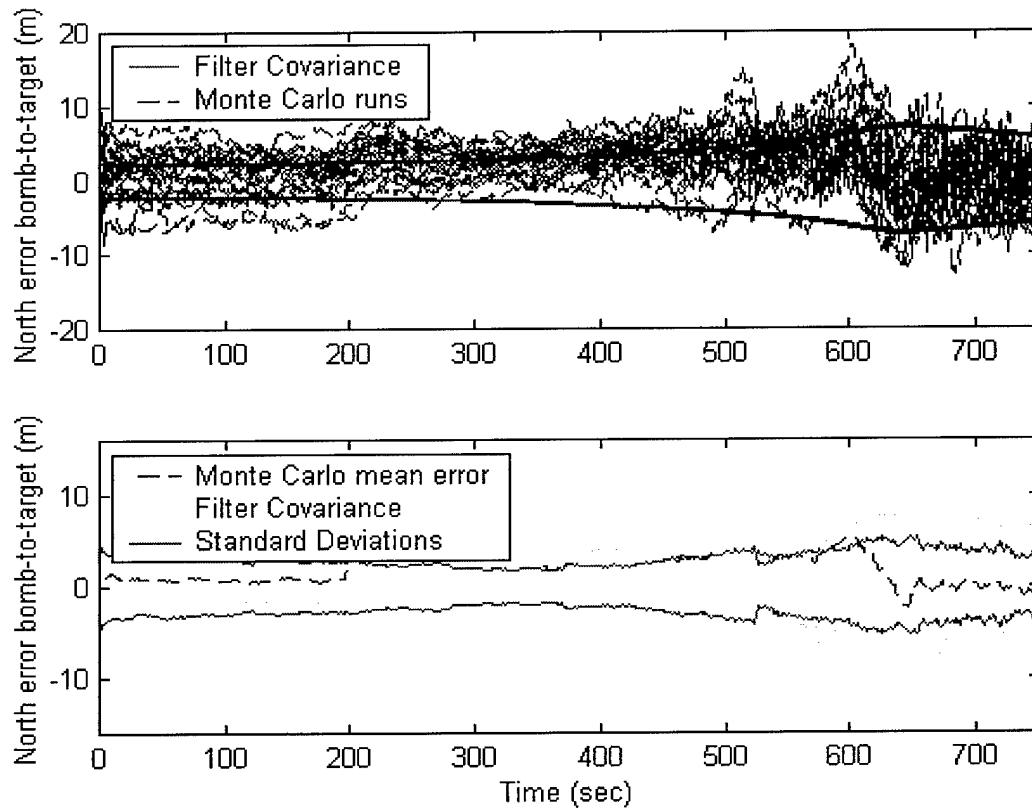


Figure 45. Case 8 – North Error Bomb-to-Target

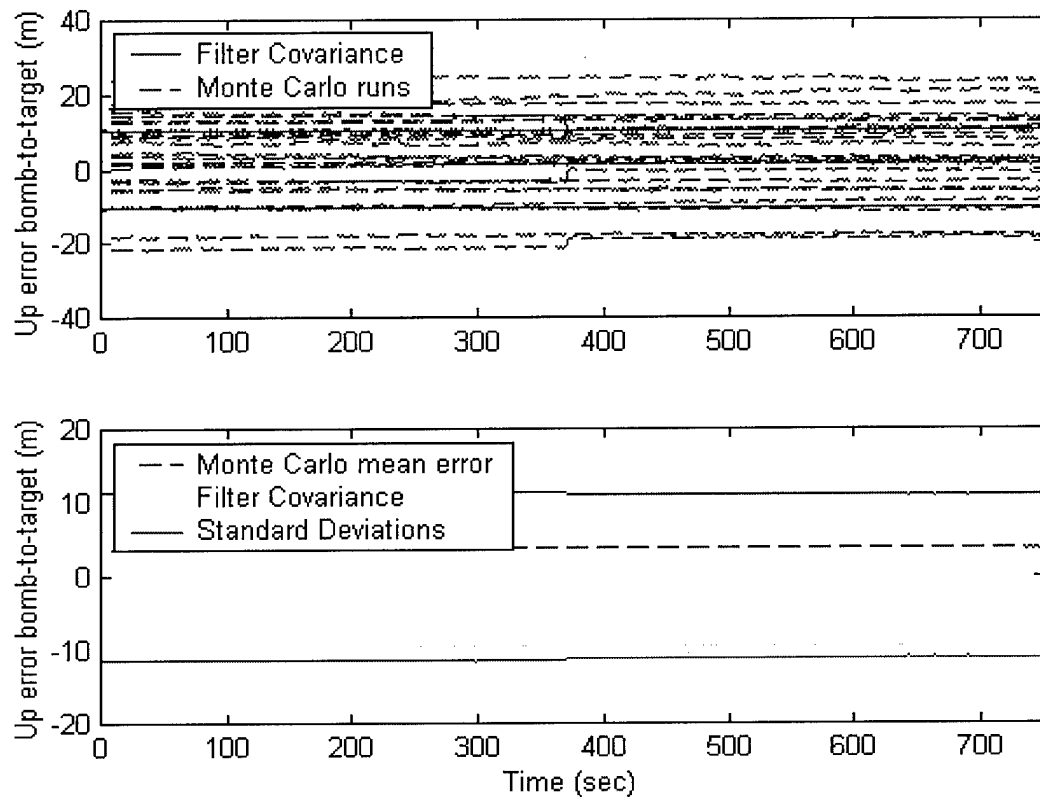


Figure 46. Case 8 – Up Error Bomb-to-Target

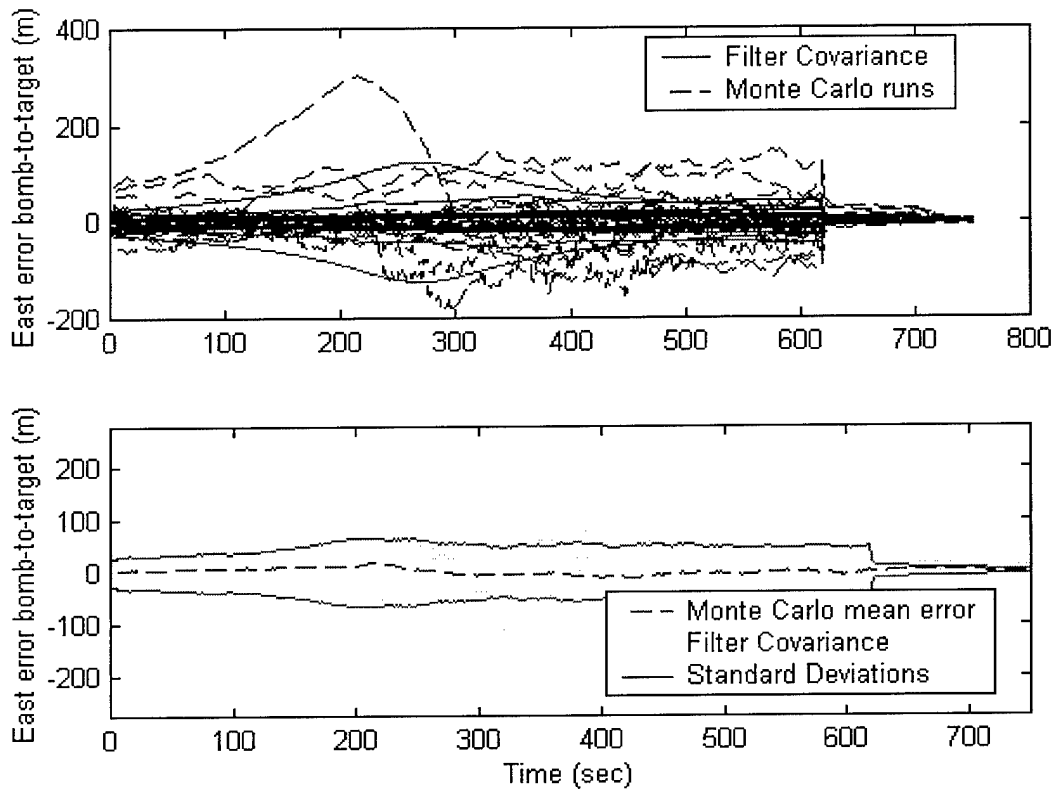


Figure 47. Case 9 – East Error Bomb-to-Target

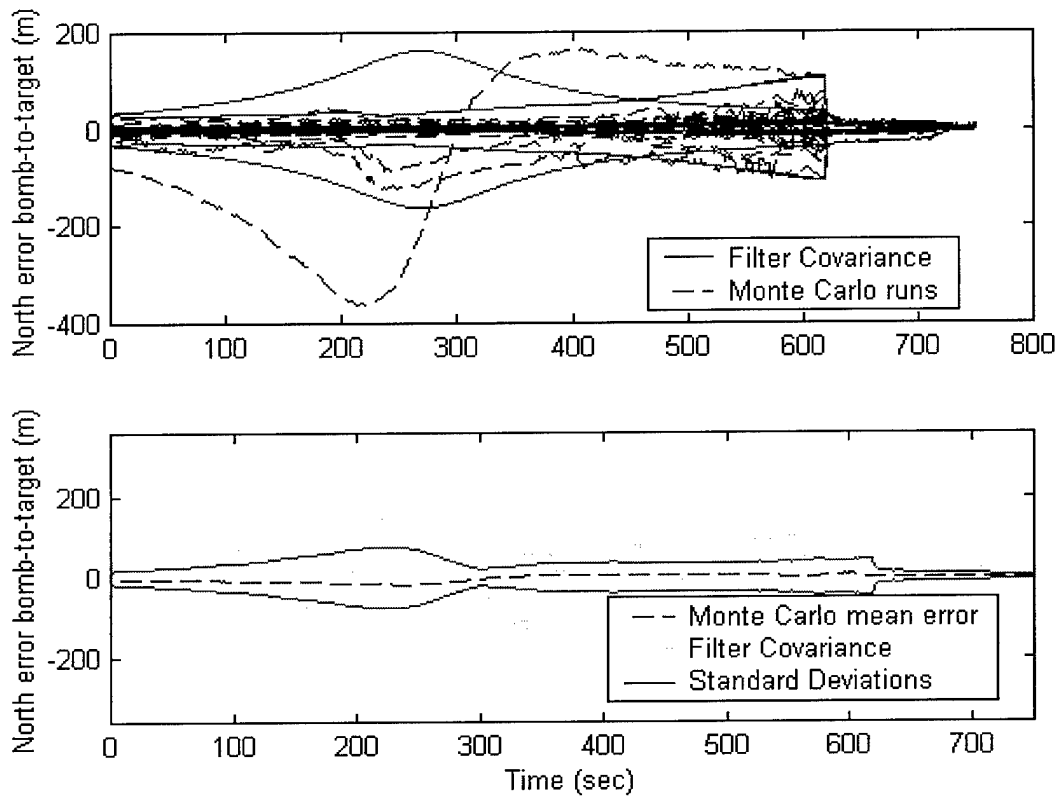


Figure 48. Case 9 – North Error Bomb-to-Target

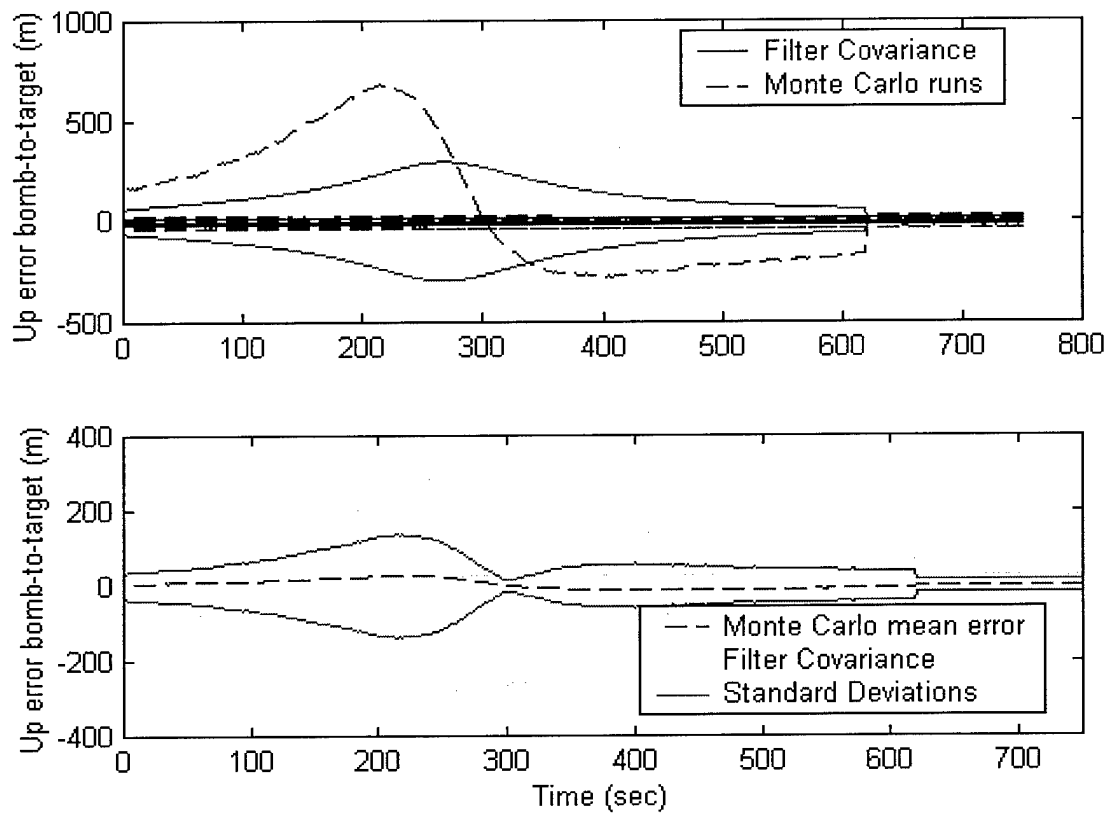


Figure 49. Case 9 – Up Error Bomb-to-Target

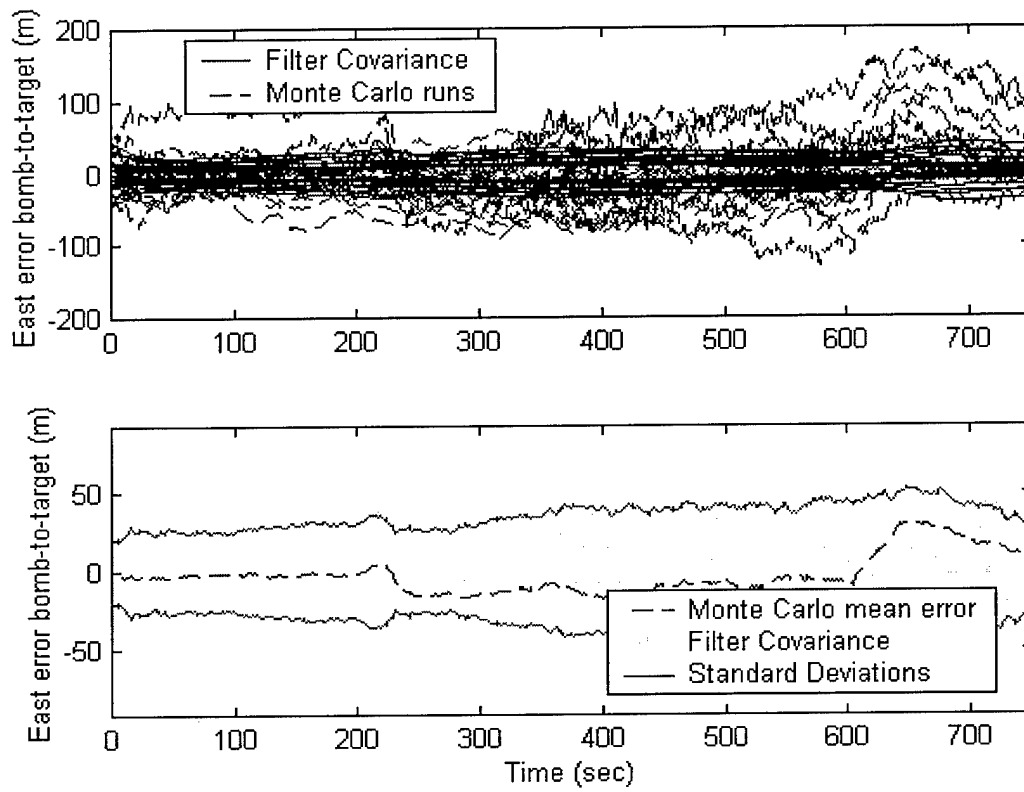


Figure 50. Case 10 – East Error Bomb-to-Target

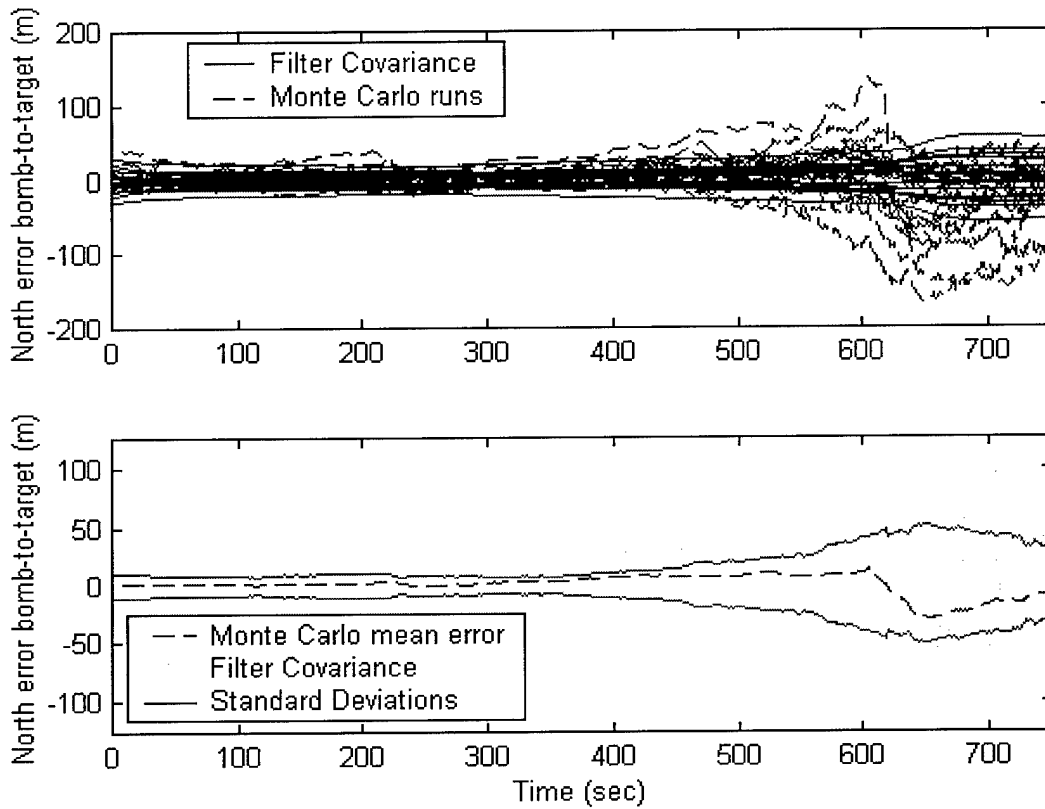


Figure 51. Case 10 – North Error Bomb-to-Target

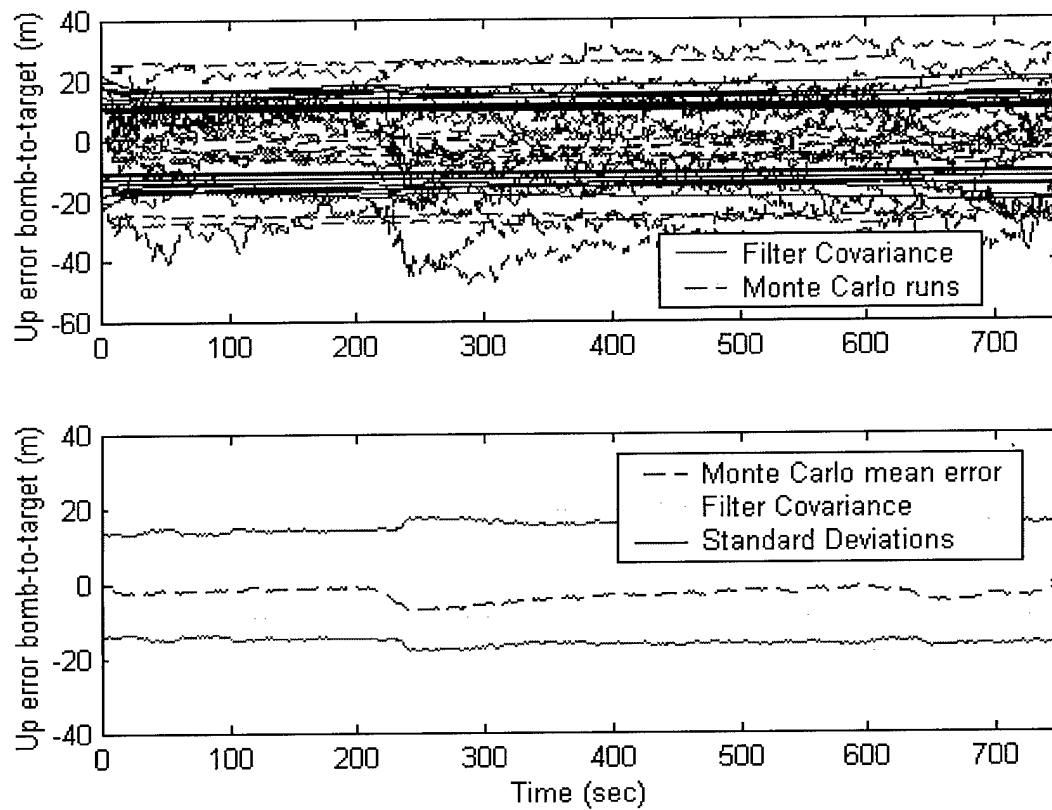


Figure 52. Case 10 – Up Error Bomb-to-Target

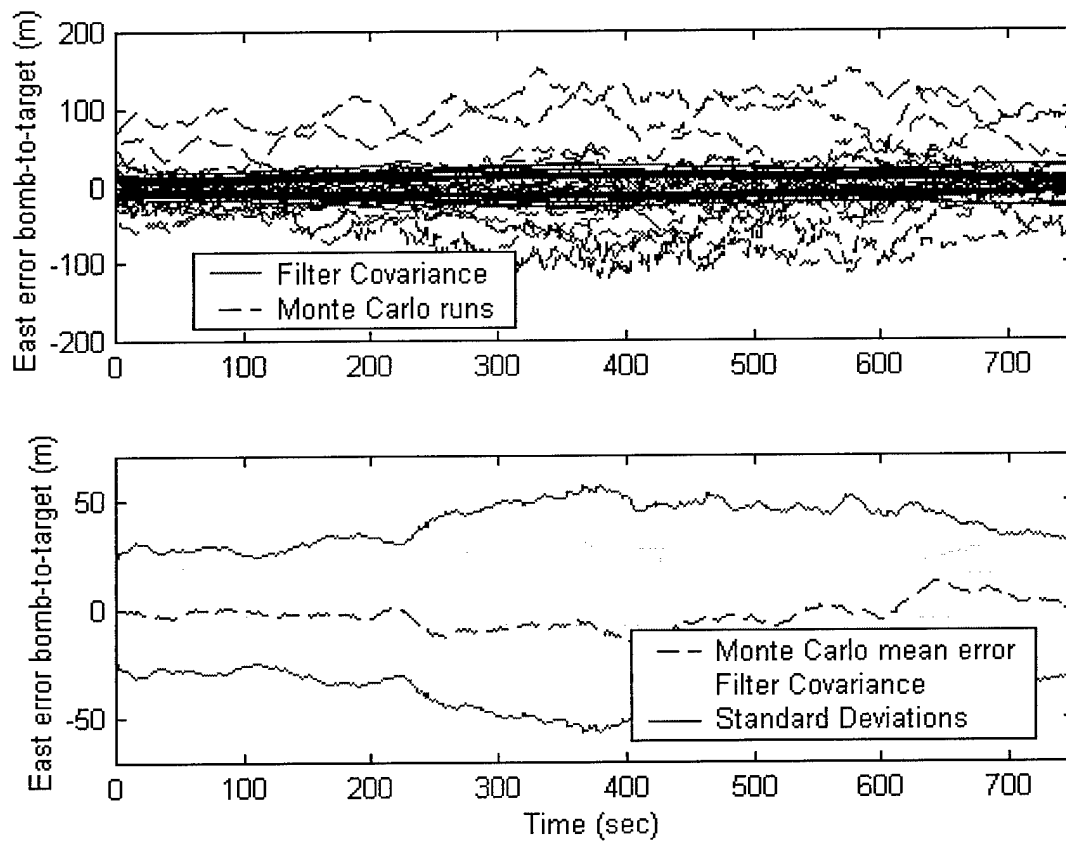


Figure 53. Case 11 – East Error Bomb-to-Target

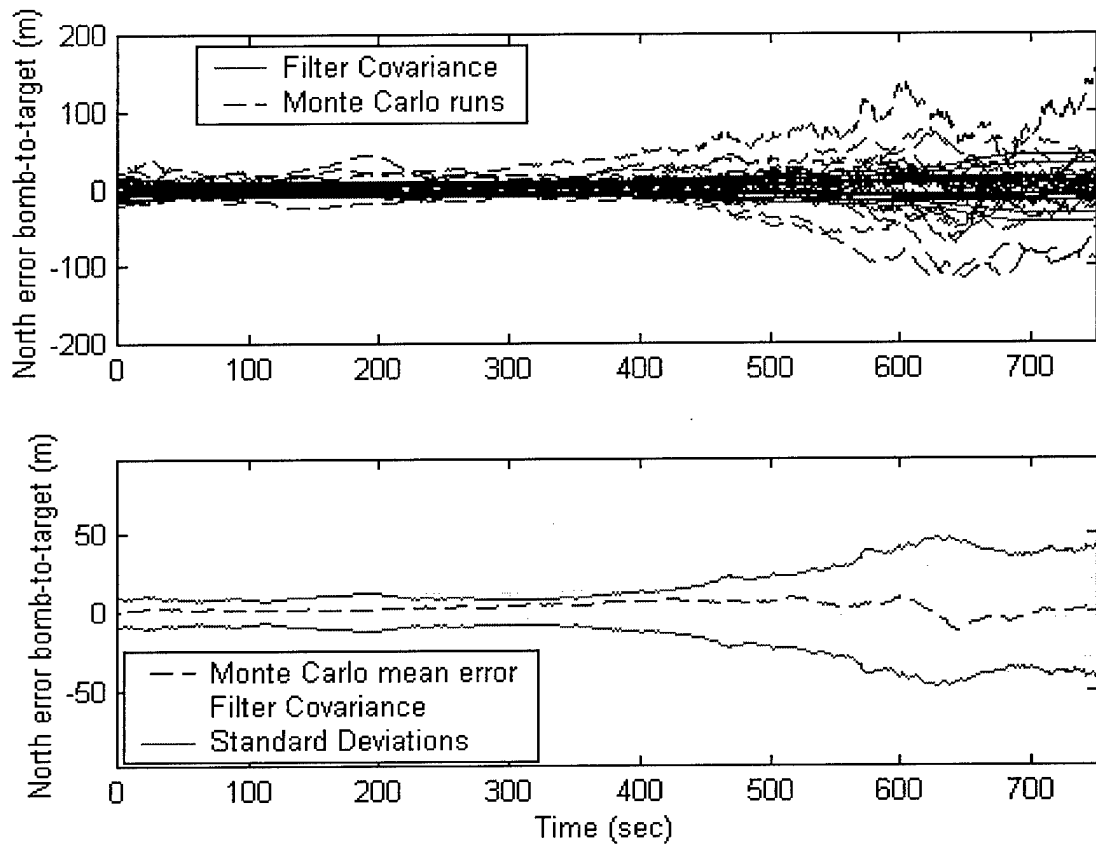


Figure 54. Case 11 – North Error Bomb-to-Target

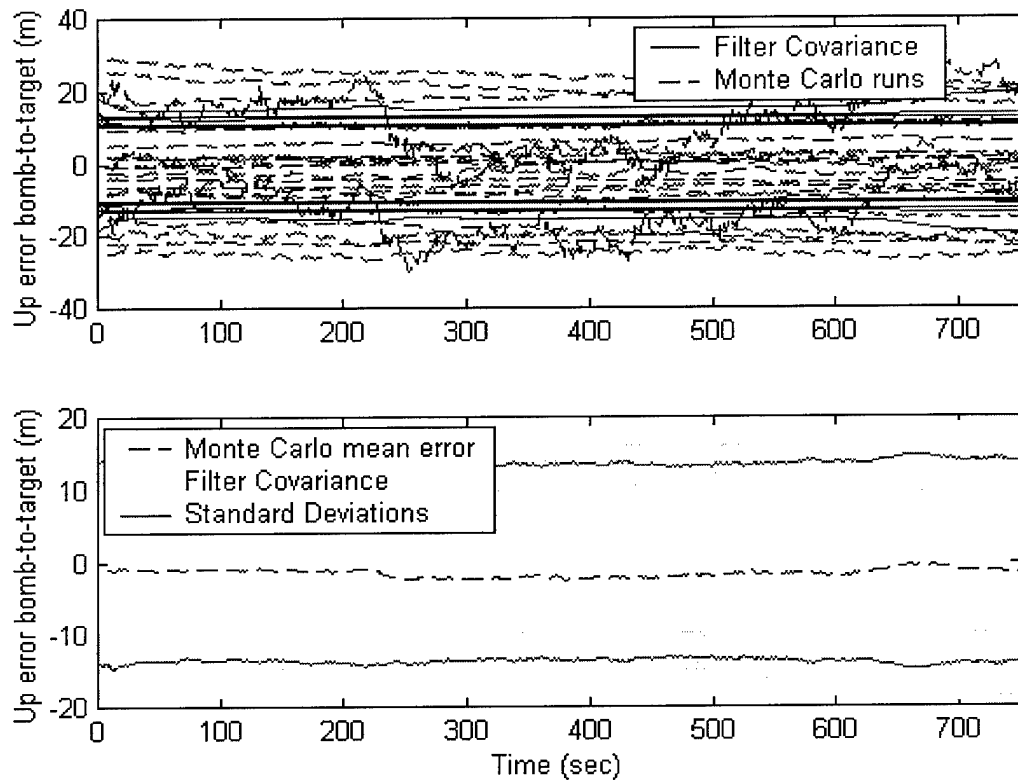


Figure 55. Case 11 – Up Error Bomb-to-Target

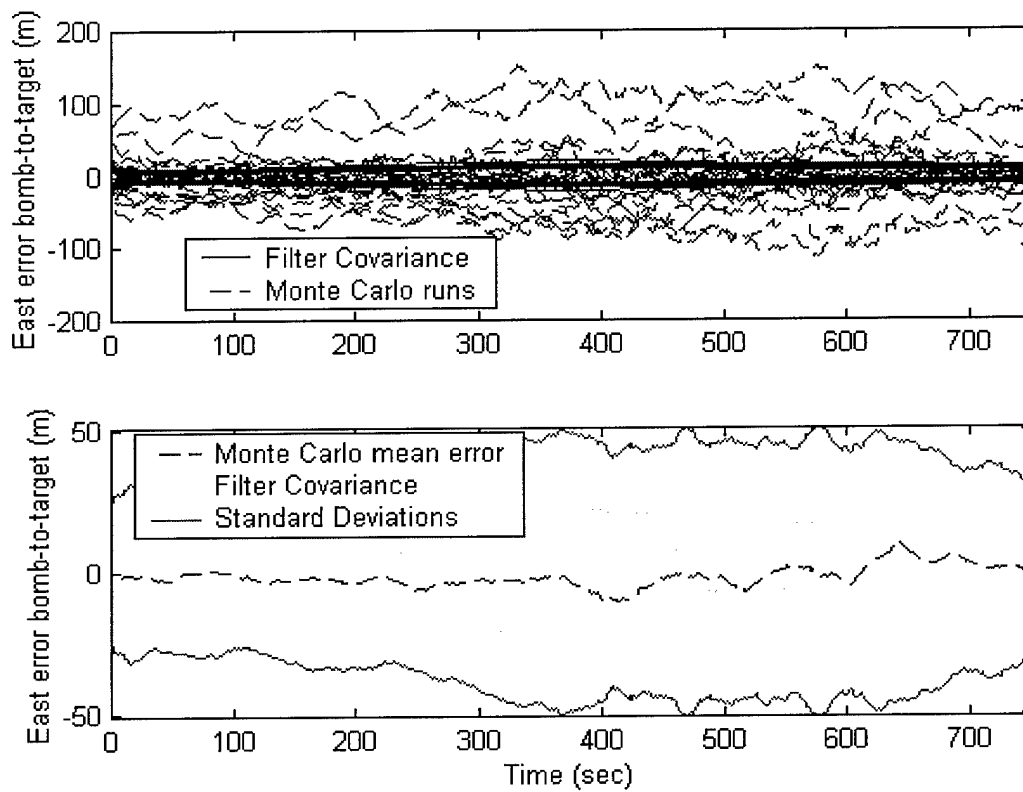


Figure 56. Case 12 – East Error Bomb-to-Target

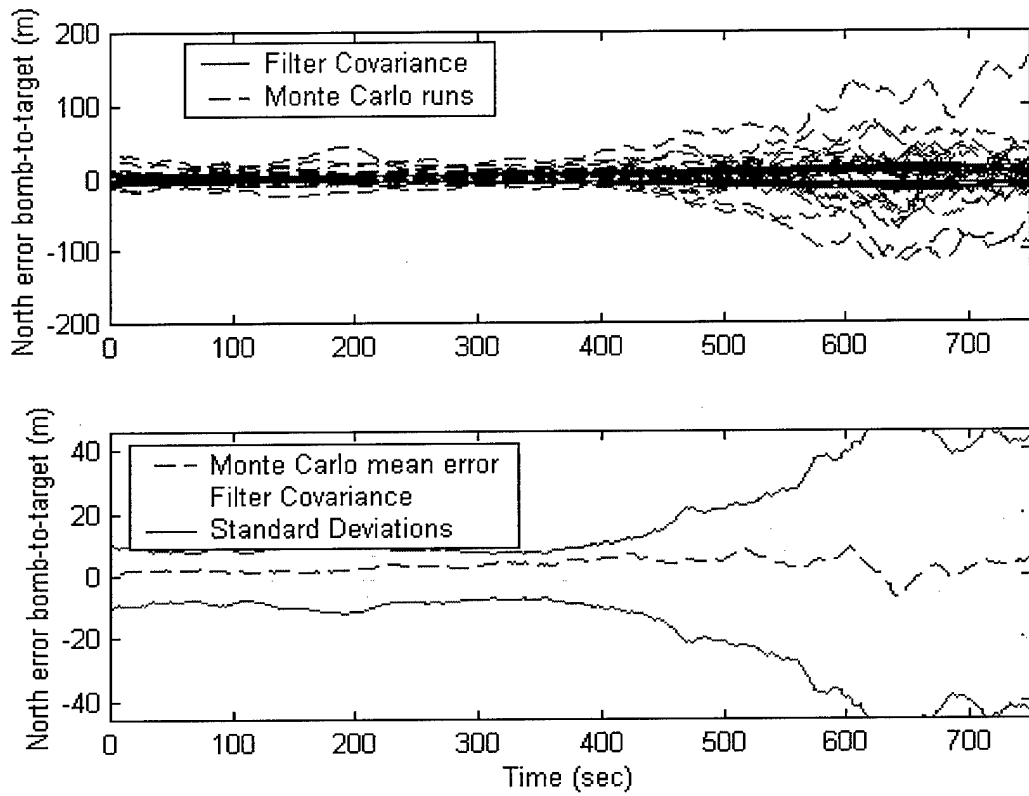


Figure 57. Case 12 – North Error Bomb-to-Target

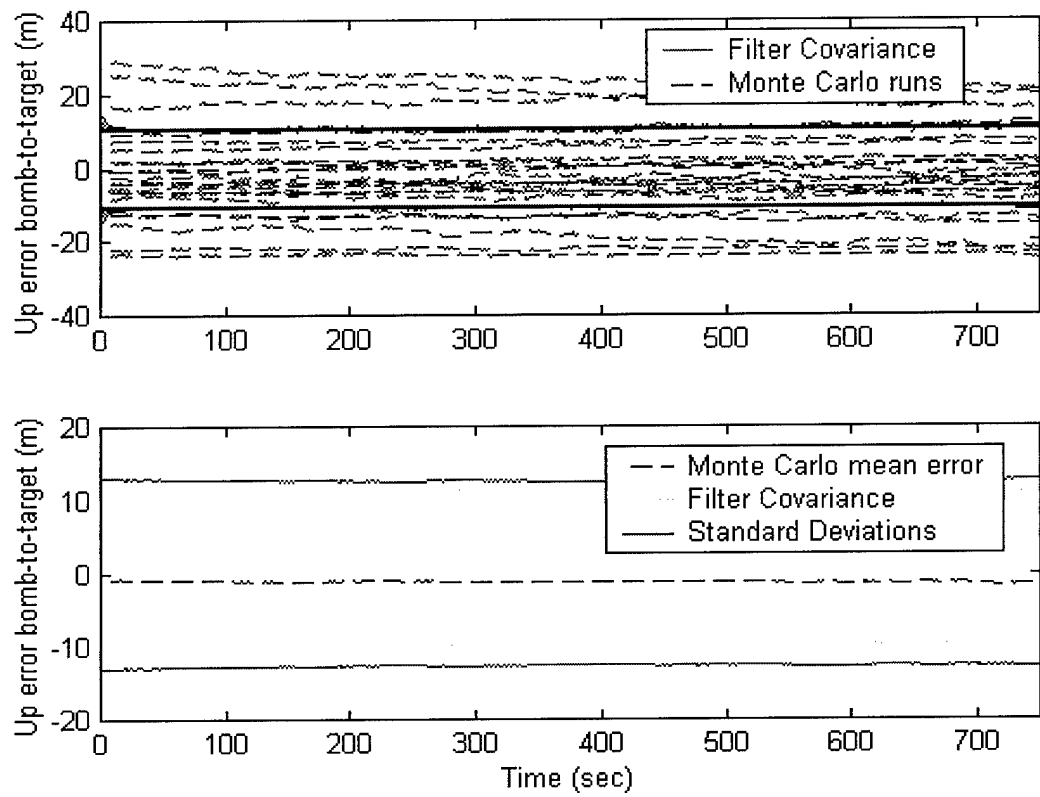


Figure 58. Case 12 – Up Error Bomb-to-Target

Bibliography

- [1] "Affordable Moving Surface Target Engagement Program Enters Second Phase." Online News Article http://www.af.mil/news/Sep2000/n20000928_001500.shtml 2 Oct 2000.
- [2] Braasch, Michael S. "INS Toolbox for MATLAB." Athens OH: GPSSoft LLC, 1998. WWW Site <http://www.gpssoftnav.com>.
- [3] Braasch, Michael S. "Chapter 14. Multipath Effects," in Global Positioning System: Theory and Applications Volume I . Ed. Bradford Parkinson, James Spilker. Washington, DC: American Institute of Aeronautics and Astronautics, Inc., 1995.
- [4] Braasch, Michael S. Class handout, Navtech Course 650: GPS and DGPS Multipath Effects and Modeling. Salt Lake City, UT, September 19, 2000.
- [5] Braasch, Michael S. Associate Professor, Ph.D., P.E., Ohio University. Personal Interview. 20 July 2001.
- [6] Castleberg, Paul A. "GMTI Radar for Affordable Moving Surface Target Engagement (AMSTE)." Naval Postgraduate School, Short Course Slides, March 1, 2000.
- [7] Clynch, James. Class handout, Navtech Course 730: GPS Propagation and Broadcast Ephemeris Errors: GPS Error Sources After SA, Salt Lake City, UT, September 18, 2000.
- [8] Collins, J. Paul and Richard B. Langley. "Estimating the Residual Tropospheric Delay for Airborne Differential GPS Positioning." Proceedings of ION National Technical Meeting 1997, Kansas City, MO, September 1997.
- [9] Dana, Peter H. "Global Positioning System Overview." n. pag. http://www.colorado.edu/geography/gcraft/notes/gps/gps_f.html 1 May 2000
- [10] Dodson, A.H., W. Chen, H.C. Baker, N.T. Penna, and G.W. Roberts. "Assessment of EGNOS Tropospheric Correction Model." Proceedings of ION National Technical Meeting 1999, Nashville, TN, September 14-16, 1999.
- [11] Dowdle, John and Karl Flueckiger. "Submeter Navigation Grid System Concept" Proceedings of IEEE Position Location and Navigation Symposium, San Diego, CA, March 13-16, 2000.
- [12] "Error Sources." n. pag. <http://www.mercat.com/QUEST/Error.htm>. November 16, 2000.
- [13] Gilson, W. "NIMA DTED Error Characteristics", February 23, 1999.

- [14] Gilson, William. "Affordable Moving Surface Target Engagement (AMSTE); Precision Fire Control Tracking (PFCT); Error Budget." Slides from Presentation MIT Lincoln Laboratory, May 4, 1999.
- [15] Godet, Jérémie, Joël Dantepal, and others. "Multipath Error Analysis and Calibration for GPS Differential Phase." Proceedings of ION National Technical Meeting 1999, San Diego, CA, January 25-27, 1999.
- [16] "GPS Error Sources." n. pag.
<http://www.colorado.edu/geography/gcraft/notes/gps/gps.html>. November 16, 2000.
- [17] Hartman, Bob "DARPA's AMSTE GPS Developments" Slides, November 17, 1999.
- [18] Henderson, Paul E. And John F. Raquet. "Development and Testing of a Multiple Filter Approach for Precise DGPS Positioning and Carrier-Phase Ambiguity Resolution." Proceedings of ION National Technical Meeting 1999, Nashville, TN, September 14-16, 1999.
- [19] Kaplan, Elliott D., "Understanding GPS: Principles and Applications." Boston: Artech House, 1996.
- [20] Kovach, Karl. "New User Equivalent Range Error (UERE) Budget for the Modernized Navstar Global Positioning System (GPS)." Proceedings of ION National Technical Meeting 2000, Anaheim, CA, January 26-28, 2000.
- [21] Lachapelle, Gérard. Class handout, Navtech Course 500A: High Accuracy GPS Positioning Techniques & Applications I., Salt Lake City, UT, September 18, 2000.
- [22] Lachapelle, Gérard and Ning Luoand. "Centimeter Level Relative Positioning of Distributed Moving Platforms Using GPS Carrier Phase Observables." Proceedings of 55th Annual Meeting of the Institute of Navigation. Cambridge, MA, June 28-30, 1999.
- [23] Layne, Jeffery R. And Erik P. Blasch. Integrated Synthetic Aperture Radar and Navigation Systems for Targeting Applications: Final Report for Period 12/01/92-12/01/93. Wright-Patterson AFB OH: Wright Lab, September 1997 (AD-A337532).
- [24] Mac Millan, A. J., J. M. Clifford, and others. "CAPE – CRPA Associated Position Errors." Proceedings of ION National Technical Meeting 2000, Anaheim, CA, January 26-28, 2000.

- [25] Maybeck, Peter S. Stochastic Models, Estimation and Control, I. New York: Academic Press, Inc., 1979. Republished Arlington VA: Navtech, 1994.
- [26] Maybeck, Peter S. Stochastic Models, Estimation and Control, II. New York: Academic Press, Inc., 1982. Republished Arlington VA: Navtech, 1994.
- [27] Mendes, V.B., and R.B. Langley. "A Comprehensive Analysis of Mapping Functions Used in Modeling Tropospheric Propagation Delay in Space Geodetic Data." Proceedings of ION National Technical Meeting, Nashville, TN September 15-18,1998.
- [28] Murphy, Tim, Robert Snow, and Michael Braasch. "GPS Multipath on Large Commercial Air Transport Airframes." Navigation: Journal of The Institute of Navigation, Volume 43, Number 4, Winter 1996-1997.
- [29] Raquet, J., G. Lachapelle, T.E. Melgård. "Test of a 400 km x 600 km Network of Reference Receivers for Precise Kinematic Carrier-Phase Positioning in Norway." Proceedings of ION National Technical Meeting, Nashville, TN September 15-18,1998.
- [30] Raquet, John F. Class Handouts, EENG 533, Navigation Using the GPS. School of Engineering, Air Force Institute of Technology (AU), Wright-Patterson AFB OH, Spring 2000.
- [31] Raquet, John F. Class Handouts, EENG 633, Advanced GPS Theory and Applications. School of Engineering, Air Force Institute of Technology (AU), Wright-Patterson AFB OH, Summer 2000.
- [32] Ray, J.K. and M.E. Cannon. "Code Range and Carrier Phase Multipath Mitigation Using SNR, Range and Phase Measurements in a Multi-Antenna System." Proceedings of ION National Technical Meeting 1999, Nashville, TN, September 14-16, 1999.
- [33] Schueler, Torben, Guenter W. Hein and Bernd Eissfeller. "Improved Tropospheric Delay Modeling Using an Integrated Approach of Numerical Weather Models and GPS." Proceedings of ION National Technical Meeting 2000, Salt Lake City, UT, September 19-22, 2000.
- [34] Sennott, James. Class handout, Navtech Course 140A: Differential GPS I., Salt Lake City, UT, September 19, 2000.
- [35] Spilker, J.J. Jr. . "Chapter 13. Tropospheric Effects on GPS," in Global Positioning System: Theory and Applications Volume I. Ed. Bradford Parkinson, James Spilker. Washington, DC: American Institute of Aeronautics and Astronautics, Inc., 1995.

- [36] Spilker, J.J. Jr. . "Chapter 2. GPS Navigation Data," in Global Positioning System: Theory and Applications Volume I . Ed. Bradford Parkinson, James Spilker. Washington, DC: American Institute of Aeronautics and Astronautics, Inc., 1995.
- [37] Spilker, J.J. Jr. . "Chapter 1. Differential GPS," in Global Positioning System: Theory and Applications Volume II . Ed. Bradford Parkinson, James Spilker. Washington, DC: American Institute of Aeronautics and Astronautics, Inc., 1995.
- [38] "Synthetic Aperture Radar an Overview (SAR)." Mid-Term Project – Spring 1998, ASE 389 University of Texas at Austin. n. pag.
<http://www.ae.utexas.edu/courses/ase389/midterm/cary/sar-report.htm>.
 November 14, 2000.
- [39] Tsujii, Toshiaki, Jinling Wang, Chris Rizos, Masatoshi Harigae, Toshiharu Inagaki. "Estimation of Residual Tropospheric Delay for High-Altitude Vehicles: Towards Precise Positioning of a Stratosphere Airship." Proceedings of ION National Technical Meeting 2000, Salt Lake City, UT, September 19-22, 2000.
- [40] "Understanding the Global Positioning System." n. pag.
<http://www.montana.edu/places/gps/understd.html>. November 16, 2000.
- [41] "US Air Force Eyes Next Revolution in Close Air Support," Jane's International Defense Review: 3: 3 (October 2000).
- [42] Vanek, Barry J. "GPS Signal Offset Detection and Noise Strength Estimation in a Parallel Kalman Filter Algorithm." MS thesis, AFIT/GE/ENG/99M-30. School of Engineering, Air Force Institute of Technology (AU), Wright-Patterson AFB, OH, March 1999. (AD-A361773).
- [43] Welby, Stephen, Program Manager. "Affordable Moving Surface Target Engagement." DARPA Special Projects Office. n. pag.
<http://www.darpa.mil/spo/programs/affordmovingsurfacetarget.htm>. October 24, 2000.
- [44] Witko, Jeff and Jose Caussade. "Continued Need for PGMs," GPS for Air and Space Power, No. 228, ANSER Corp., November 13, 2000.
- [45] Wormley, Samuel J. "GPS Errors & Estimating Your Receiver's Accuracy." Iowa State University. n. pag.
http://www.cnde.iastate.edu/staff/swormley/gps/gps_accuracy.html. November 17, 2000.

- [46] Young, Brian J. "An Integrated Synthetic Aperture Radar/Global Positioning System/Inertial Navigation System for Target Geolocation Improvement." MS thesis, AFIT/GE/ENG/99M-32. School of Engineering, Air Force Institute of Technology (AU), Wright-Patterson AFB OH, March 1999 (AD-A3618000).
- [47] Zhang, JiHong. "Precise Estimation of Residual Tropospheric Delays in a Spatial GPS Network." Proceedings of ION National Technical Meeting 1999, Nashville, TN, September 14-16, 1999.
- [48] Zhang, Z "Impact of Rubidium Clock Aiding on GPS Augmented Vehicular Navigation." MS Thesis, published as Report No. 20112, Department of Geomatics Engineering, The University of Calgary.1997

Vita

As an Air Force dependant, Captain Daryl J. Burnette has traveled the world and in 1992 landed in Glendale, AZ where he graduated from Cactus High School. In May 1996, he graduated with a Bachelor of Science Degree in Electrical Engineering from Tulane University and was commissioned as a Second Lieutenant in the United States Air Force. Captain Burnette began his career at Vandenberg AFB attending the Undergraduate Space and Missile Training course. Upon graduation, he chose 2d Space Launch Squadron as his first assignment. As a mission-ready Launch Crew Commander for the Delta II rocket, he served as the single point of contact for all issues involving the Advanced Research Global Observation Satellite (ARGOS) spacecraft, the only military payload to be launch on a West Coast Boeing Delta II rocket. As Satellite Operations Controller, Captain Burnette coordinated the spacecraft community's communication requirements, incorporated spacecraft processing into the Delta II countdown manual and was the Air Force link between the civilian contractor and payload personnel on all spacecraft requirements. He was also a trainer for Vandenberg's Guardian Challenge Operation team which won the coveted Schiever Trophy for Best Spacelift Wing in Space Command in 1999. In August 1999, he was selected to attend the Graduate School of Engineering and Management, Air Force Institute of Technology to receive a Masters Degree in Electrical Engineering with a focus in Stochastic Estimation and Control and GPS Navigation. Upon graduation, he will be assigned to the Information Directorate, Air Force Research Laboratory, Wright-Patterson AFB, Ohio.

REPORT DOCUMENTATION PAGE			Form Approved OMB No. 0704-0188		
Public reporting burden for the collection of information is estimated to average 1 hour per response, including the time for reviewing instructions, searching existing data sources, gathering and maintaining the data needed, and completing and reviewing the collection of information. Send comments regarding this burden estimate or any other aspect of this collection of information, including suggestions for reducing this burden, to Washington Headquarters Services, Directorate for Information Operations and Reports, 1215 Jefferson Davis Highway, Suite 1204, Arlington, VA 22202-4302, and to the Office of Management and Budget, Paperwork Reduction Project (0704-0188), Washington, DC 20503.					
1. REPORT DATE (DD-MM-YYYY) 20-03-2001		2. REPORT TYPE Master's Thesis		3. DATES COVERED Aug 1999 - Mar 2001	
4. TITLE AND SUBTITLE USING GPS AS A REFERENCE SYSTEM TO HIT A MOVING TARGET			5a. CONTRACT NUMBER		
			5b. GRANT NUMBER		
			5c. PROGRAM ELEMENT NUMBER		
			5d. PROJECT NUMBER		
6. AUTHOR(S) Burnette, Daryl J. Captain, USAF			5e. TASK NUMBER		
			5f. WORK UNIT NUMBER		
			8. PERFORMING ORGANIZATION REPORT NUMBER AFIT/GE/ENG/01M-04		
7. PERFORMING ORGANIZATION NAMES(S) AND ADDRESS(S) Air Force Institute of Technology Graduate School of Engineering and Management (AFIT/EN) 2950 P Street, Bldg 640 Wright-Patterson AFB OH 45433-7542			10. SPONSOR/MONITOR'S ACRONYM(S)		
			11. SPONSOR/MONITOR'S REPORT NUMBER(S) N/A		
9. SPONSORING/MONITORING AGENCY NAME(S) AND ADDRESS(ES) DARPA Special Projects Office Attn: Stephen Patrick Welby 3701 N. Fairfax Drive Arlington, VA 22203-1714 Phone: 703-248-1545					
12. DISTRIBUTION/AVAILABILITY STATEMENT APPROVED FOR PUBLIC RELEASE, DISTRIBUTION UNLIMITED.					
13. SUPPLEMENTARY NOTES					
14. ABSTRACT <p>The Affordable Moving Surface Target Engagement (AMSTE) project attempts to develop affordable solutions to the precise moving target surface target engagement problem. Up to this point, most of the error analysis performed for the AMSTE project has been at the error variance level, generating root-sum-square (RSS) total errors from error budgets consisting of constant error variances. In reality, the level of error for both Global Positioning System (GPS) positioning and radar targeting systems is highly dependent upon the given situation (such as the distance between sensor and target, the altitude differences, etc.) This research generates a more comprehensive model of the GPS errors based upon the underlying physics of the situation. It focuses on differential tropospheric errors and multipath, as these are the primary error source in a differential GPS targeting system.</p> <p>In addition to the error model development, a code-based differential GPS and differential ranging approach is implemented in simulation using a Kalman filter. This approach uses GPS measurements collected by each of the sensors and the weapon, and it uses ranging measurements from the sensors to the bomb and the target. Multiple cases are run varying 1) the number of GPS satellite measurements tracked by each receiver, 2) whether or not the common GPS errors are estimated, and 3) whether or not the bomb is tracked with the same radar sensors that are tracking the target. The horizontal DRMS position error during the terminal phase of the bomb trajectory drops from about 6 meters to about 3.5 meters.</p>					
15. SUBJECT TERMS Global Positioning System, GPS, Differential Global Positioning System, DGPS, GPS Errors, DGPS Errors, GPS Targeting, DGPS Targeting, Synthetic Aperture Radar, Kalman filter, Targeting, Sensor Fusion					
16. SECURITY CLASSIFICATION OF:		17. LIMITATION OF ABSTRACT	18. NUMBER OF PAGES	19a. NAME OF RESPONSIBLE PERSON	
a. REPORT	b. ABSTRACT			c. THIS PAGE	Raquet, John F. Major USAF
U	U	U	134	19b. TELEPHONE NUMBER (Include area code) 937-255-3636 x4580	